Eduardo José Novaes Menezes

Wind Turbine Structural Control

Recife

2022

Eduardo José Novaes Menezes

Wind Turbine Structural Control

Thesis presented to the Graduate Program in Mechanical Engineering of the Federal University of Pernambuco, in order to obtain the title of Ph.D. in Mechanical Engineering.
Concentration Area: Energy

Universidade Federal de Pernambuco – UFPE

Centro de Tecnologia e Geociências

Programa de Pós-Graduação em Engenharia Mecânica

Supervisor: Alex Maurício Araújo, Ph.D.

Recife

2022

Catalogação na fonte:
Bibliotecária Margareth Malta, CRB-4 / 1198

M543w Menezes, Eduardo José Novaes.
Wind turbine structural control / Eduardo José Novaes Menezes. – 2022.
134 f.: il., fig.

Orientador: Prof. Dr. Alex Maurício Araújo.
Tese (Doutorado) – Universidade Federal de Pernambuco. CTG. Programa de Pós-Graduação em Engenharia Mecânica. Recife, 2022.
Inclui referências e apêndice.

1. Engenharia mecânica. 2. Turbinas eólicas. 3. Análise estrutural. 4. Método dos elementos finitos. 5. Redução de carregamento. 6. Controle estrutural. I. Araújo, Alex Maurício (Orientador). II. Título.

UFPE

621 CDD (22. ed.) BCTG/2023-58

Eduardo José Novaes Menezes

Wind Turbine Structural Control

Thesis presented to the Graduate Program in Mechanical Engineering of the Federal University of Pernambuco, in order to obtain the title of Ph.D. in Mechanical Engineering.
Concentration Area: Energy

Approved in August 25th, 2022.

Alex Maurício Araújo, Ph.D.
Universidade Federal de Pernambuco

Nadège Sophie Bouchonneau da Silva, Ph.D.
Universidade Federal de Pernambuco

Unai Fernandez-Gamiz, Ph.D.
Universidad del País Vasco / Euskal Herriko Unibertsitatea

Pedro André Carvalho Rosas, Ph.D.
Universidade Federal de Pernambuco

José Ângelo Peixoto Da Costa, Ph.D.
Instituto Federal de Pernambuco

This work is dedicated to my family.

"Gravity explains the motions of the planets
but it cannot explain who set the planets in motion.
God governs all things,
and knows all that is or can be done."
Isaac Newton (1643-1727)

Abstract

Wind energy is one of the most important power sources in supplying world energy consumption nowadays. The transition to a clean-based energy has created the demand for wind turbines (WTs) of extremely large dimensions, with very flexible design. In this context, the structural analysis and control of WTs has a fundamental role in the mitigation of loads and increasing the fatigue life of the structure. Significant research has been devoted to the issues of aeroelastic loads, simulation software, structural control and load reductions of WTs. The present thesis is included in this field of research, contributing with developments in the structural analysis and in the state-space control, H-infinity control, and model predictive control (MPC) applied to WTs. Therefore, the thesis deals with two main pathways: (1) the development of a proprietary tool for the structural analysis of wind turbines, based on finite-element procedures and (2) the development and application of control strategies to reduce WT structural loads and the results of them in terms of WT fatigue damage, based on turbulent simulations. The results show an effectiveness and superiority of the WT advanced control strategies employed, demonstrating a good rotor speed regulation and reduction of structural loads and oscillations.

Keywords: Wind turbines. Structural analysis. Finite-Element Method. Load mitigation. Structural control.

Resumo

A energia eólica é uma das fontes de energia mais importantes para suprir o consumo mundial de energia. A transição para um consumo de energia baseado em energia renovável levou ao desenvolvimento de turbinas eólicas (TEs) de grandes dimensões, com projetos estruturais de elevada flexibilidade. Nesse contexto, a análise e o controle estrutural de TEs têm papel fundamental na mitigação de cargas e no aumento da vida em fadiga da estrutura. Significativo esforço de pesquisa tem sido dedicado às questões do carregamento aero-elástico, simulação computacional de TEs, controle estrutural e redução de cargas estruturais. Esta tese está inserida neste campo de pesquisa, contribuindo com desenvolvimentos na análise estrutural e no controle em espaço de estados, controle H-infinito e controle preditivo baseado em modelo (MPC), aplicado às TEs. Portanto, a tese apresenta dois caminhos principais: (1) o desenvolvimento de uma ferramenta própria para a análise estrutural de turbinas eólicas, baseada em procedimentos de elementos finitos e (2) o desenvolvimento e aplicação de estratégias de controle para reduzir as cargas estruturais da TE, que são verificadas com base em simulações de vento turbulento. Os resultados mostram a efetividade e superioridade dos métodos de controle utilizados, apresentando uma regulação de velocidade do rotor adequada e a redução das cargas estruturais e das oscilações.

Palavras-chave: Turbinas eólicas. Análise estrutural. Método dos Elementos Finitos. Redução de carregamento. Controle estrutural.

List of Figures

Contents

1 INTRODUCTION

1.1 Wind energy overview

The wind energy has been used as a power source since the antiquity. In fact, many ancient civilizations have used wind as the driving force in sailing ships, for commercial trade and human migrations (ROHATGI, 1998). The first register of a machine designed to harness wind energy is the prototype of Hero of Alexandria, from the 1st century BC, in his book Pneumatics (MANWELL; MCGOWAN; ROGERS, 2010). The next historical register of wind energy dates from the 9th century AD, when there are registers of windmills used by the persians. These were vertical-axis machines and used to grain milling. The presence of windmills in China, used to drain rice fields and made from bamboo and fabric, is also related in this time. In Europe, the first appearances of wind energy dates from the middle age, in northern Europe. These were different from the persian wind mills, being horizontal-axis machines. They were used for nearly any mechanical task, including water pumping, grinding grain, sawing wood and powering tools. They were constructed with 4 blades and mounted in individual posts. An example of a early european windmill is shown in Fig. 1. The wind energy continued to be an important power source in Europe

Figure 1 – Early european windmill

Source: UN Climate Change. Available in: https://www.un.org/en/climatechange/what-is-renewable-energy. Access in August 14th, 2022

Figure 2 – Modern wind turbines

Source: UN Climate Change. Available in: https://www.un.org/en/climatechange/what-is-renewable-energy. Access in August 14th, 2022

until the Industrial Revolution, when the coal and steam power have overcome all the other power sources. The importance of windmills have remained reduced until their initial use to electricity, dating from the end of the 19th century. The danish engineer Paul La Cour is between the first to build a windmill driving a dynamo, back to 1891. From this time and during the first half of 20th century, there has been a development of wind turbines (WTs) in the range of less than 1 MW, for specific uses. The strong wind energy development became relevant from the mid 1970s, with the oil crisis and the growing environmental conscience about the issues caused by fossil fuels. In the following years, many wind turbines manufacturers have appeared and wind energy has gained importance, especially in Europe and in the north-american state of California. The wind turbines have begun to be installed in wind farms or wind parks (EUROPE, 2022). By the early 2000s, commercial wind turbines reached 2 MW of rated power. The evolution has continued, and as of today there are 5 MW and 10 MW wind turbines, and there is planned design for 15 MW or even larger capacity machines (GAERTNER et al., 2020). Additionally, in the recent years, the installation of offshore wind turbines has been widespread. Examples of modern wind turbines are shown in Fig. 2, presenting onshore and offshore turbines. In summary, the current wind turbines are large-scale machines, with huge dimensions and reaching several mega-watts of power. On the other hand, the need for energy transition has increasingly received impulse. This is mainly due to the escalation of the environmental crisis. According to the Intergovernmental Panel on Climate Change (IPCC), organ of the United Nations (UN) for climate changes matters, the limitation of global temperature increase to 1.5ºC in 2100 compared to pre-industrial levels would be the ideal to weaken the effects of global warming in ecosystems and in the human life. A 2ºC increase is pointed as the superior threshold to ensure tolerable impacts in the life in the planet. Indeed, this was the limit adopted by the Paris Agreement, in the end of 2015, by 192 countries (IPCC, 2018). Further, the Paris Agreement also established the limitation of greenhouse gas emissions from human activity to the same levels that trees, soil and oceans can absorb naturally, known as net zero, between 2050 and 2100 (BRIGGS, 2021). The achievement

Figure 3 – World installed wind power evolution

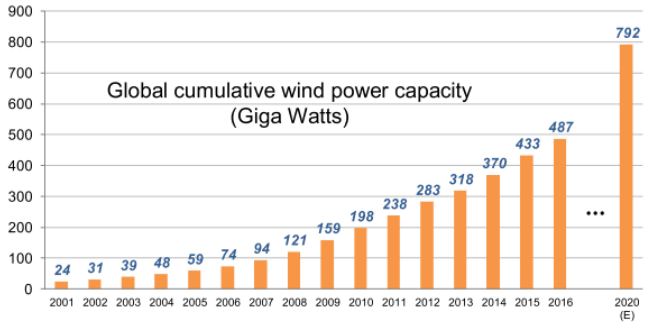

Source: (GWEC, 2022)

of these goals will require massive investments in renewable sources in the next decades, including even more wind energy. At the same time, energy transition has been pursuit as a manner of the national governments to attain energy self-sufficiency, particularly in the face of the recent political instabilities (IEA, 2022), which have been motivating clean energy development to free countries from gas dependence.

In this context, the wind energy has performed a fundamental role as one of the most important and profitable renewable energy sources. The world has seen its installed wind power capacity passes from 198 GW in 2010 to 792 GW in 2020, as shown in Fig. 3. In 2022, this number is of 837 GW. Projections indicate that, to achieve the net zero by 2050, the installed capacity worldwide should ideally increase to 3000 GW already by 2030. However, based on current growth rates, the capacity in this year should attain 1200 GW of power (GWEC, 2022). In either scenario, the wind energy growth is very significant. Brazil's situation fits in the increasing wind power importance. The country has passed from the incipient wind power production of 0.22 GW in 2005 to the current 21 GW. Brazil is today the 7th country in wind power installed capacity and the projections are of constant growth over the next years (EPBR, 2022). It is worth noting that 80% of Brazil's wind farms are located in the Northeast region. As one can see, the wind energy presents a great potential of growth, both in a global and local scale. This whole outline of renewable energy sources and specifically of wind energy has led to the development of increasingly larger wind turbines, raising structural issues, as presented in the next sections.

1.2 Large wind turbines and structural issues

Given the need for wind energy development, the wind turbines have reached enormous dimensions. Nowadays, the typical wind turbines attain 100 m of hub-height and 120 m of blade length (ENERGY, 2021). This happens because one of the fundamental challenges of renewable energy is the competitiveness and cost regarding conventional sources. The increase in size allows to obtain economies of scale for wind energy cost.

Nevertheless, the increase in wind turbine dimensions and in rated capacity per WT implies some technological challenges. In particular, the WT designs have become more flexible and lighter, in order to admit the increased size. This, on its turn, makes the structure more susceptible to dynamic actions and structural loads, which may lead to the structural failure. One of the main concerns of the designers is about the fatigue of the structure, but failures related to ultimate strength are also plausible to occur. Thus, the knowledge and study about WTs structures is a crescent subject, and the structural analysis of WTs is more and more necessary. There has been considerable research in the field of WTs structural dynamics.

The early works date to the 1980s, when helicopter-specific computer programs were used to simulate wind turbine dynamics, such as MOSTAS and REXOR (NASA, 1977). Along the years, WT simulation softwares were developed, taking into account the specific characteristics of these machines. Amongst them, one can cite the GH Bladed (DNV, 2022), HAWC2 (DTU, 2022), and FAST (more recently, OpenFAST) (NREL, 2022). These softwares couple aerodynamics, aeroelastic and control models, in order to simulate the WT as a whole, giving WT power and loads in several WT components. They enable the WT designers to verify the structural loads in different wind conditions, speeding up the design process. In the control models, it is possible to simulate generator torque, yaw and pitch control, and test the effects of the executed controls in the WT structures. Many research works have been executed using the WT simulation softwares, including (JONKMAN, 2010; HAN; LEITHEAD, 2014; RINKER et al., 2020). In (JONKMAN, 2010), e.g., a complete loads analysis is run, verifying the wind turbine behavior under different IEC-61400 conditions. In (HAN; LEITHEAD, 2014), the concern about fatigue loads is studied using the Bladed software. In (RINKER et al., 2020), turbine loads are analyzed comparing HAWC2 and OpenFAST. Even though the use of simulation WT specific software is very common, studies modelings structural dynamics through finite-element method and computational fluid dynamics are also present. As examples, the work of (BI K.; HAO, 2017) use a finite-element approach to analyze the structural loads in the WT tower. (MUYAN; COKER, 2020) have researched the ultimate load in the WT blades considering flap and edgewise forces, with finite-elements. On its turn, (TAVARES; BOUWMAN; PAEPEGEM, 2022) use shell and solid elements to analyze torsional loading of the blades. An instance of CFD applied to structural loads can be found in (HALVO, 2019). Regardless the method, it is important to emphasize that structural analysis and structural loads have always been of concern, since e.g. the work of (SULLIVAN, 1982) and (PEREIRA, 1993), passing to (BOSSANYI, 2000), until most recent works such as (MENG et al., 2019) and (CHEN et al., 2022).

1.3 Wind turbine structural control

The wind turbine is a complex system, that receives a completely variable input, the wind, and should deliver a controlled and well-conditioned output, the electrical power, in a safe and efficient manner. To accomplish this task, control systems are fundamental. There are four main control systems in a wind turbine: the yaw control, the generator torque control, the pitch control and the supervisory control. The later is the responsible for the high-level WT tasks, such as turn-on and turn-off the machine. The other three control systems correspond to the operational tasks. Yaw control is responsible for turning the WT rotor in the direction of the prevailing wind, trying to guarantee that the wind direction be always perpendicular to the rotor, during normal operation. Generator torque control is responsible for changing the WT speed during partial load, when the wind is below the rated, to maximize power production. Pitch control is responsible for limiting power production, when the wind is above the rated, by changing blade pitch angles. This is essential to prevent generator overheating or WT mechanical damages due to the high speed winds.

The main objective of the referred control systems is to provide a suitable operation of the WT. This involves maximizing the efficiency and minimizing the costs, by running the WT under optimal conditions. In this broader context of efficiency and cost, it can be included in the control systems scope an additional objective, which is the reduction or mitigation of structural loads. This consists what can be denominated wind turbine structural control. Reducing loads can increase the efficiency and decrease the wind energy costs by a twofold path: it makes possible the building of larger WTs, able to produce more power and get economies of scale, and it gives these turbines a longer useful life, reducing costs per generated MW of power. Wind turbine structural control is therefore a essential issue of wind energy in its path to reduce cost and increase competitiveness.

In commercial WTs, the existent control systems have some structural control functions. Specifically, generator torque control is usually designed to damp tower side-side vibrations, and pitch control, besides limiting the power, damp tower fore-aft vibrations. However, there has been much research in this field, proposing new control methods, strategies and functions for the WT control systems, all with the objective of mitigating WT loads (see Chap. 2). In this way, the WT structural control seeks to be improved and extended, in order to obtain more profitable WTs.

Pitch control is the most used control system to attain structural control, since it modifies the blade pitch angles, thereby modifying all the WT dynamic response. Additionally, because it works in above rated winds, in full-load region, it deals with the operational condition in which the WT is subjected to the most severe loads, making the load reduction a very demanding requirement. Conventional pitch control relies on proportional-integral-derivative (PID) control, which regulates rotor speed to a constant

value, what causes the WT power to remain controlled (DNV, 2002; ABBAS; WRIGHT; PAO, 2020). The tower fore-aft damping is included as a simple proportional control. Research includes the use of individual pitch control (IPC) to mitigate tower and blade loads (CHEN; STOL, 2014a; SOLINGEN et al., 2015; HOU et al., 2019). In this type of pitch control, each blade receives independent pitch input to minimize asymmetrical loads. Further, the use of advanced control methods is very frequent in the literature. Intelligent and heuristic control is used with e.g. neural networks (POULTANGARI; SHAHNAZI; SHEIKHAN, 2012; ATA, 2015) and fuzzy logic (VAN et al., 2015). Frequency and time-domain control comprises H_∞ methods (NAVALKAR et al., 2014; TAKAHASHI et al., 2020), linear quadratic regulator (RITTEL, 2021), feedforward control (KOERBER; KING, 2013; FENG; SHENG, 2014), Fault-Tolerant Control (BADIHI; ZHANG, 2018), state-space methods (MENEZES et al., 2018) and Model Predictive Control (MPC) (JAIN et al., 2015; LIU; WU; KONG, 2019). In all these works, the objective of reducing wind turbine loads is the major concern.

1.4 Thesis objectives

Following the path outlined in the previous sections, and given the importance of WT structural dynamics and control for the advancement of wind energy, the objectives of the present thesis are:

- Review the literature concerning wind turbine structural control.
- Develop methods to analyze wind turbine structural dynamics, including a proprietary modeling tool.
- Develop wind turbine dynamics modeling to be used in control design.
- Control design of IPC, H_∞, and MPC pitch control systems in order to mitigate WT loads.
- Analyze the fatigue life of the WT considering the developed controls to proof their benefits.

1.5 Thesis structure

This work is organized as follows: Chapter 1 has described the introduction and the context of the subject. Chapter 2 contains the literature review concerning WT structural control. Chapter 3 presents WT structural dynamics modeling, including a discussion about the existent methods to carry out the analysis. Chapter 4 describes the development of a proprietary tool to model WT dynamics. Chapter 5 contains the WT model used for

control purposes and debates the control design process. Chapter 5 presents the results, including a fatigue life analysis. Chapter 6 concludes the thesis discussing the results.

2 LITERATURE REVIEW

2.1 Generalities about wind turbine control

Unlike other energy sources, the wind is not controllable. The wind flux is a strongly random process, variable both in time and in space. This variability leads to a complex conversion of energy, as WTs are subjected to a non-uniform and transient resource, variable mechanical loads and non-linear dynamics (LARSEN; NIELSEN, 2006). Control makes possible to cope with this variability and produce energy in a reliable and cost-effective manner.

The main objectives of the control systems embedded in a WT are maximize power production, mitigate dynamic as long as static mechanical loads and guarantee a continuous supply of energy to the grid, according to the utilities requirements (WANG et al., 2013). For achieving these goals, the WTs should have a supervisory control system, which manages turbine operation, and operational control systems dedicated to regulate turbine parameters to the desired set-points (LUBOSNY et al., 2007). The blade pitch angle, the yaw angle and the generator torque are major parameters to be controlled in a WT. The pitch angle is directly related to the blade‘s aerodynamic efficiency, and its control implies controlling the wind torque, enabling smooth power production and reduced mechanical loads. The generator torque control allows varying the WT rotor‘s speed following a Maximum Power Point Tracking (MPPT) strategy, for extracting as much as possible power from the wind. The yaw angle control is quite simple and aims to move the WT rotor into the wind's prevailing direction. The means of controlling these parameters depend on the current WT technology and have evolved from passive to active ones. One can distinguish WTs in variable-speed WT (VSWT) and fixed-speed WT (FSWT), as well as variable-pitch WT (VPWT) and fixed-pitch WT (FPWT). The early WTs were fixed-pitch and fixed-speed, which had no torque generator neither pitch angle control. The power regulation was achieved by passive means, namely the phenomenon of aerodynamic stall (MULJADI; PIERCE; MIGLIORE, 1998). Although the FSWT and FPWT still exist, almost all modern WTs are VSWT and VPWT (BURTON et al., 2011).Thus, the today‘s WTs usually have both pitch angle and generator torque control systems, as well as a yaw-angle control system. The last one has a too slower dynamics than the other control systems and so has not much interest for control engineers (JOHNSON et al., 2006).

Additionally, the WTs should have control of the power delivered to the grid, in order to accomplish a well-conditioned energy supply. It must be controlled to have reduced flicker, suitable voltage levels and little harmonics (YANG; TIAN, 2015). Furthermore,

Figure 4 – Wind turbine power curve

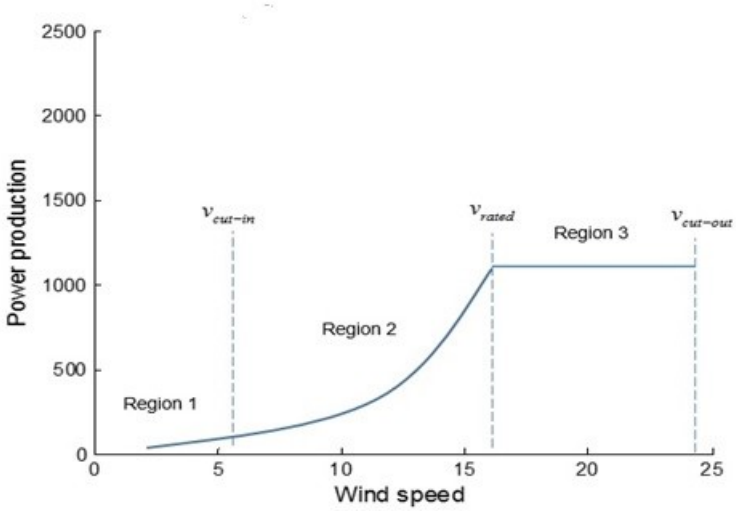

Source: Author (2022)

grid integration of WTs is a complex task due to the random nature of the wind, which can cause problems to grid frequency stability. In this aspect, the contribution of WT control systems for grid frequency regulation has been becoming a very important concern and a pulsating field of research, due to the increasing participation of wind power in grid power systems.

2.2 Control objectives and operational regions of WTs

The control objectives of WTs determine the moment of operation of each WT control system. The definition of control objectives is dependent on the wind turbine operational regions, shown in Fig. 4. These are closely related to the wind speed and one can identify three operational regions according to the wind speed (NJIRI; SöFFKER, 2016). In the so-called Region 1, below the cut-in wind speed, there is no production of electrical power, as the wind speed is too low and the produced power would not compensate the losses in the turbine operation. In this operational region, the turbine should be stopped or in idle mode. Region 2, between the cut-in and the rated wind speed, has an increasing power production as the wind increases progressively. In Region 2 the WT is in the partial-load regime. In Region 3, wind reaches rated speed and WT enters in full-load regime. Power production must be limited to the WT rated power, for ensuring operation within the safety limits of generator speed and WT mechanical loads. Some authors also identify a Region 2.5, where the WT rotor has achieved rated speed but the torque is still below its rated value (AHO; PAO; HAUSER, 2013). One can also consider

the additional Region 4, after the cut-out wind speed, where the WT must be switched off due to the very high wind regimes. The power extracted from the wind can be expressed according to Eq. 2.1 (ROHATGI; VAUGHN, 1994)

$$P_w = \frac{1}{2}\rho A C_p v^3 \tag{2.1}$$

where P_w is the power extracted from the wind, ρ is the air density, A is the rotor swept area, v is the wind speed and C_p is the so-called power coefficient, which depends on the pitch angle β and on the tip speed ratio λ. Tip speed ratio is defined by the relation between linear velocity on the tip blade and wind speed, according to Eq. 2.2

$$\lambda = \frac{\Omega R}{v} \tag{2.2}$$

where Ω is the rotor speed and R is the rotor radius. Field tests and simulations have shown that the power coefficient $C_p(\lambda, \beta)$ is maximum for a predetermined optimal pitch angle (β_{opt}) and optimal tip speed ratio (λ_{opt}), which are specific constants for each particular WT. When operating in Region 2 the WT rotor speed should be varied to maintain this optimal tip speed ratio as the wind changes its speed, for ensuring the maximum power production. The way the rotor speed is varied is the Maximum Power Point Tracking (MPPT) strategy. In Region 3, the control objective changes from maximizing to limiting power, as well as limiting rotor speed and torque. The generator torque is maintained constant at its rated value and the pitch angle should be controlled to reduce the power coefficient and aerodynamic efficiency. Thereby, constant rated power is extracted from the wind. One can summarize control objectives for the operational regions of WTs as follows:

- Regions 1 and 4: The WT should be out of operation, commanded by the supervisory control.
- Region 2: Maximize power production via MPPT strategies and generator torque control, which is the control system typically active in this region; the generator torque control should be a trade-off between generator torque actuation and optimal power production.
- Region 2.5: The rated speed should be maintained constant and the torque should be slightly increased until its rated value, ensuring a smooth transition between Regions 2 and 3.
- Region 3: Power production should be limited to the rated power via pitch control, which is the control system typically active in this region. Additionally, as the wind speed is above rated, the control objective of mechanical load reduction becomes important due to the high wind speeds that can damage the WT structure.

2.3 Structural control

2.3.1 Overview

In this section, the research works regarding wind turbine structural control are reviewed. It is worth noting that the focus here is in pitch control, since this is the main system responsible for load mitigation. A complete review regarding all the WT control systems can be found in (MENEZES; ARAúJO; SILVA, 2018).

Pitch control allows to change the pitch angle of WT's blades in order to control its aerodynamic efficiency. The pitch angle is a major WT parameter as it determines the flow angle of attack. Thus, turning the blades around their own axes changes the relative wind flow and consequently the aerodynamic loads exerted on the rotor. Moreover, the power coefficient $C_p(\lambda, \beta)$ varies according to the pitch angle and consequently the power capture varies as well. Therefore, pitch angle control has a twofold role: power regulation and load reduction. These are fundamental in operation on Region 3, where the power production must be limited to the rated one and the high wind speeds impose severe loads to WT structure and rotor (JOHNSON et al., 2011). Different concepts have been proposed along the years for power regulation and load reduction of WTs. The early WTs were controlled by passive means using the blades' aerodynamic characteristics. The airfoils were designed to stall when subjected to high wind regimes, which is called passive stall control. None additional actuator was necessary, thus a simple and low-cost power control was realized. However, the controllability was very limited as it was based on a natural stall phenomenon without any active control. In passive stall control, the WT is subjected to more power fluctuations, torque spikes and varying load effort.

For overcoming these drawbacks, modern WTs use active pitch control, with pitch actuators. In Region 3, the generator torque is usually imposed to be constant while the pitch control should be working to maintain constant rotor speed. While changing the pitch angle the control system is also changing the wind torque and accelerating or decelerating the turbine. As torque and speed are set to be constant, the power production is limited and mechanical loads are reduced, reaching the control objectives of Region 3. Typically, the pitch control loop uses only the rotor speed as feedback signal and the pitch commanded value is the same for the three blades. This is the so-called collective pitch control (CPC). A modern researched pitch control with the specific aim of load reduction is the method of individual pitch control (IPC). Both CPC and IPC techniques are reviewed in the following.

2.3.2 Collective Pitch Control

This is the traditional method of pitch control, which is largely implemented in commercial turbines (NJIRI; SöFFKER, 2016). The commanded pitch is sent collectively

for the blades, meaning that the same control action is taken in each one of them. Usually, CPC implementation relies on a simple PID (proportional-integral-derivative) control law, with rotor speed variation being the error signal for the closed-loop control. A systematic simulation-based procedure for selecting the PID control gains can be found in (HAND; BALAS, 2002). As the WT is a nonlinear system, applying a linear control law such as this simple PID requires linearization around an operating point. Different operational conditions degrade controller's performance and hence gain scheduling techniques can be necessary for improving efficiency. Such techniques are present in the literature (LI et al., 2015). Although PID control with gain scheduling is the classical CPC implementation, the constant pursuit for load reduction has motivated the rise of modern CPC approaches in many research works. Robust and adaptive methods are used to overcome modelling uncertainties. (FROST; BALAS; WRIGHT, 2009) develop adaptive pitch control with concerns to disturbance rejection. This work is followed by (FROST; BALAS; WRIGHT, 2009), where this adaptive controller is extended with a Residual Mode Filter (RMF) to avoid WT mode shapes be excited during operation, especially in turbulent conditions. On the other hand, nonlinear modelling is used in (BOUOUDEN et al., 2012), where fuzzy methods develop a T-S (Takagi-Sugeno) model for pitch control purposes. A hybrid Fuzzy-PI control is considered in (DUONG et al., 2014), where the focus is CPC to smooth power fluctuations. Controllers based on neural networks, although less present in the literature, can also be envisaged (NAJD; GOREL; HAMMOOD, 2020). CPC with fault tolerant control (FTC) has been researched for installations of hard maintenance, such as offshore WTs. Fault tolerant capability is essential to reduce WT downtimes and fault detection and FTC are pointed as critical research fields for the wind industry. In (MAZARE; TAGHIZADEH; GHAF-GHANBARI, 2021) the authors propose a FTC considering both actuator and sensor failures. Another approach is used by (LUZAR; WITCZAK, 2014). System identification is proceeded by neural network for assembling a Linear Parameter Varying (LPV) system, which allows handling system nonlinearities and develop an active fault tolerant controller. Promising field of research is predictive and feedforward CPC, due to the advances in LIDAR (Light Detection and Ranging) applications. LIDAR is a sensing technology used to remotely measure the wind speed based on laser diffraction. An early work considering feedforward-CPC has simulation proven significant load reductions, in order of 10% (HARRIS et al., 2006). Since them, many papers have demonstrated such benefits. (DUNNE et al., 2011) consider LIDAR measurements to design a feedforward controller using a non-causal series expansion for inverse-model control. Inverse-models aim on cancelling disturbances affecting controlled outputs. The proposed controller has performed better than baseline CPC feedback control. A more research conducted by (KOERBER; KING, 2013) suggests a Model Predictive Control (MPC) designed using LIDAR measurements as preview information. MPC is by definition a multivariable and constraint handling method. Authors use torque and pitch

as control signals and consider constraints on pitch rate. MPC allows an optimization procedure and the simulations show better performance than the traditional PID controller. Finally, field tests proving effectiveness of feedforward CPC can be found in (SCHLIPF et al., 2014).

2.3.3 Individual pitch control

IPC is the most recent development in pitch control, which has been intensively researched in the last years, but still not completely implemented in commercial WTs. It is expected to be largely applied in the next generation of turbines to shift WT's design for more and more larger and flexible blades (TANG et al., 2021). IPC is a technique frequently pointed in the literature as capable of reducing loads and fatigue damage (BOSSANYI, 2003; GEYLER; CASELITZ, 2007; PETROVIć; JELAVIć; BAOTIć, 2015). It makes the WT control system an inherently Multiple-Input-Multiple-Output (MIMO) system, since it requires individual pitch commands for each blade and the presence of additional sensors. These could be strain gauges or accelerometers enabling measuring of variables such as blade root moment or tower displacement. Based on the additional measures, the controller performs an additional control action that is individual to each blade. The aim is to adjust the pitch angle to reduce the blade root moment or damping structural modes. Individual pitch command works in a different frequency range from the collective pitch one. The pure CPC has the objective of regulating rotor speed while IPC envisages little adjustments in pitch angle for reducing stresses. Although simulations prove the benefits of using IPC, the field tests and practical implementation remain in course (SOLINGEN et al., 2015). In the point of view of hardware, the challenge remains about sensors reliability, as the modern WTs are already equipped with individual pitch actuators for each blade. Sensors installed at the blades would operate under harsh conditions and have difficult maintenance (EHLERS; DIOP; BINDNER, 2007). There is also a concern about the wear in individual pitch mechanisms due to the increased actuation cycle (JELAVIć; PETROVIć; PERIć, 2010). Despite these practical questions, IPC papers generally focus on control methods and this is a fertile research field. Early proposals of IPC relied on feedback control based on structural sensors (BOSSANYI, 2005). The most recent development consists in using LIDAR technology for feedforward control. The preview information about wind inflow provided by LIDAR allows the control system to act in advance to incoming wind events, as gusts or disturbances. (LAKS et al., 2011) compare feedforward IPC to the IPC feedback only, based on H_∞ techniques. Simulations results show reductions in damage equivalent loads (DEL), a standard measure of fatigue damage. A technical report from the U.S. National Renewable Energy Laboratory (NREL) deals with different LIDAR-based strategies for IPC, comparing preview time and LIDAR implementations (DUNNE, 2012). Feedforward strategies using MPC, which is a MIMO method in nature, are also very suitable for IPC. In an early study conducted

by (HENRIKSEN, 2007) a linear MPC controller is proposed, while (KUMAR; STOL, 2009) suggest a scheduling procedure, which allows improved performance due to the most refined tuning. LIDAR preview along with local inflow measurements are used to develop a more precise MPC controller in the work of (KRAGH; HANSEN, 2010). Short-term wind field predictions can also be used for MPC purposes and are considered in a the research of (SPENCER et al., 2013). At last, one can cite hybrid methods as the most recent advance in MPC pitch control, presented in (NAVALKAR et al., 2014). In this research, authors consider a repetitive control (RC), which is a modern 'learning' control technique, helped by MPC for constraint handling goals. Another focus of research is related to IPC applications in offshore WTs. Researchers have considered the possibility of using individual pitch to help in stabilization of proposed floating WT platforms. IPC based on disturbance accommodating control can be envisaged for barge and tension leg platforms (NAMIK; STOL, 2011) MPC is also a feasible alternative in offshore WTs, developed for reducing blade loads and yaw rolling of a barge platform (CHAABAN; FRITZEN, 2014). Besides offshore applications, studies of IPC effects on ultimate loads affecting the WT are present. In fact, the traditional IPC aims to mitigate fatigue loads, but it can also be profitable for reducing ultimate loads (BOTTASSO et al., 2014). Finally, confirming IPC as a future trend for larger WTs, the work of (CHEN; STOL, 2014b) and references therein, considers IPC performance in very large WTs with rating up to 15MW, through an upscaled model, obtaining good results. On the other hand, field tests in normal scale were performed by (BOSSANYI; FLEMING; WRIGHT, 2013) on NREL's experimental WT CART3 (3-bladed Control Advanced Research Turbine). The tests show once again an effective load reduction, as it was expected. The most recent field tests were carried out by (OSSMANN et al., 2021), where H_∞ control was tested in a multi-megawatt scale turbine of the University of Minnesota.

2.3.4 Selected control methods

The selected control methods to perform WT structural control in this thesis include: conventional PI control, state-space control, H_∞ control and Model Predictive Control. The conventional PI control will work as a baseline comparison. The other three controls will have the objective of mitigating wind turbine loads while maintaining correct wind turbine operation in Region 3. Therefore, these control methods use the pitch control system as the actuator. The methods were chosen based on the literature review, since they are advanced control algorithms capable of reducing WT loads in different conditions and have presented promising results. The objective here is to compare and analyze them regarding their benefits, especially the increase in fatigue life.

3 WIND TURBINE STRUCTURAL DYNAMICS

3.1 Methods for modeling wind turbine structural response

A mathematical model is the first step in any engineering analysis. It should be defined according to the user needs, since there is not a perfect model and there are different degrees of complexity (BOYCE; DIPRIMA, 2012). For understanding the wind turbine structural dynamics, the following models are possible (MANWELL; MCGOWAN; ROGERS, 2010):

- Finite-element method

  The finite-element method (FEM) is an ubiquitous technique in several fields of engineering. It consists in a method to solve differential equation which do not present simple or feasible analytic solution. The basic principle is to divide the physical domain in small parts (the 'elements') that are connected in points denominated 'nodes'. The fundamental physical equations are then established for each element using trial functions, often called shape functions. After establishing the mathematical relationships for each element, the individual contributions are summed over the entire domain, originating the FEM matrices. Then, conventional solution methods are used to solve the problem, such as Gauss-Elimination for matrices and Runge-Kutta method for the temporal solution. Even though the FEM is mainly used for structural problems, it can be applied to any kind of problem where differential equations are present. Therefore, despite less common, it is also used in heat transfer, fluid and even in electromagnetic problems.

- Lumped-parameter method

  This method is used to analyze simple systems where the components are well defined and isolated, and when distributed effects are not significant. In this case, the mass of each component can be supposed to be concentrated in certain points. Other parameters as stiffness and damping can also be considered lumped. For example, the drive train of a wind turbine in reality consists of a number of rotating components, such as the rotor itself, shafts, gears, and the generator rotor. In modeling a drive train it is common to characterize it as a few lumped inertias and stiffnesses (MANWELL; MCGOWAN; ROGERS, 2010).

- Modal analysis

The modal analysis is a method originated from the theory of vibrations. In that case, the dynamic behavior of the system was described by calculating the response for each vibration mode. By the principle of modal superposition, the overall dynamic response is obtained through summing of the vibration modes (BATHE, 2006). The structure is modeled in several degrees-of-freedoms (DOFs), and a vibration mode correspond to a particular movement shape of the DOFs. The number of DOFs depend on the degree of refinement of the analysis. The idea of modal analysis can be extended to any other mechanical problem that can be characterized by DOFs. This is precisely the case of how WTs are modeled, as it will be shown in the next sections.

- Multibody analysis

  At last, the final modeling technique which is worth noting is the multibody analysis. It consists in a modeling dedicated to systems which present relative movement between its components, and it is largely employed in the analysis of mechanisms. Multibody analysis considers the constraint equations that establish the connections amongst the elements of the system, and use these equations to describe the dynamics from the primary input to the system. It is very suitable for WT modeling, since the WT is a multibody system by nature.

3.2 Hybrid modal-multibody approach

In this thesis, the modeling chosen to the WT structural dynamics is a hybrid modal-multibody approach, using the WT simulation software FAST and OpenFAST. As discussed in the previous section, the multibody analysis works very well for wind turbine dynamics, allowing to model the relative movement between the several components of the WT, including the blades, hub, generator/drive-train, nacelle, and tower. However, in order to get a more precise modeling, it is essential to analyze the behavior within these components. One approach would be model the entire WT by using finite-elements. Given the large size and complexity involved, this would have an elevated computational burden. Indeed, FEM is more utilised in WT analysis to model specific components, such as the blades (WANG et al., 2016; NOEVER-CASTELOS; MELCHER; BALZANI, 2022) and the tower (TOMCZAK, 2021). One possible solution is to use modal analysis to model the flexible components, focusing in the first vibration modes. Thus, a finite-element approach can be used to find the vibration modes of the tower and the blades. Limiting the analysis to the first two modes, the structural dynamics can be parameterized in terms of the multibody analysis, considering the flexible tower and blades as bodies with limited degrees-of-freedom.

This is precisely the approach taken here. The wind turbine is modeled considering until 22 DOFs:

- Platform translation and rotation (6 DOFs)
- Tower flexibility in the fore-aft and side-side directions, with 2 flexible modes in each direction (4 DOFs)
- Nacelle yaw (1 DOF)
- Variable generator speed (1 DOF)
- Drive-train transmission (1 DOF)
- Blade flexibility, with 2 flexible modes in flap direction and 1 flexible mode in edge direction (9 DOFs, considering a 3-bladed turbine and a total of 3 DOFs per blade)

To implement the above modeling, it is necessary to define several reference frames or coordinate systems, in which the DOFs will be defined. The primary reference frame is the inertial reference, attached to the Earth (E). In this reference, the WT defined DOFs are the movements of sway, heave and surge (translations) and roll, pitch and yaw (rotations). These are used for offshore WTs, but they can also model onshore foundations. The second coordinate system is shown in the WT of Fig. 5. It is attached to the tower base and translates and rotates with the platform. In this coordinate system, the DOFs of tower fore-aft (aligned with x-axis) and tower side-side (aligned with y-axis) are defined. The third coordinate system is shown in Fig. 6 and it is fixed to the tower top. It translates

Figure 5 – Tower base wind turbine coordinate system

Source: (JONKMAN; JR., 2005)

and rotates with the platform, and bends with the tower bending in both fore-aft and side-side directions. None DOF is defined in this system, but it is necessary for the overall modeling. The fourth coordinate system is coincident with the previous one, but it yaws

Figure 6 – Tower top coordinate system

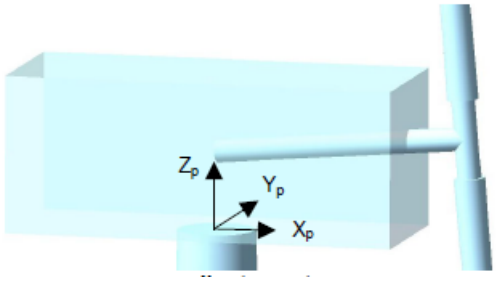

Source: (JONKMAN; JR., 2005)

Figure 7 – Nacelle yaw system

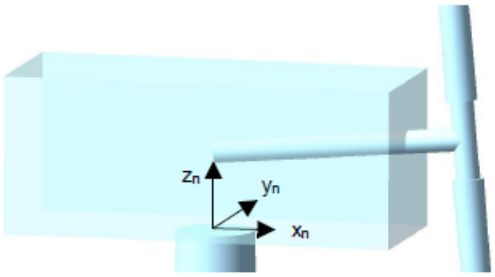

Source: (JONKMAN; JR., 2005)

with the nacelle, with coordinates x_n, y_n and z_n, as shown in Fig. 7. The DOF of nacelle yaw angle is defined in this system. The next two coordinate systems are the shaft and azimuth references, and have all the movement of the previous ones. However, they are located at the WT rotation axis. The shaft coordinate system is located at the shaft origin, considering the angle of shaft tilt. The azimuth coordinate system is located at the same spot, but it does rotate with the rotor. They are shown overlapped in Fig. 8 and involve the definition of the generator azimuth DOF and of the drive train torsion DOF. In the

Figure 8 – Shaft and azimuth coordinate systems

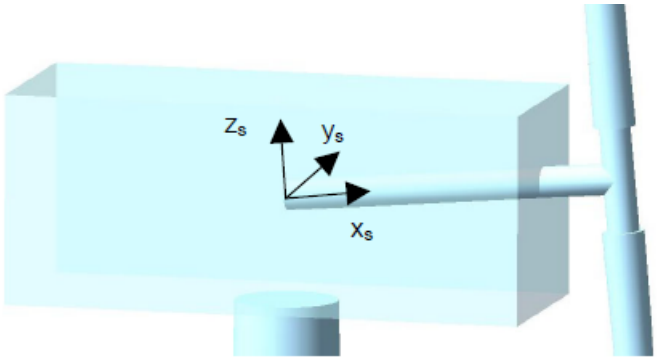

Source: (JONKMAN; JR., 2005)

following, we have the coned coordinate system, which is located at the hub taking into account the pre-cone angle of the blades. Finally, the last coordinate systems are fixed at

Figure 9 – Coned coordinate system (left) and blade coordinate systems (right)

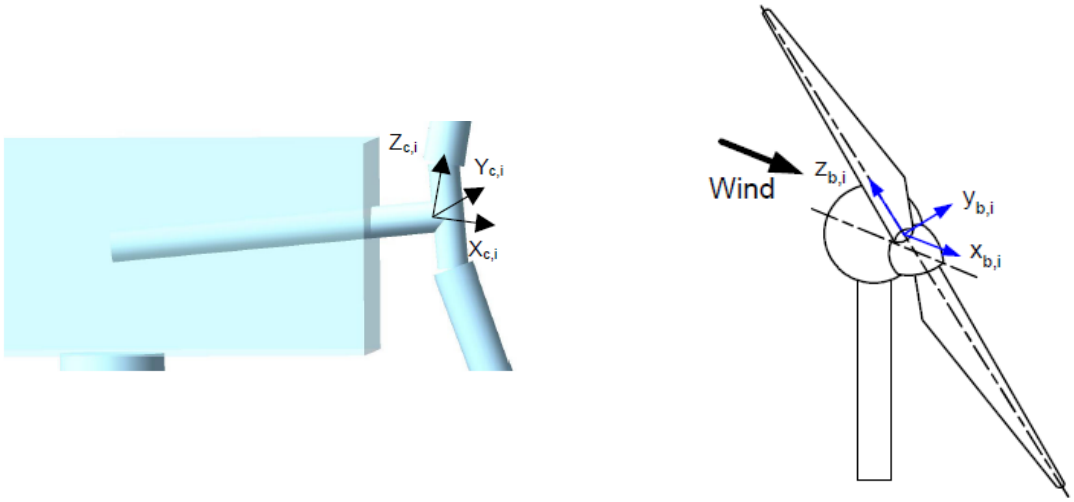

Source: (JONKMAN; JR, 2005)

the blades themselves and they are located at the blade roots; in these systems, the DOFs of flap (aligned with the x-axis) and edge (aligned with the y-axis) are defined. The last coordinate systems are shown side by side in Fig. 9.

The mounting of the equations of motion begins with the setting of the position vector for each important component, which should be defined recursively. The first position vector is of the platform reference point Z, defined in the inertial frame $z1 - z2 - z3$:

$$r_Z = q_{Sg} z_1 + q_{Hv} z_2 + q_{Sw} z_3 \tag{3.1}$$

where q_{Sg}, q_{Hv}, q_{Sw} are the DOFs of surge, heave and sway, respectively. The next relevant position vectors are the platform mass center point Y and a tower point T, defined with respect to the already defined Z:

$$r_{ZY} = P_{CM} z_t \tag{3.2}$$

$$r_{ZT} = (\phi_1^{TFA}(h) q_{TFA1} + \phi_2^{TFA}(h) q_{TFA2}) x_t + (\phi_1^{TSS}(h) q_{TSS1} + \phi_2^{TSS}(h) q_{TSS2}) y_t \tag{3.3}$$

where P_{CM} is the position of platform mass center, q_{TFA1} is the first tower fore-aft DOF, q_{TFA2} is the second tower fore-aft DOF, q_{TSS1} is the first tower side-side DOF, q_{SS2} is the second tower side-side DOF. both in fore-aft and side-side directions. The $\phi_{i's}$ are the mode shapes of the tower, which should be obtained separately considering the structural characteristics of the tower (see Chap. 4 for more details). The next two points are defined from the tower top T_{top} until the hub mass center C and from C to the apex of the coning angle:

$$r_{T_{top}C} = C_x x_s + C_y y_s + C_z z_s \tag{3.4}$$

$$r_{CQ} = (Q_x) x_c \tag{3.5}$$

The vector of the blades position are defined in the blades system for a generic point S in the blade, established relative to the apex coning point:

$$r_{QS} = (\phi_1^{BF1}(r)q_{BF1} + \phi_2^{BF2}(r)q_{BF2})x_b + (\phi_3^{BE}(r)q_{BE})y_b \tag{3.6}$$

where q_{BF1} is the first blade flap DOF, q_{BF2} is the second blade flap DOF, q_{BE} is the blade edge DOF, all of them defined in the blade coordinate system. The $\phi_{i's}$ are the mode shapes of the tower, which should be obtained separately considering the structural characteristics of the blade.

The previous established equations determine the WT kinematics. In order to get the WT kinetics, we need to apply the balance of forces. An approach to simplify the number of equations and obtain the overall dynamics is based on the Kane's method (KANE; LEVINSON, 1985), which consider the concept of generalized active forces F_i and generalized inertia forces F_i^*, for each DOF i:

$$F_i + F_i^* = 0 \qquad (i = 1, 2, ..22) \tag{3.7}$$

The generalized active and inertia forces are obtained by taking the dot product between forces and moments with the respective velocities. Kane's dynamic is, in practice, an alternative to Lagrange multipliers. Therefore,

$$F_i = \sum_{i=1}^{22} {}^E v_r{}^{X_j} \cdot F^{X_j} + {}^E \omega_r{}^{X_j} \cdot M^{X_j} \tag{3.8}$$

$$F_i^* = \sum_{i=1}^{22} {}^E v_r{}^{X_j} \cdot -m_j \, {}^E a^{X_j} + - {}^E \omega_r{}^{X_j} \cdot \dot{H}^{X_j} \tag{3.9}$$

where the linear and angular velocities are written in terms of the DOFs, using the defined coordinate systems. Active forces involve the wind and water (for offshore WTs) external forces and the internal structural damping and stiffness forces. After executing the dot products, considering the velocities as the derivative of the position vectors deduced in the previous section, the WT equations of motion reduce to a matrix equation:

$$M(q, t) = f(\dot{q}, q, t) \tag{3.10}$$

where M is the generalized mass matrix and f is the generalized force matrix. After the mounting of Eq.3.10, time-domain solution techniques can be used to solve for the several DOFs.

3.2.1 OpenFAST software

The OpenFAST software is a tool of WT simulation which has evolved from the ancient FAST developed by the National Renewable Energy Laboratory (NREL). It fits in the broader category of WT simulation softwares, along with the GH Bladed, HAWC2,

Flex5, and Simpack (ABBAS et al., 2022). These programs incorporate sophisticated models of both turbulent- and deterministic-wind inflow; aerodynamic, gravitational, and inertial loading of the rotor, nacelle, and tower; elastic effects within and between components and in the foundation; and mechanical actuation and electrical responses of the generator and of the control and protection systems (JONKMAN, 2007). OpenFAST utilizes the modal-multibody approach developed in this chapter and thus it is the chosen software to simulate the WTs in this thesis. Additionally, it includes an embedded aerodynamic model through AeroDyn (NING et al., 2015), which will allow to simulate the aerodynamic loads input to the turbine.

3.2.2 Chosen turbine model

The chosen WT model to be simulated in this work needs to be representative of current installed wind turbines and yet have the data disclosed, such as structural tower and blade properties and airfoil characteristics. The NREL 5 MW reference wind turbine meets these requirements and has a size and rating compatible with the commercial WTs today, even though it is a little above in terms of power and dimensions. This WT model is widely used in the academia, since the majority of WT designs are not disclosed and are protected by industrial confidentiality. It is worth noting that other Reference Wind Turbines (RWTs) exist, even though NREL 5 MW RWT is the most widespread. See for example the RWTs documented in (BAK et al., 2013) and (RINKER; DYKES, 2018). The main characteristics of NREL 5 MW RWT are described in Table 1

Table 1 – NREL 5MW turbine general characteristics

NREL 5 MW RWT	
Rating	5 MW
Rotor orientation, configuration	Upwind, 3 blades
Control	Variable speed, variable pitch
Rotor diameter	126 m
Tower height	90 m
Cut-in, rated, cut-out wind speed	3 m/s, 11.4 m/s, 25 m/s
Rated rotor speed	12.1 rpm

Source: Author (2022)

4 FINITE-ELEMENT MODELING

4.1 Finite-elements and the modal-multibody approach

In the previous chapter, we have developed a dynamics modeling approach to cope with the WT structural dynamics in a suitable level of precision and computational burden, considering the trade-off between them. However, it was emphasized that in the modal-multibody approach it was necessary to model the first flexible modes of the tower and the blades. This can be done using finite-elements in order to introduce the finite element method in our modeling. Since this calculation of flexible modes is running at once (off-line), it does not introduce excessive computation load, even though it increases the precision of the model. The flexible mode shapes are given as inputs to the modal-multibody equations, which consider them by means of the tower and blades DOFs. Indeed, the positions of the whole tower and blades are determined making the product between the tower top DOFs or blade tip DOFs by the input mode shapes. OpenFAST uses a separate tool, Modes, to calculate the mode shapes. The objective here is to develop our own modeling tool to calculate the tower and blades mode shapes, using the finite element method.

4.2 Finite Element Method

Finite element method (FEM) is an important and frequently indispensable part of engineering analysis and design. Finite element computer programs are widely used in practically all branches of engineering for the analysis of structures, solids, and fluids (KOUTROMANOS, 2018). FEM consists in a numerical method to solve differential equations that do not have analytical solution in a simple or feasible way. It is based in the discretization of the physical domain in individual elements and nodes, for which the fundamental physical equations are established, using interpolation functions to determine the physical variables within each element. The individual elements equations are then assembled in global matrices considering the contribution of each element. These are solved using traditional numerical and integration techniques in terms of each node variable. The solution for every point of the original domain is obtained through the nodes solution and the used interpolation functions. Due to this procedure, the FEM is especially well suited for structural analysis. An example of application of FEM analysis is shown in Fig. , with gradient colors representing the field of stresses. Given a general system modeled using a differential formulation such as the one in Eq. 4.1

$$L(\phi) = f \tag{4.1}$$

where L is a differential operator and f the forcing function, the FEM formulation is constructed using the physical modeling expressed as the minimization of a given functional Π,

$$\delta\Pi = 0 \tag{4.2}$$

where Π is obtained by integration of Eq. 4.1. The basic step in the finite element procedures is to assume a solution of the form

$$\overline{\phi} = \sum_{i=1}^{n} a_i \psi_i \tag{4.3}$$

where f_i are the interpolation functions and a_i the node coefficients to be determined. The assumed solution $\overline{\phi}$ is then substituted in Eq. 4.2 according to the Galerkin method, in which the residuals are weighted over the solution domain. The residual is calculated as the difference between the approximated solution and the exact solution, so that $R = f - L(\overline{\phi})$. The assumed solution is defined within each element, and each ψ_i constitutes what is called a shape function. The application of Galerkin method to Eqs. 4.1-4.2 results in

$$\int_D \psi_i R dD = 0, i = 1, 2...n \tag{4.4}$$

where D is the solution domain and n is the number of interpolation functions or nodes. This is the general formulation of the finite element method and it is valid to all physical domains.

4.3 Finite element method applied to structural analysis

One of the most common applications of FEM is related to structural analysis. Indeed, the finite element procedures were developed originally to cope with structural calculations. Using the general formulation developed in the previous section, it is possible to bring the FEM procedures to the structural context through the following standard guidelines to run FEM structural analysis:

1. Idealize the total structure as an assemblage of individual elements interconnected at structure points denominated ‘nodes’
2. Choose shape functions defined within each element that are suitable to describe the structure behavior and the problem complexity
3. Calculate the contribution of each element using the shape functions and the fundamental physical relationships (balance of forces)
4. Execute the sum of the contributions of each element, obtaining global mass, damping, and stiffness matrices. Further, consider the external applied forces and boundary conditions

5. Solving the resulting equation system and obtain the solution at each structural node

It is important to emphasize that the choice of the elements and shape functions are critical decisions in the finite element analysis. Nowadays, there is a large amount of available elements and shape functions developed and implemented in commercial FEM softwares. In this work, the objective is to use the FEM to model the structural response of the wind turbine and obtain the mode shapes needed by OpenFAST using a proprietary software developed by the author. In order to do this, the wind turbine tower and blades are modeled as cantilevered beams, assuming the Bernoulli beam theory. Accordingly, beam elements with 3 degrees-of-freedom are used to model the dynamic wind turbine behavior. The first step in the FEM analysis carried out here is to model the dynamic equations of the Bernoulli beam. Next, the finite element modeling is executed and the FEM equations are developed. Finally, the dynamic equations are solved and the results are presented and compared to other modeling solutions.

4.3.1 Bernoulli beam dynamic equations

The objective here is to perform a dynamic analysis of Bernoulli beam, under bending and axial loads. These constitute the main wind turbine drivers, since torsional loading is less significant. In order to do this, the problem is divided into axial modeling and bending modeling. Further, the basic Bernoulli assumption that the plane sections remain plane after deformation is considered.

For the axial modeling, be $N(x)$ the axial force resulting from axial deformation in each beam section and q_x a distributed axial force. Considering the balance of forces in the x-direction,

$$\sum F_x = 0 \Rightarrow N(x+\Delta x) - N(x) + \int_x^{x+\Delta x} q_x(\eta) d\eta \tag{4.5}$$

Taking the limit when $\Delta x = 0$,

$$\frac{dN}{dx} + q_x(x) = 0 \tag{4.6}$$

Considering that $N(x)$ is given by the Hooke constitutive law as a function of the axial displacement u,

$$N(x) = \int_{A(x)} \sigma_{xx} dA = EA\frac{du}{dx} \tag{4.7}$$

substituting in Eq. 4.6, it is possible to get

$$\frac{d}{dx}\left(EA\frac{du}{dx}\right) + q_x(x) = 0 \tag{4.8}$$

This completes the modeling for the static axial case. However, the dynamic modeling is wanted. For this, the fundamental law of dynamics is written in terms of the density $\rho(x)$

and the area $A(x)$, where F is the resulting force, as in

$$F(x) = \rho(x)A(x)\ddot{u}(x,t) \tag{4.9}$$

$F(x)$ is composed by the previous defined q_x and $N(x)$. For the dynamic analysis, q_x must be calculated in two parcels: the external distributed applied force and the damping force, related to the damping coefficient $C(x)$ and the displacement first derivative $\dot{u}(x,t)$. Therefore,

$$q_x = q_{0x} + \frac{d}{dx}\left(CA\frac{d\dot{u}(x,t)}{dx}\right) \tag{4.10}$$

Combining Eqs. 4.8-4.10, the final form of axial modeling is

$$-\frac{d}{dx}\left(EA\frac{du(x,t)}{dx}\right) - \frac{d}{dx}\left(CA\frac{d\dot{u}(x,t)}{dx}\right) + \rho(x)A(x)u(x,t) = q_{0x} \tag{4.11}$$

For the transversal modeling, be $V(x)$ the shear force at an arbitrary section and $M(x)$ the bending moment. Considering the balance of forces in the y-direction,

$$\sum F_y = 0 \Rightarrow V(x+\Delta x) - V(x) + \int_x^{x+\Delta x} q_y(\eta)d\eta \tag{4.12}$$

Taking the limit when $\Delta x = 0$,

$$\frac{dV}{dx} + q_y(x) = 0 \tag{4.13}$$

At this point, it must be observed that the shear force is obtained by the derivative of the bending moment:

$$V(x) = -\frac{dM}{dx} \tag{4.14}$$

and that the bending moment can be calculated, according to the beam theory, using the angle of deflection θ and the transversal displacement $v(x)$, through the following relationships:

$$\theta = \frac{dv}{dx}; M = EI\frac{d\theta}{dx} = EI\frac{d^2v}{dx^2} \tag{4.15}$$

Substituting in Eq. 4.13,

$$-\frac{d^2}{dx^2}\left(EI\frac{d^2v}{dx^2}\right) + q_y(x) = 0 \tag{4.16}$$

This concludes the static case. For the dynamic analysis, analogously to the axial modeling, it is needed to include the inertia and the damping terms, resulting in the final equation form:

$$\frac{d^2}{dx^2}\left(EI\frac{d^2v(x,t)}{dx^2}\right) + \frac{d^2}{dx^2}\left(CI\frac{d^2\dot{v}(x,t)}{dx^2}\right) + \rho(x)A(x)\ddot{v}(x,t) = q_{0y} \tag{4.17}$$

4.3.2 Assemblage of the finite element equations

In order to obtain the finite element equations that will be solved, the developed dynamic beam equations must undergo the application of Galerkin method, doing the

integration over the domain weighted by the shape functions. For the cases axial and transversal, this results in

$$\int_0^L \rho(x)A(x)f_i\ddot{u}dx + \int_0^L EA\frac{df_i}{dx}\frac{du}{dx} + CA\frac{df_i}{dx}\frac{d\dot{u}}{dx}dx = \int_0^L q_{0x}f_i dx$$
$$\int_0^L \rho(x)A(x)f_i\ddot{v}dx + \int_0^L EI\frac{d^2f_i}{dx^2}\frac{d^2v}{dx^2} + CI\frac{d^2f_i}{dx^2}\frac{d^2\dot{v}}{dx^2}dx = \int_0^L q_{0y}f_i dx \tag{4.18}$$

where L is the beam length and, by simplicity, the Neumann and mixed boundary conditions were omitted. These will be included as concentrated loads or displacements in the finite element matrices. Additionally, abuse of notation allows to use f_i as the shape function symbol for both cases and substitute $u(x,t)$ and $v(x,t)$ by u and v.

The mesh construction, corresponding to beam analysis, is carried out by rectangular elements obtained by the division of the beam length in equal parts. For the shape functions, they are defined within each element, being zero outside it. Also, they are related to node displacements. For the axial case, the shape functions are two linear functions for each element, corresponding to one function per node. Therefore, the assumed solution within a generic element between nodes i and j is

$$\phi(x) = u_i\frac{x_i - x}{x_i - x_j} + u_j\frac{x_j - x}{x_j - x_i} \tag{4.19}$$

where x is the axial coordinate along the beam and x_i, x_j are the coordinates of nodes i and j. For the transversal case, each node have two degrees-of-freedom. Thus, a polynomial function of order 3, containing 4 constants, is chosen as the assumed solution

$$\phi(x) = a_0 + a_1x + a_2x^2 + a_3x^3 \tag{4.20}$$

in which a_0, a_1, a_2 and a_3 are determined in order to have

$$\begin{aligned} \phi(x_i) = v_i \quad \phi(x_j) = v_j \\ \phi_i'(x_i) = \theta_i \quad \phi'(x_j) = \theta_j \end{aligned} \tag{4.21}$$

where v_i, θ_i, v_j and θ_j are the transversal displacement and deflection for nodes i and j.

The substitution of these assumed solutions and shape functions in Eq. 4.18, with the appropriate mathematical procedures, will result in the finite element matrices. Establishing h_e as the generic element length, the following matrices are obtained

- Axial case

$$M_e = \frac{\rho A h_e}{6}\begin{bmatrix} 2 & 1 \\ 1 & 2 \end{bmatrix}$$

$$C_e = \frac{CA}{h_e}\begin{bmatrix} 1 & -1 \\ -1 & 1 \end{bmatrix}$$
$$K_e = \frac{EA}{h_e}\begin{bmatrix} 1 & -1 \\ -1 & 1 \end{bmatrix}$$
$$F_e = \frac{q_{0x} h_e}{2}\begin{bmatrix} 1 \\ 1 \end{bmatrix} \tag{4.22}$$

- Transversal case

$$M_e = \frac{\rho A h_e}{420}\begin{bmatrix} 156h_e & 22h_e & 54 & -13h_e \\ 22h_e & 4h_e^2 & 13h_e & -3h_e^2 \\ 54 & 13h_e & 156 & -22h_e \\ -13h_e & -3h_e^2 & -22h_e & 4h_e^2 \end{bmatrix}$$

$$C_e = \begin{bmatrix} 12 & 6h_e & -12 & 6h_e \\ 6h_e & 4h_e^2 & -6h_e & 2h_e^2 \\ -12 & -6h_e & 12 & -6h_e \\ 6h_e & 2h_e^2 & -6h_e & 4h_e^2 \end{bmatrix}$$

$$K_e = \frac{EI}{h_e^3}\begin{bmatrix} 12 & 6h_e & -12 & 6h_e \\ 6h_e & 4h_e^2 & -6h_e & 2h_e^2 \\ -12 & -6h_e & 12 & -6h_e \\ 6h_e & 2h_e^2 & -6h_e & 4h_e^2 \end{bmatrix}$$

$$F_e = \frac{q_{0y}}{12}\begin{bmatrix} 6h_e \\ h_e^2 \\ 6h_e \\ -h_e^2 \end{bmatrix} \tag{4.23}$$

These are element matrices, which need to be assembled together to form the global structural matrices. The assemblage is carried out according to the position of each element in the mesh. For the rectangular elements considered, the mounting of global matrices is executed through the following rules:

$$\begin{bmatrix} G(i,i) & G(i,j) \\ G(j,i) & G(j,j) \end{bmatrix} = \begin{bmatrix} G_{e_{ij}}(1,1) & G_{e_{ij}}(1,2) \\ G_{e_{ij}}(2,1) & G_{e_{ij}}(2,2) \end{bmatrix} \tag{4.24}$$

where G is a generic matrix (M, C, or K).

4.3.3 Structure of the program

Using the above established equations, a finite-element computer program was developed to determine WT mode shapes. The program was written in MATLAB language and the source codes are in the Appendix. The logic structure is as presented below:

- Main.m: The main program, containing the matrices assemblies, the temporal solution (using Newmark method) and the calculation of eigenvalues and eigenvectors.
- Parametros.m: Contains the user definitions about the analyzed structure, in our case, the tower length, density, structural damping and stiffness, points of application of concentrated loads and points of boundary conditions (in our case, these conditions reflect a cantilevered beam).
- Malha.m: Contains the definition of the mesh, determining the number of elements and the connection nodes.
- momI.m, area.m, elast.m, amort.m, rho.m: These are functions which allow the user to define variations of the key structural parameters (inertia moment, area, elasticity (stiffness) coefficient, damping coefficient and density), over the beam length

4.4 Results

In this section, we will test the developed program to verify its correctness.

- Case 1: Axial loading, cantilevered beam. $F = 100N$ at the beam end, without distributed force.

  Initial conditions: $u(x,0)$=0 and $\dot{u}(x,0) = 0$

  Boundary conditions: $u(0,t) = 0$ and $EA\frac{du}{dx}(L,t) = 100N$

  Structural and geometric parameters: $L = 1m$, $A = 0.1m^2$, $I = 8.33.10^{-4}m^4$, $E = 200.10^5Pa$, $\rho = 10000kg/m^3$, $C = 100kNm/s$

  Mesh: 8 rectangular elements

  Exact solution: The axial displacement at the beam end shall converge for $u(L,t) = \frac{PL}{EA} = 5.10^{-5}m$.

  Solution: The solution is shown in Fig. 10, where one can see the value converges to the expected $5.10^{-5}m$.

Figure 10 – Axial displacement, flexible beam

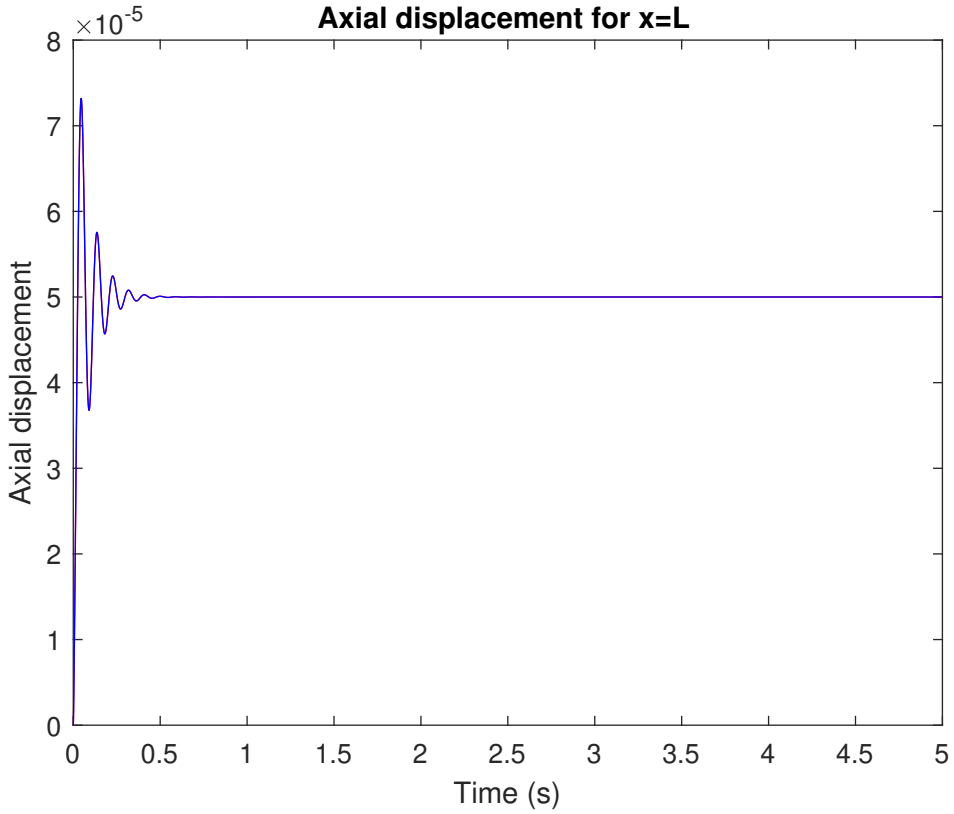

Source: Author (2022)

- Case 2: Transversal loading, cantilevered beam. $F = 100N$ at the beam end, without distributed force.

  Initial conditions: $v(x,0)$=0 and $\dot{v}(x,0) = 0$

  Boundary conditions: $v(0,t) = 0$ and $-\frac{dM}{dx}(L,t) = 100N$

  Structural and geometric parameters: $L = 1m$, $A = 0.1m^2$, $I = 8.33.10^{-4}m^4$, $E = 200.10^5 Pa$, $\rho = 10000kg/m^3$, $C = 50kNm/s$

  Mesh: 8 rectangular elements

  Exact solution: The axial displacement at the beam end shall converge for $u(L,t) = \frac{PL^3}{EI} = 0.002m$.

  Solution: The solution is shown in Fig. 11, where one can see the value converges to the expected $0.002m$. It is important to emphasize that the speed of convergence is lower than the axial case, due to the inferior damping coefficient.

- Case 3: Comparing the calculation of mode shapes using the program with exact mode shapes calculated analytically.

  Given the Eq. 4.17, to obtain the mode shapes in analytical form, one must consider

Figure 11 – Transversal displacement, flexible beam

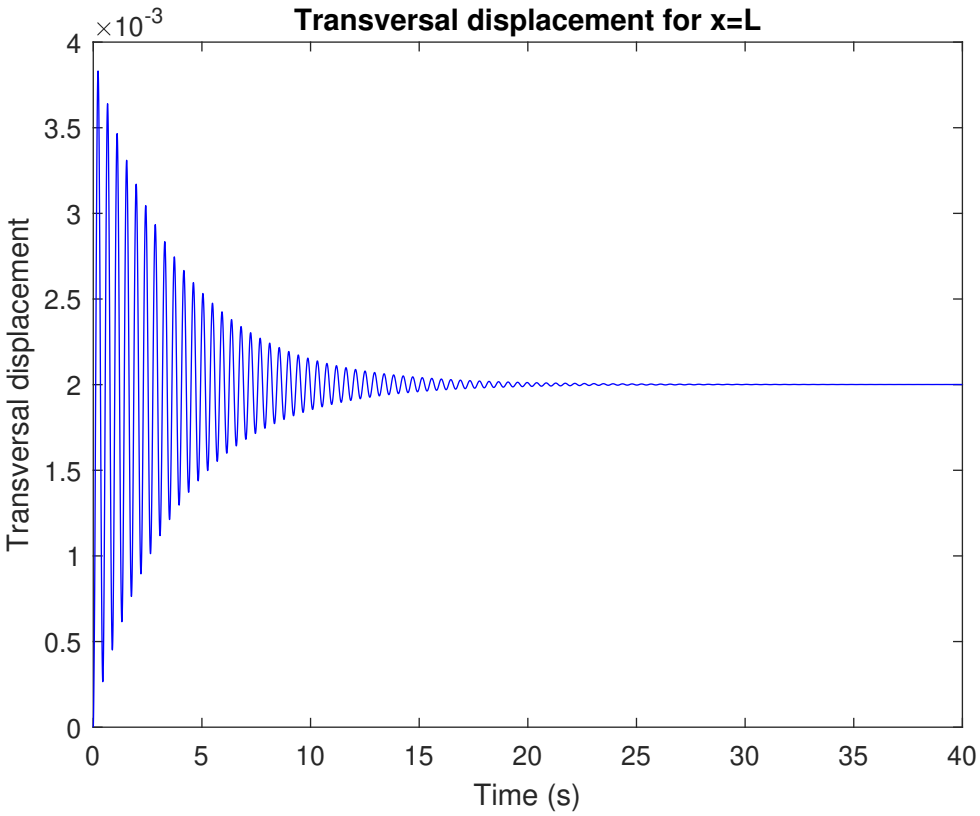

Source: Author (2022)

the damping-free equation and external force equals to zero, getting:

$$EI\frac{d^4}{dx^4}v(x,t) + \rho(x)A(x)\ddot{v}(x,t) = 0 \tag{4.25}$$

Assuming the harmonic solution is given by

$$v(x,t) = V(x)\cos(\omega t - \theta) \tag{4.26}$$

Substituting Eq. 4.26 in Eq. 4.25,

$$\frac{d^4V}{dx^4} - \lambda^4 W = 0 \tag{4.27}$$

$$(\lambda L)^4 = \frac{\rho A\omega^2 L^4}{EI} \tag{4.28}$$

The analytical solution for the above equation can be found as:

$$V(x) = C_1 sinh(\lambda x) + C_2 sinh(\lambda x) + C_3 sinh(\lambda x) + C_4 sinh(\lambda x) \tag{4.29}$$

Imposing the boundary conditions of a cantilevered beam, the solution constants can be found from the system:

$$\begin{bmatrix} 0 & 1 & 0 & 1 \\ \lambda & 0 & \lambda & 0 \\ \lambda^2 sinh(\lambda L) & \lambda^2 cosh(\lambda L) & -\lambda^2 sinh(\lambda L) & -\lambda^2 cosh(\lambda L) \\ \lambda^3 cosh(\lambda L) & \lambda^3 sinh(\lambda L) & -\lambda^3 cosh(\lambda L) & -\lambda^3 sinh(\lambda L) \end{bmatrix} \cdot \begin{bmatrix} C_1 \\ C_2 \\ C_3 \\ C_4 \end{bmatrix} = \begin{bmatrix} 0 \\ 0 \\ 0 \\ 0 \end{bmatrix} \tag{4.30}$$

In order to the above system have solution, we need the determinant of the coefficients matrix to be zero, what leads us to:

$$cos(\lambda L)cosh(\lambda L) + 1 = 0 \tag{4.31}$$

The solutions of this equation can be calculated as:

$$\lambda_1 L = 1.875 \tag{4.32}$$

$$\lambda_2 L = 4.694 \tag{4.33}$$

$$\lambda_3 L = 7.854 \tag{4.34}$$

$$\lambda_4 L = 10.995 \tag{4.35}$$

With the obtained values, it is possible to calculate the natural frequencies and the mode shapes, substituting in Eqs. 4.28-4.29. Finally, for verification of the finite-element program, one can consider a beam with the following characteristics (STRESSER, 2021):

Table 2 – Characteristics of the verified beam

Length	2m
Width	0.1m
Thickness	0.03m
Density	7850kg/m
Elasticity modulus	200 GPa

Source: Author (2022)

In this case, applying the finite-element method and the analytical solution, it is possible to obtain the same results. For increasing precision, this time 20 elements are used. The analytical and computational results are presented side by side in Table 3.

As remains clear from the previous table, the FEM developed program provides accurate results.

4.5 Conclusions

In this chapter, a finite-element modeling for the WT structural dynamics was developed. As a result, a finite-element program has been developed and validated against

Table 3 – Comparison between analytical and FEM solutions

Analytical solution	FEM solution
6.1154 Hz	6.1154 Hz
38.3243 Hz	38.3244 Hz
107.3091 Hz	107.3108 Hz

Source: Author (2022)

analytical solutions. This program allows to obtain the vibration characteristics of the tower and the blades, which can be input in the modal-multibody approach of Chapter 3.

5 WIND TURBINE CONTROLLERS

5.1 Introduction

In this chapter, the objective is to develop several wind turbine controllers and verify their benefits, in terms of reduction of vibration loads of the WT. Following the path consolidated in the previous chapters, the aim is to develop a pitch control system, which should control rotor speed (and thus power) in the Region 3 operation of the turbine. The turbine is modeled using a modal-multibody approach, and from the obtained models, control systems are designed. Following that, both steady and turbulent simulations are carried out to verify the control performance. Simulations are run using OpenFAST to implement the modal-multibody model and Simulink to implement the developed controls.

The control systems developed here include the traditional PID control, which will serve as a baseline comparison, state-space controllers (MENEZES et al., 2018), H_∞ and model predictive controllers.

5.2 Classical PID control

The PID control is the most widespread control method, in all industrial fields (GOLNARAGHI; KUO, 2017). It is very appreciated by its simplicity and effectiveness, with the control law given by:

$$u(t) = K_p e(t) + K_i \int_0^t e(\tau)d\tau + K_d \frac{de(t)}{dt} \tag{5.1}$$

where $e = r - y$ is the error signal between the reference (r) and the output (y). K_p, K_i, K_d are the proportional, integral and derivative gains, respectively.

5.3 State-space control

The state-space control is used here through the technique of full-state feedback. It is used to determine the location of all system closed-loop poles and so determine its dynamic response. Due to this, the method is also called control by pole placement. A state-space system is modeled according to Eq. 5.2, reproduced below:

$$\begin{aligned} \dot{\mathbf{x}} &= \mathbf{A}\mathbf{x} + \mathbf{B}\mathbf{u} + \mathbf{B_d}\mathbf{u_d} \\ \mathbf{y} &= \mathbf{C}\mathbf{x} + \mathbf{D}\mathbf{u} \end{aligned} \tag{5.2}$$

where $\mathbf{A}$ is called the state matrix, $\mathbf{B}$ is the control matrix, $\mathbf{B_d}$ is the disturbance matrix, $\mathbf{C}$ is the output matrix $\mathbf{D}$ is the direct transmission matrix, and $\mathbf{D_d}$ is the direct transmission

disturbance matrix. The state vector is represented by $\mathbf{x}$ and the output vector by $\mathbf{y}$. The dynamic response of this system is determined by its closed-loop poles (TANG et al., 2021), which are the eigenvalues of the state matrix. Indeed, the dynamic response of the homogeneous state-space equation is:

$$x(t) = e^{\mathbf{A}t}x(0) \tag{5.3}$$

where $x(0)$ are the initial conditions. It can be shown that, if A is a diagonal matrix, its exponential is given by:

$$e^{\mathbf{A}t} = \mathbf{P}\begin{bmatrix} e^{\lambda_1 t} & . & . & 0 \\ . & . & & . \\ . & & . & . \\ 0 & . & . & e^{\lambda_n t} \end{bmatrix}\mathbf{P^{-1}} \tag{5.4}$$

where λ_1 ... λ_n are the matrix eigenvalues and $\mathbf{P}$ is the matrix which makes $\mathbf{A}$ diagonal. One can diagonalize a matrix using its eigenvectors. If $\mathbf{P}$ is the eigenvectors matrix for an eigenvectors base, it is well known that the matrix $\mathbf{P^{-1}AP}$ is a diagonal matrix. Using the transformation $\mathbf{x} = \mathbf{Pz}$ to represent the Eq. 5.2 in an eigenvectors base, one obtains:

$$\mathbf{\dot{z}} = \mathbf{P^{-1}APz} + \mathbf{P^{-1}Bu} + \mathbf{P^{-1}B_d u_d} \tag{5.5}$$

Thus, the solution for the state Eq. 5.2 can also be expressed as:

$$\mathbf{z(t)} = \begin{bmatrix} e^{\lambda_1 t} \\ e^{\lambda_2 t} \\ . \\ . \\ . \\ e^{\lambda_n t} \end{bmatrix} \tag{5.6}$$

By Eq. 5.6 the dynamic response depends on the eigenvalues. These, on the other hand, are the closed-loop poles of the controlled system transfer function, either real or complex. In the time-domain, the responses corresponding to these poles are, respectively:

$$z(t) = e^{\lambda t}z(0) \tag{5.7}$$

$$\lambda = -\xi\omega_n \pm \omega_n\sqrt{1-\xi^2} \tag{5.8}$$

$$z(t) = e^{-\xi\omega_n t}\left(cos(\omega_n\sqrt{1-\xi^2}\frac{\xi}{\sqrt{1-\xi^2}sin(\omega_n\sqrt{1-\xi^2})}\right)z(0) \tag{5.9}$$

where ξ is the damping coefficient and ω_n the natural frequency corresponding to each pole.

Analyzing Eqs. 5.7 and 5.9, useful results can be obtained. First, for attaining stability the eigenvalues must be negatives or have negative real parts, in order to obtain decreasing exponential terms. Second, for complex eigenvalues, the damping coefficient increases as much as the real part is distant from the imaginary axis. Therefore, placing the closed-loop poles in a suitable way, one can increase the damping of structural modes, reducing the wind turbine loads. For pole placement, the control input vector is set as a linear combination of the system states:

$$\mathbf{u} = -\mathbf{K}\mathbf{x} \tag{5.10}$$

Introducing the control input the system dynamics is modified to:

$$\dot{\mathbf{x}} = (\mathbf{A} - \mathbf{B}\mathbf{K})\mathbf{x} + \mathbf{B_d}\mathbf{u_d} \tag{5.11}$$

The full-state feedback gain $\mathbf{K}$ is then calculated such that the new state matrix $\mathbf{A} - \mathbf{B}\mathbf{K}$ has the eigenvalues (closed-loop poles) in the desired positions. It is easy to show that this can be accomplished since the system attends certain controllability conditions (OGATA, 2010).

5.4 H_∞ control

The chosen control method to reduce wind turbine structural loads is the H_∞ optimal control. This is a more recent control theory diverging from the classical approaches of root-locus and Bode diagram control design techniques, which are fundamentally dependent on the expertise of the control engineer to tune the controller parameters. H_∞ approach is based on a optimization procedure, that allows to obtain the controller giving the minimal transference of energy between disturbance and output, while stabilizing the closed-loop system. For a linear, time-invariant system $\Gamma : L^2_m(R) \longrightarrow L^2_p(R)$ the ∞-norm is given by:

$$||\Gamma||_\infty = \sup_{\omega \in R} ||G(j\omega)||_2 \tag{5.12}$$

where $||G(j\omega)||_2$ is the spectral norm of the p x m matrix $G(j\omega)$ and $G(s)$ is the transfer function matrix of Γ. Therefore, the ∞-norm of a system describes the maximum energy gain of the system and corresponds to the peak value of the largest singular value of the frequency response matrix over the whole frequency axis. This norm is called the H_∞-norm, since we denote by H_∞ the linear space of all stable linear systems (GU; PETKOV; KONSTANTINOV, 2005). Given the desired output of a closed-loop control system y with controller matrix K and transfer function matrix G, the classical control relationships apply:

$$y = (I + GK)^{-1}GKr + (I + GK)^{-1}d \tag{5.13}$$

$$u = K(I + GK)^{-1}r - K(I + GK)^{-1}d \tag{5.14}$$

$$e = (I + GK)^{-1}r - (I + GK)^{-1}d \tag{5.15}$$

where e is the error between the reference and the output, r is the desired reference, u is the control signal, and d the disturbance, all in transfer function form, while I is the identity matrix. As it is evident from the above equations, in order to have a small error and less interference from disturbance, it is necessary to reduce the maximum energy gain between y and d, represented by the H_∞ norm of the function $(I + GK)^{-1}$. This function is called in H_∞ control design the sensitivity function (S). However, purely minimizing S may not be sufficient to attain all performance requirements of the controller K. In this case, weighting functions can be used to give a desired shape to S. Therefore, the H_∞ control problem becomes the search for the stabilizing controller K that minimizes the following H_∞ norm

$$\min_{K stabilizing} ||W_1 S|| \tag{5.16}$$

where the term stabilizing refers to the need of the calculated K of making the closed-loop system stable and W_1 is a weighting function. Further, the product KS should be minimized and shaped, in order to limit the control signal effort (u), as it can be inferred by analyzing Eq. 5.14. Indeed, if KS is not considered in the H_∞ design the control energy required by u could become unfeasible. Therefore, the H_∞ optimization problem is extended and becomes

$$\min_{K stabilizing} \left\| \begin{matrix} W_1 S \\ W_2 K S \end{matrix} \right\| \tag{5.17}$$

The choice of the weighting functions should be defined according to the model of the controlled system (plant) and will be presented in the next sections. The solution of the optimization equations can be obtained through the solve of Riccati equations (NISE, 2019) or using one of the available computational approaches, such as MATLAB (MATHWORKS, 2017) or Python implementations (BEAZLEY; JONES, 2018).

5.5 Model Predictive Control

Model predictive control is a recent development of control theory, which uses a model of the plant to predict its behavior, considering the present and the future inputs. At each time step, the controller solves an optimization problem to determine not only one control input, as in other control methods, but a control trajectory, made up of all the future control inputs over a pre-determined temporal window. This period of time is called the control horizon. To calculate the control trajectory, the controller uses a prediction of the behavior of the plant over a time window called the prediction horizon. Prediction and control horizons need not be equal, even though the control horizon need to be smaller than the prediction (PRODAN; ZIO, 2014; LIO et al., 2014). The optimization solved by the controller deals with the following quadratic programming problem:

$$J = \sum_{i=1}^{N_p} (R_y - Y) Q (R_y - Y)^T + \sum_{i=1}^{N_c} U R U^T \tag{5.18}$$

where N_p is the prediction horizon, N_c is the control horizon, R_y is the desired set-point (reference), Y are the plant ouputs, and U are the control inputs. R and Q are weighting matrices that takes into account the effect of the control effort (represented by u) and the control error (represented by $R_y - Y$. Model predictive controller consists in the solution of the previous quadratic optimization, using a numerical technique, which can be the active-set method, the interior point convex or the trust-region-reflective (CHAPRA; CANALE, 2021). Since these are constraint-handling algorithms, constraints may be imposed to the optimization problem of Eq. 5.18.

5.6 Results

5.6.1 Baseline controllers

5.6.1.1 Developed controllers

The pitch baseline controllers developed here are representative of the controllers used in commercial WTs installed worldwide. These controllers are based on simple PID algorithms and are developed from a linear model of the WT containing only one DOF, which is the rotor azimuth. The baseline controllers are:

- Baseline DLL NREL 5 MW Controller developed by NREL
- Classical PID controller based on 1-DOF model
- State-space controller based on 1-DOF model

The baseline controllers will have their performance evaluated and will be used as comparison basis for advanced controllers.

5.6.1.2 Baseline DLL NREL 5MW Controller developed by NREL

5.6.1.2.1 Control design

This controller was developed along with the reference wind turbine (RWT, see Sec. 3.2.2) NREL 5 MW to be used with it during simulations (JONKMAN et al., 2009). It was implemented as a DLL to run inside FAST/OpenFAST. Nonetheless, we have developed a Simulink model of this controller, implementing all its characteristics from the DLL source code within MATLAB. This will make easier the process of comparison with another controllers.

The Baseline DLL Controller uses a PID control, designed using a linear model of the turbine obtained through FAST simulations. Like the other baseline controllers, the model is built with only one DOF, which is the rotor azimuth. The model for control

design relates the rotor speed with aerodynamic torque and generator torque, as in Eq. 5.19:

$$T_{Aero} - N_{Gear}T_{Gen} = (I_{Rotor} + N_{Gear}^2)\frac{d}{dt}(\Omega_0 + \Delta\Omega) = I_{Drivetrain}\Delta\dot{\Omega} \tag{5.19}$$

where T_{Aero} is the low-speed shaft aerodynamic torque, T_{Gen} is the high-speed shaft generator torque, N_{Gear} is the high-speed to low-speed gearbox ratio, $I_{Drivetrain}$ is the drivetrain inertia cast to the low-speed shaft, I_{Rotor} is the rotor inertia, I_Gen is the generator inertia relative to the high-speed shaft, Ω_0 is the rated low-speed shaft rotational speed, $\Delta\Omega$ is the small perturbation of low-speed shaft rotational speed about the rated speed, $\Delta\dot{\Omega}$ is the low-speed shaft rotational acceleration, and t is the time. In Region 3, the Baseline DLL controller considers the generator power is kept constant, which leads to generator torque being inversely proportional to generator speed, as in:

$$T_{Gen}(N_{Gear}\Omega) = \frac{P_0}{N_{Gear}\Omega} \tag{5.20}$$

where P_0 is the rated power and Ω is the low-speed shaft rotational speed. Assuming negligible variation of aerodynamic torque with rotor speed, the aerodynamic torque in Region 3 can be written as:

$$T_{Aero}(\theta) = \frac{P_0(\theta, \Omega_0)}{\Omega_0} \tag{5.21}$$

where θ is the blade pitch angle. Expanding Eqs. 5.20 and 5.21 in a first-order Taylor series, we obtain

$$T_{Gen} \approx \frac{P_0}{N_{Gear}\Omega_0} - \frac{P_0}{N_{Gear}\Omega_0^2}\Delta\Omega \tag{5.22}$$

$$T_{Aero} \approx \frac{P_0}{\Omega_0} + \frac{1}{\Omega_0}\frac{\partial P}{\partial\theta}\Delta\theta \tag{5.23}$$

where $\Delta\theta$ is a small perturbation of the blade-pitch angles about their operating point. With proportional-integral-derivative (PID) control, this is related to the rotor-speed perturbations by

$$\Delta\theta = K_p N_{Gear}\Delta\Omega + K_i \int N_{Gear}\Delta\Omega(t)dt + K_d N_{Gear}\Delta\dot{\Omega} \tag{5.24}$$

where K_p, K_i, and K_d are the blade-pitch controller proportional, integral, and derivative gains, respectively. Using $\dot{\phi} = \Delta\Omega$, combining the above expressions and simplifying, the equation of motion for the rotor-speed error becomes:

$$\left[I_{Drivetrain} + \frac{1}{\Omega_0} - \frac{\partial P}{\partial\theta}N_{Gear}K_d\right]\ddot{\phi} + \left[\frac{1}{\Omega_0} - \frac{\partial P}{\partial\theta}N_{Gear}K_p - \frac{P_0}{\Omega_0^2}\right]\dot{\phi} + \left[\frac{1}{\Omega_0} - \frac{\partial P}{\partial\theta}N_{Gear}K_i\right]\phi = 0$$

$$M_\phi\ddot{\phi} + C_\phi\dot{\phi} + K_\phi\phi = 0 \tag{5.25}$$

where, for the sake of simplicity, we substitute the extended terms by M_ϕ, C_ϕ, and K_ϕ. The previous Eq. 5.25 demonstrates that the closed-loop system responds as a second-order

system, with natural frequency and damping ratio

$$\omega = \sqrt{\frac{K_\phi}{M_\phi}} \tag{5.26}$$

$$\xi = \frac{C_\phi}{2\sqrt{K_\phi M_\phi}} \tag{5.27}$$

Most authors recommend neglecting derivative gain, and thus the Baseline DLL Controller sets $K_d = 0$. Besides, following the guidelines in (HANSEN; HANSEN; LARSEN, 2005), desirable values for the natural frequency and damping are $\omega = 0.6$ and $\xi = 0.6 \sim 0.7$. This specification allows to calculate K_p and K_i:

$$K_p = \frac{2 I_{Drivetrain} \Omega_0 \xi \omega}{N_{Gear}\left(-\frac{\partial P}{\partial \theta}\right)} \tag{5.28}$$

$$K_i = \frac{I_{Drivetrain} \Omega_0 \omega^2}{N_{Gear}\left(-\frac{\partial P}{\partial \theta}\right)} \tag{5.29}$$

As it possible to infer from Eqs. 5.28 and 5.29, the main parameter influencing control gains is the partial derivative of power with respect to blade pitch $\frac{\partial P}{\partial \theta}$, which results from the linearization process. In the Baseline DLL Controller, $\frac{\partial P}{\partial \theta}$ is calculated in other points other than the linearization point, in order to ensure suitable performance. The values of $\frac{\partial P}{\partial \theta}$ are shown in Table 4.

Table 4 – Variation of $\frac{\partial P}{\partial \theta}$ with wind speed

Wind speed (m/s)	Rotor speed (rpm)	Pitch angle (°)	$\frac{\partial P}{\partial \theta}$
11.4	12.1	0.00	-28.24E6
12.0	12.1	3.83	-43.73E6
13.0	12.1	6.60	-51.66E6
14.0	12.1	8.70	-58.44E6
15.0	12.1	10.45	-64.44E6
16.0	12.1	12.06	-70.46E6
17.0	12.1	13.54	-76.53E6
18.0	12.1	14.92	-83.94E6
19.0	12.1	16.23	-90.67E6
20.0	12.1	17.47	-94.71E6
21.0	12.1	18.70	-99.04E6
22.0	12.1	19.94	-105.90E6

Source: (JONKMAN, 2007)

A gain-scheduling procedure is utilized to take into account the variation of $\frac{\partial P}{\partial \theta}$. Using the results of Table 4 it is verifiable that this variation is linear and the following relation holds,

$$\frac{1}{\frac{\partial P}{\partial \theta}} = \frac{1}{\frac{\partial P}{\partial \theta}(\theta = 0)\left(1 + \frac{\theta}{\theta_K}\right)} \tag{5.30}$$

where $\frac{\partial P}{\partial \theta}(\theta = 0)$ is the blade pitch sensitivity at $\theta = 0$ and θ_K is the pitch angle at which the pitch sensitivity has doubled from the original value at $\theta = 0$. The Eq. 5.30 has put the linear variation of blade pitch sensitivity in an appropriate form to be included in the equations for K_p and K_i, which become

$$K_p = \frac{2 I_{Drivetrain} \Omega_0 \xi \omega}{N_{Gear} \left[-\frac{\partial P}{\partial \theta}(\theta = 0) \right]} GK(\theta) \tag{5.31}$$

$$K_i = \frac{I_{Drivetrain} \Omega_0 \omega^2}{N_{Gear} \left[-\frac{\partial P}{\partial \theta}(\theta = 0) \right]} GK(\theta) \tag{5.32}$$

where $GK(\theta)$ is the gain-scheduling factor, deduced from Eq. 5.30 and given by:

$$GK(\theta) = \frac{1}{1 + \frac{\theta}{\theta_K}} \tag{5.33}$$

For the structural properties and design characteristics of NREL 5 MW RWT, the resulting final control gains at $(\theta = 0)$ calculated using Eqs. 5.31-5.32 are

$$K_p = 0.01883 \tag{5.34}$$

$$K_i = 0.0081 \tag{5.35}$$

$$K_d = 0 \tag{5.36}$$

At last, it is important to establish the minimum and maximum limits for blade pitch angle value and for blade pitch change rate. The limits are set to $\theta_{min} = 0°$ and $\theta_{max} = 90°$. The minimum value corresponds to maximum aerodynamic power (which is the typical pitch angle at partial-load in Region 2) and is the initial pitch angle once the wind turbine changes from Region 2 to Region 3. The maximum value corresponds to the fully feathered blade with minimum torque. The blade pitch rate was set to $8°/s$, corresponding to the General Electric (GE) long-blade test program for 5 MW machines.

5.6.1.2.2 *Considerations about generator torque control*

Even though this is not the focus of the present thesis, which has chosen to aim at pitch control system for structural and power control at Region 3, it is important to have a generator torque control model, for the sake of completeness. This also allows to have a full operational wind turbine model, which could be used for future research in generator torque control algorithms, coupled generator torque-blade pitch controls (see e.g., (NEJAD et al., 2016) and (BINSBERGEN; WANG; NEJAD, 2020)), and simulations of transition between Regions 2 and 3. The Baseline DLL Controller also contains a generator torque control. It follows the industry-standard torque control law,

$$T_{Gen} = k \Omega^2 \tag{5.37}$$

$$k = \frac{1}{2} \rho \pi R^5 \frac{C_{P_{opt}}}{\lambda_{opt}} \tag{5.38}$$

where the generator torque in Region 2 is defined according to the quadratic law 5.37. This has been shown in numerous research (MENEZES; ARAúJO; SILVA, 2018) to ensure maximum power production in variable speed wind turbines, by changing the rotor speed in Region 2 accompanying the wind speed variations. The constant k is a turbine-specific parameter that depends on air density ρ, turbine rotor radius R and $C_{P_{opt}}$ and λ_{opt}, which are respectively the optimal power coefficient and tip-speed ratio for power production in variable-speed operation. $C_{P_{opt}}$ and λ_{opt} depend on the airfoil design and blade properties and can be obtained from aerodynamic simulations using a CFD or a WT simulation software. In the case of the Baseline DLL Controller, they were found running AeroDyn simulations (NING et al., 2015). AeroDyn is an aerodynamics calculation program that is used by FAST and OpenFAST to calculate the aerodynamic loads. Nevertheless, it can be also run in stand-alone mode. The values of the above parameters for the NREL 5 MW RWT are $C_{P_{opt}} = 0.482$ and $\lambda_{opt} = 7.55$, giving $k = 0.02558$ Nm/rpm^2. With the rated generator speed of 1173.7 rpm, rated electric power of 5 MW, and establishing a generator efficiency of 94.4%, the rated mechanical power is 5.296610 MW and the rated generator torque is 43,093.55 Nm. Other characteristics of generator torque control involve the transitions between Regions 1 and 2 (denominated Region 1½) and Regions 2 and 3 (denominated Region 2½).Region 1½ spans the range of generator speeds between 670 rpm and 30% above this value (or 871 rpm). The transitional generator speed between Regions 2½ and 3 is defined as 99% of the rated generator speed, or 1,161.963 rpm. The generator-slip percentage in Region 2½ was taken to be 10%. These values were established by NREL for the Baseline DLL Controller based on several conceptual designs of 5 MW machines, such as (T. LINDENBURG; HOOFT, 2003) and (SYSTEMS, 2005). The designed torque control provides a generator torque characteristic curve (not shown here).

At last, the Baseline DLL Controller includes a low-pass filter in the generator speed signal. Indeed, the generator speed signal feeds the generator torque control and is also the primary signal for blade pitch control (since the latter limits aerodynamic power by controlling rotor speed in Region 3). Therefore, generator speed signal is of utmost importance. If it is not filtered, the high-frequency oscillations can enter and impair torque control and pitch control (FLEMING et al., 2017). Baseline DLL Controller low-pass filter uses a recursive, single-pole formulation with exponential smoothing (). The discrete-time recursion (difference) equation for this filter is

$$\begin{aligned} y[n] &= (1-\alpha)u[n] + \alpha y[n-1] \\ \alpha &= e^{-2\pi T_s f_c} \end{aligned} \tag{5.39}$$

where f_c is the filter corner frequency, T_s is the time step and n is the discrete counter. NREL sets $f_c = 0.25Hz$ because it corresponds to one-quarter of the first blade collective edge frequency, which has been proven to be the lower frequency excited by noise oscillations.

5.6.1.2.3 Overview of Baseline DLL Controller

The discussed Baseline DLL Controller was implemented, with the complete previous presented features, in a Simulink model. This will make possible to run complete WT simulations and execute all the required analysis. Originally, the Baseline DLL Controller is implemented as a DLL to run inside OpenFAST, written in Fortran source code. This reduces the capability of running analysis and control design. An overview of the Baseline DLL Controller is represented by its Simulink model, as shown in Figs. 12-14.

In Fig. 12, we have the general controller outline, with the generator speed measurement as the feedback variable. Blade pitch is also output from the nonlinear WT simulation model, because the generator torque control uses this information in changing between control regions. The designed filter is implemented in state-space formulation. The Pitch Controller and Torque Controller blocks contains the algorithms developed in the previous sections and their detailing is shown in Fig. 13 and Fig. 14, respectively. It is important to emphasize that provisions for future implementations of yaw controller and high-speed shaft brake models are also included in the main diagram of Fig. 12, though they are not considered at the moment. The presented diagrams summarize the main Baseline DLL Controller characteristics and consequently the NREL 5 MW RWT control system.

Figure 12 – Baseline DLL Controller - main diagram

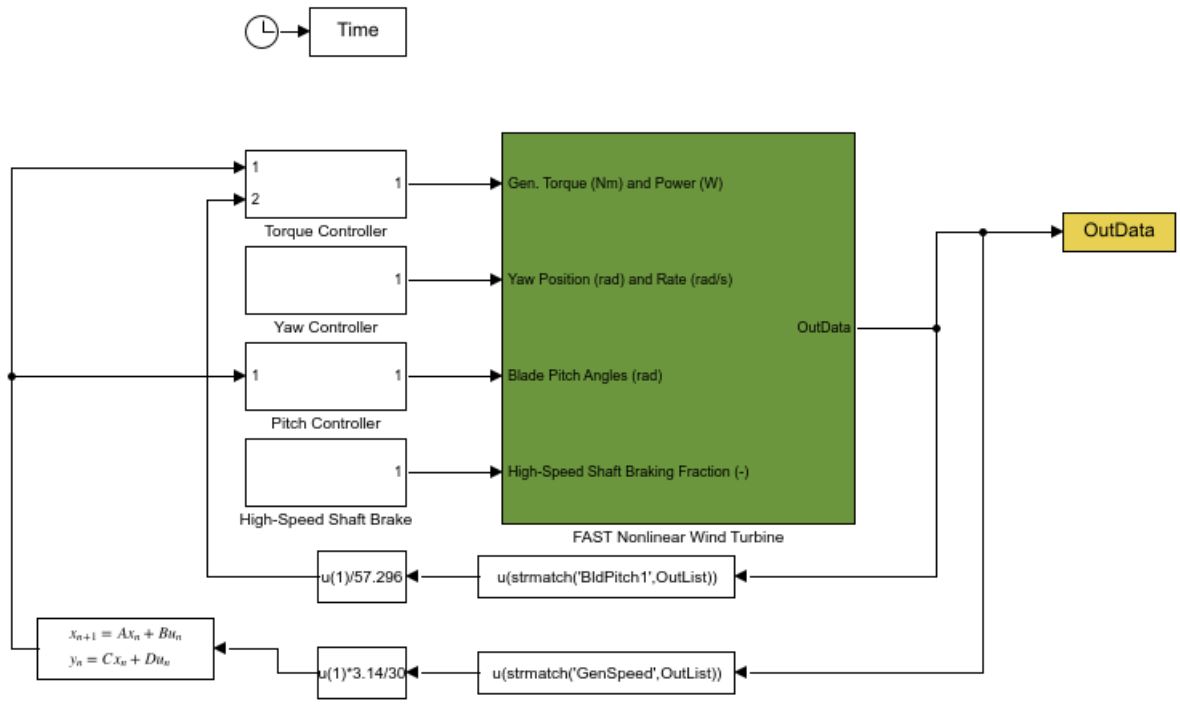

Source: Author (2022)

Figure 13 – Baseline DLL Controller - Pitch Controller diagram

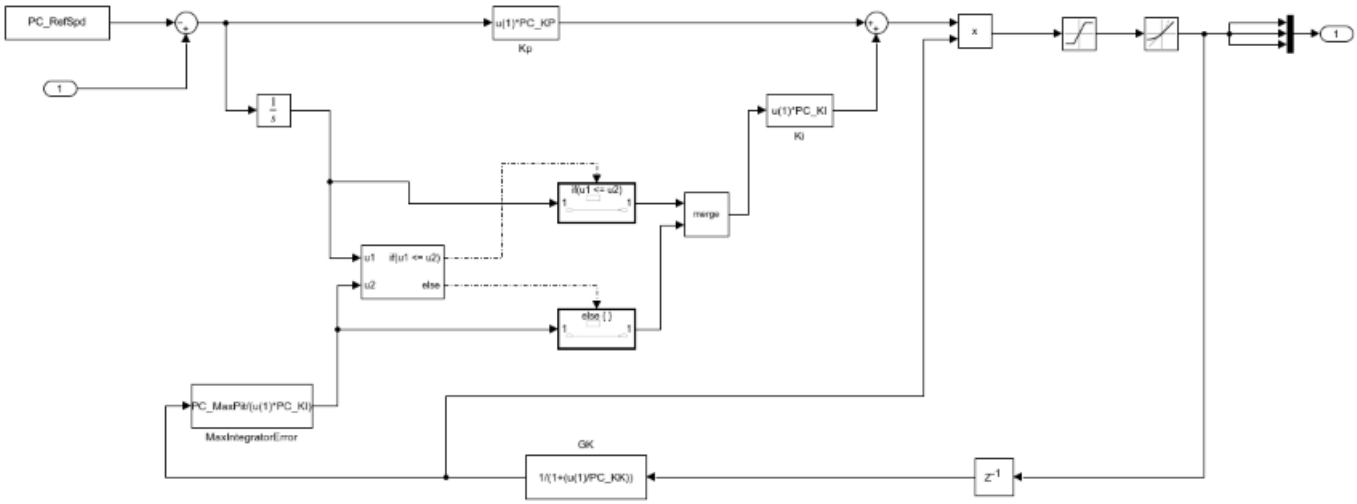

Source: Author (2022)

Figure 14 – Baseline DLL Controller - Torque Controller diagram

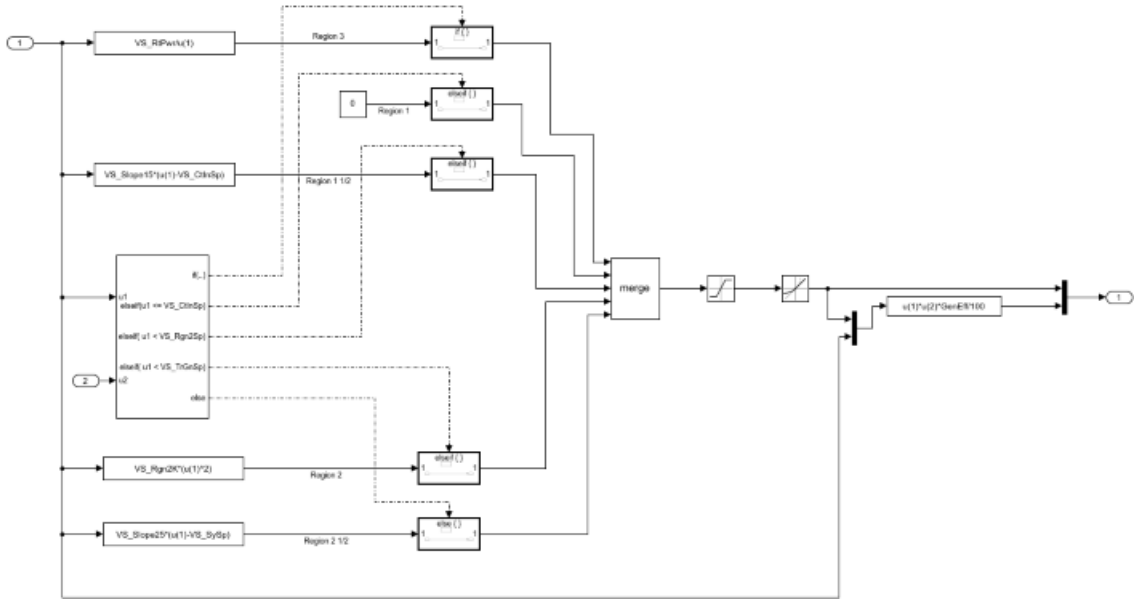

Source: Author (2022)

5.6.1.2.4 Results

Given a designed controller, the next phase in the control systems implementation is the execution of the simulations to verify control performance. This is done for the Baseline DLL Controller in this section.

5.6.1.2.5 Steady wind simulations

The first set of simulations consider steady wind conditions. Initially, the wind is considered uniform over the rotor. Afterwards, a wind variation due to wind shear

is included. In the following definitions, v is the wind speed and α is the wind shear coefficient. Therefore, steady wind simulations encompasses:

1. Uniform wind varying from $v = 14m/s$ to $v = 18m/s$
2. Hub-height wind speed varying from $v = 14m/s$ to $v = 18m/s$ with wind shear coefficient $\alpha = 0.2$, as recommended by IEC 61400-1 for on-land turbines.

1. Uniform wind varying from $v = 14m/s$ to $v = 18m/s$
As previously discussed, rotor speed regulation is the primary objective of pitch control. By controlling rotor speed to the rated value, the pitch control provides constant WT power in Region 3. Results for the rotor speed regulation are shown in Fig. 15.

Figure 15 – NREL 5 MW RWT rotor speed - Baseline DLL Controller

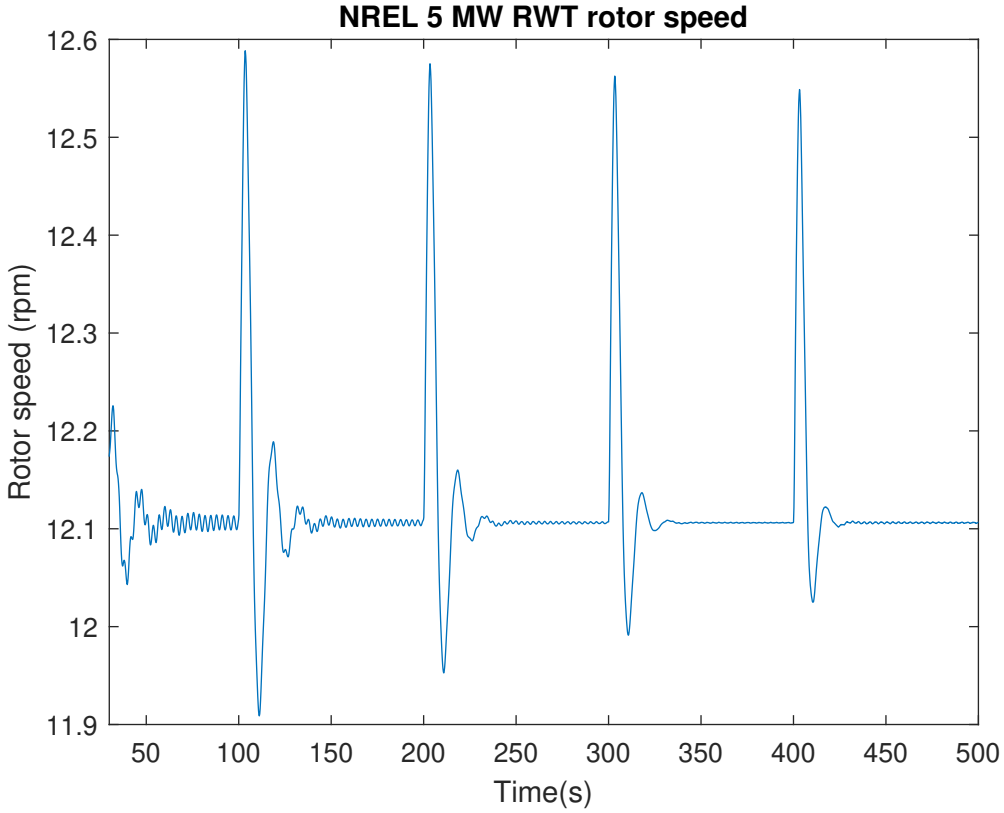

Source: Author (2022)

It is possible to observe that the rotor speed control performance is satisfactory. Other parameters of interest include turbine power and blade pitch angle, shown in Fig. 16. The latter is important because represents the control effort. From the plots, it can be concluded that the blade pitch angle presents a reasonable variation, increasing as long as the wind speed increases. For the generator power, a constant value is obtained. This was expected because the Baseline DLL Controller imposes constant generator power in Region 3.

Figure 16 – NREL 5 MW RWT commanded pitch angle (left) and generator power (right) - Baseline DLL Controller

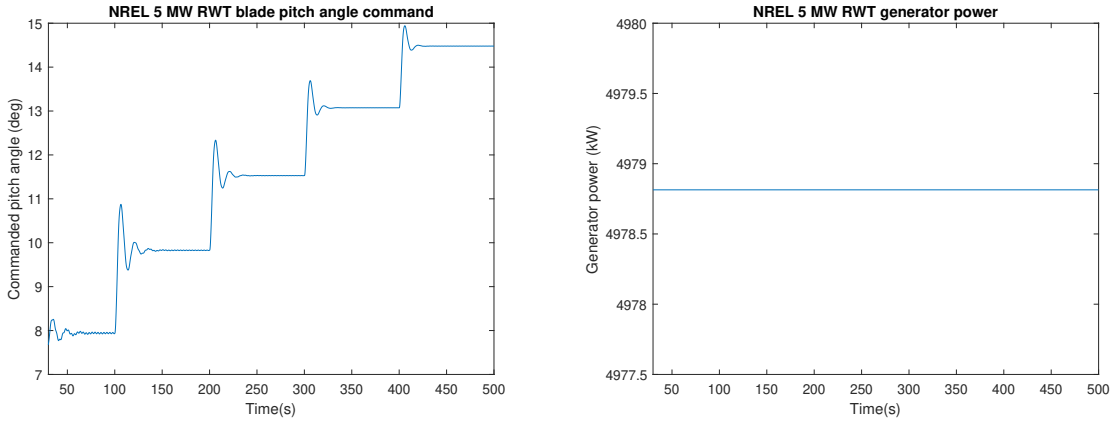

Source: Author (2022)

It is also necessary to evaluate turbine structural loads when using Baseline DLL Controller. This will allow a comparison with the other controllers developed next. Regarding structural aspects, we can observe structural loads for the tower and the blades. For the tower, Fig. 17 contains the plots of tower top fore-aft displacement and the corresponding tower base fore-aft moment. Regarding the blade, the blade root flapwise moment is shown in Fig. 18.

Figure 17 – NREL 5 MW RWT tower top fore-aft displacement (left) and tower base fore-aft moment (right) - Baseline DLL Controller

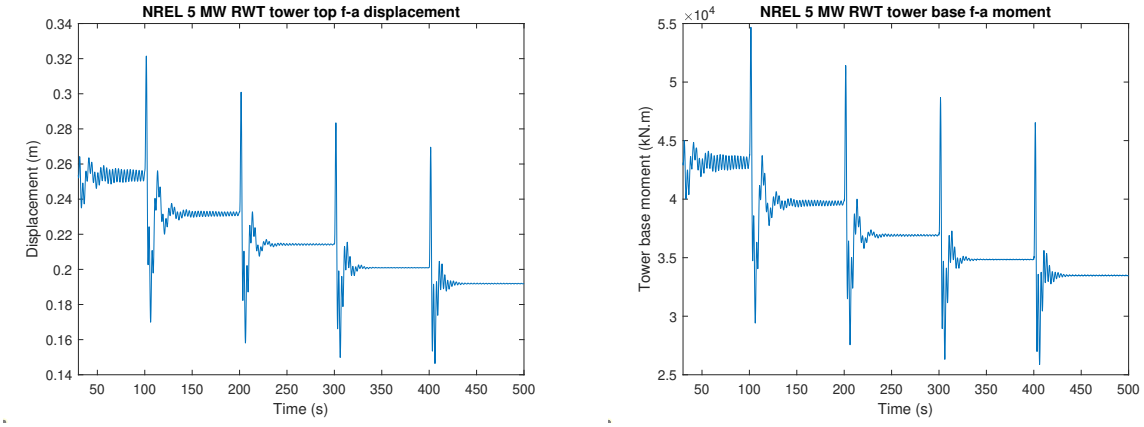

Source: Author (2022)

2. Hub-height wind speed varying from $v = 14m/s$ to $v = 18m/s$ with wind shear coefficient $\alpha = 0.2$

The results of the steady wind simulation considering wind shear are showed in Fig. 19 for rotor speed regulation. A detail of the simulation between t =100 s and t =200 s is shown in the right part of Fig. 19 emphasizing the rotor speed behavior when the wind speed rises from $v = 14m/s$ to $v = 15m/s$. It is clear that the presence of shear does not

Figure 18 – NREL 5 MW RWT blade root flapwise moment with wind shear - Baseline DLL Controller

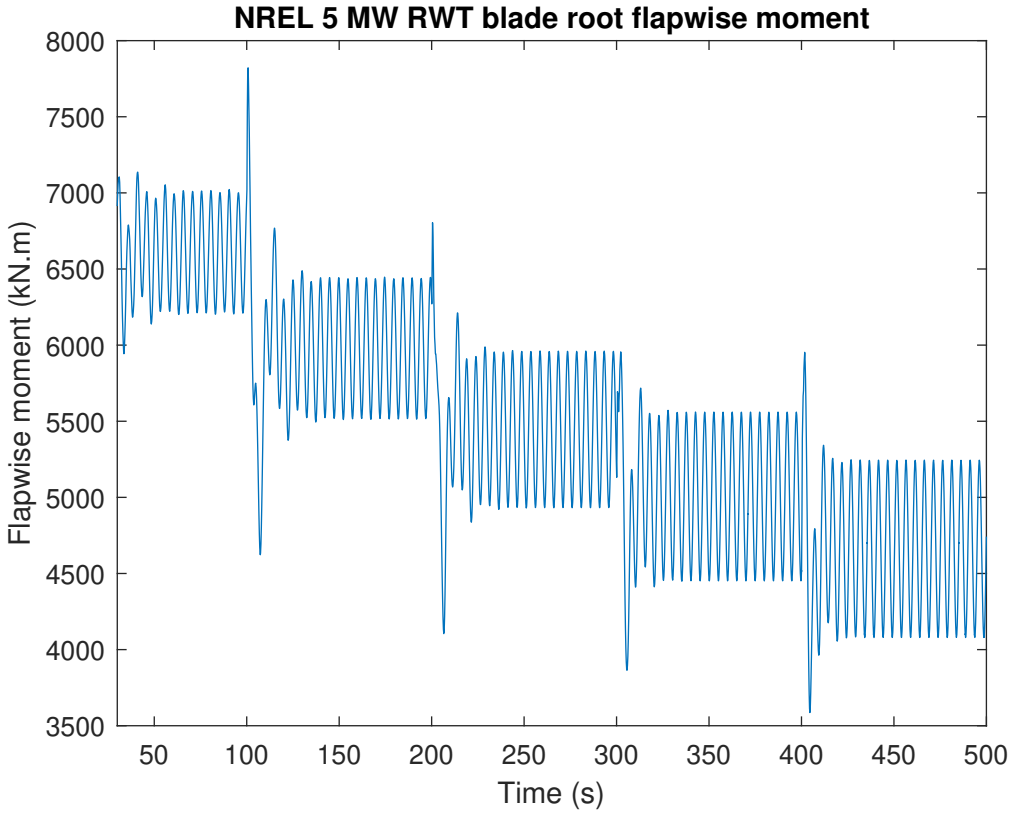

Source: Author (2022)

impair the control performance. Blade pitch angle and generator power are shown in Fig. 20, and since rotor speed has not presented significant change, pitch angle and generator power have not shown changes either. Finally, tower base fore-aft and blade root flapwise moments are shown in Fig. 21. As expected, the blade root moment variation is higher than in the case without shear, given the wind shear causes the blade to see a higher wind in the upper part of its rotation and a smaller wind speed in the lower part of its rotation.

5.6.1.2.6 Turbulent wind simulations

Unlike the previous section, the second set of simulations presented here consider turbulent wind conditions. Turbulent winds are generated using TurbSim (BUHL; MANJOCK, 2006). The following turbulence characteristics are assumed:

- $v = 18m/s$ at hub-height
- Kaimal spectral model
- IEC Turbulence Category B
- IEC Normal Turbulence Model (NTM)

Figure 19 – NREL 5 MW RWT rotor speed with wind shear - Baseline DLL Controller

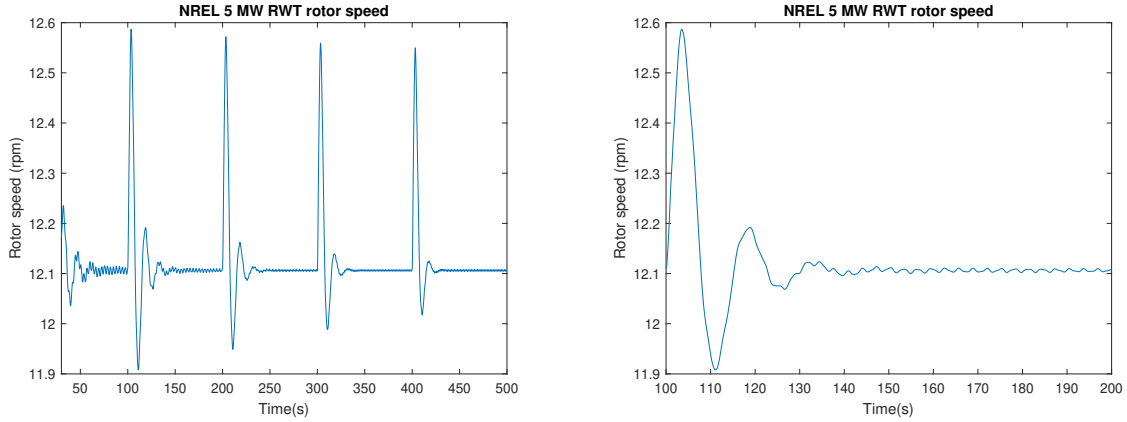

Source: Author (2022)

Figure 20 – NREL 5 MW RWT commanded pitch angle (left) and generator power (right) with wind shear - Baseline DLL Controller

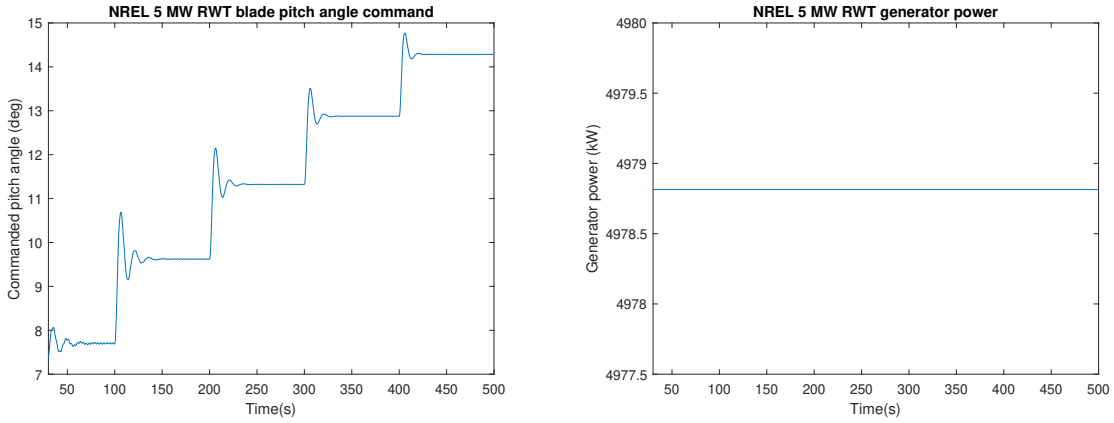

Source: Author (2022)

The rotor speed is shown in Fig. 22, together with the blade pitch angle. Given the turbulent wind, the rotor speed changes continuously, even though its mean remains over 12.1 rpm and the maximum overshoot does not surpass 13 rpm. To follow the wind speed variation, blade pitch presents a much larger control effort. The structural loads are represented in Fig. 23 by tower base fore-aft moment and blade root flapwise moment. As expected, a strong oscillation is present.

5.6.1.3 Classical PID Controller based on 1-DOF model

5.6.1.3.1 Control design

This controller design is based on the calculation of Kp, Ki and Kd using a classical transfer function approach. The modeling for control design is based on a 1-DOF model. This DOF is the rotor azimuth, since this is a baseline controller and the primary objective of pitch control is to regulate rotor speed. The model relates rotor speed perturbation $\Delta\Omega$

Figure 21 – NREL 5 MW RWT tower base fore-aft moment (left) and blade root flapwise moment (right) with wind shear - Baseline DLL Controller

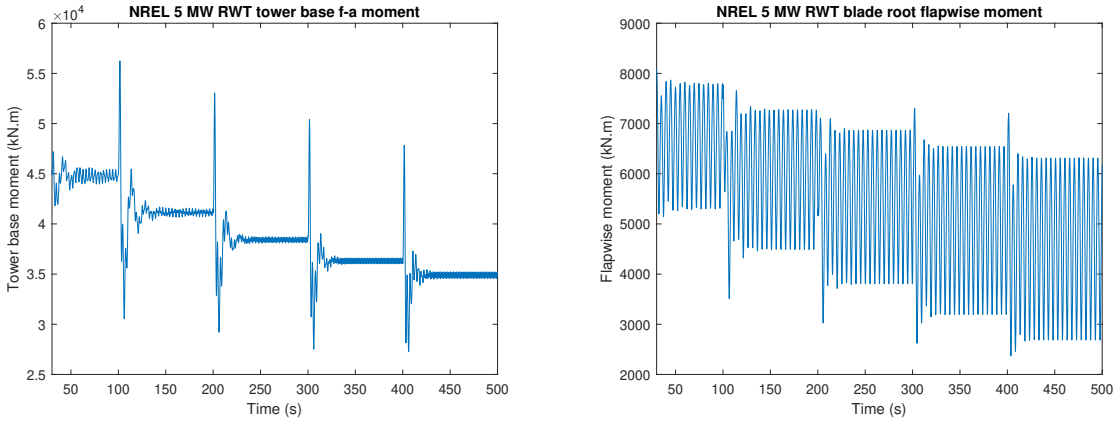

Source: Author (2022)

Figure 22 – NREL 5 MW RWT rotor speed (left) and commanded pitch angle (right), turbulent conditions - Baseline DLL Controller

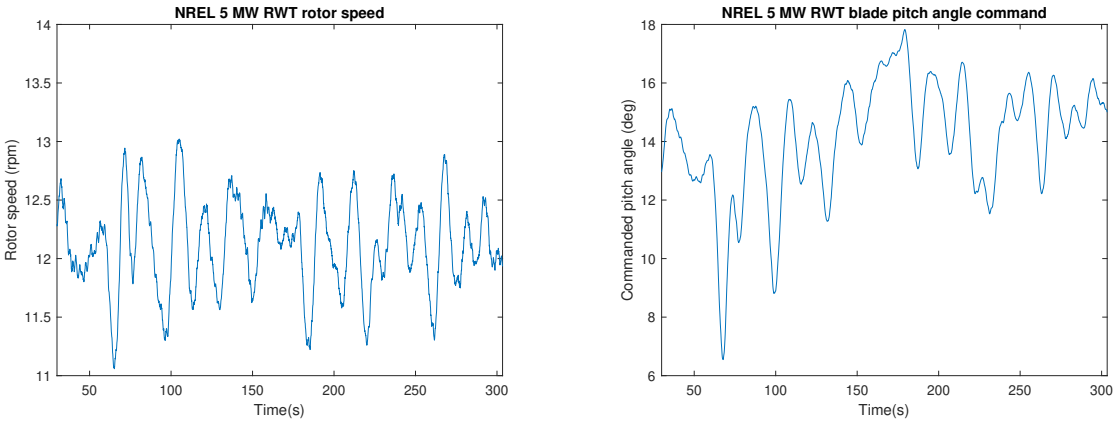

Source: Author (2022)

with wind speed perturbation Δv and pitch angle perturbation $\Delta\theta$, as in Eq. 5.40:

$$\Delta\dot{\Omega} = A\Delta\Omega + B\Delta\theta + B_d\Delta v \tag{5.40}$$

where A, B and B_d correspond to a linear model of the NREL 5 MW RWT obtained through OpenFAST simulations. These terms are related to the rotor inertia and WT characteristics. The presence of Δ indicates that these quantities were linearized around an operating point. In this case, the point is chosen in the mid-range of Region 3, with $v = 16m/s$, $theta = 12.06°$ and $\Omega = 12.1rpm$. These values represent a steady condition for the NREL 5 MW RWT dynamic system, as has been demonstrated in several works (SCHLIPF et al., 2014). Therefore, this operating point is suitable for linearization process. The Baseline DLL control imposes a pitch angle according to classical PID formulation:

$$\Delta\theta = K_p\Delta\Omega + K_i\int\Delta\Omega(t)dt + K_d\Delta\dot{\Omega} \tag{5.41}$$

Figure 23 – NREL 5 MW RWT tower base fore-aft moment (left) and blade root flapwise moment (right), turbulent conditions - Baseline DLL Controller

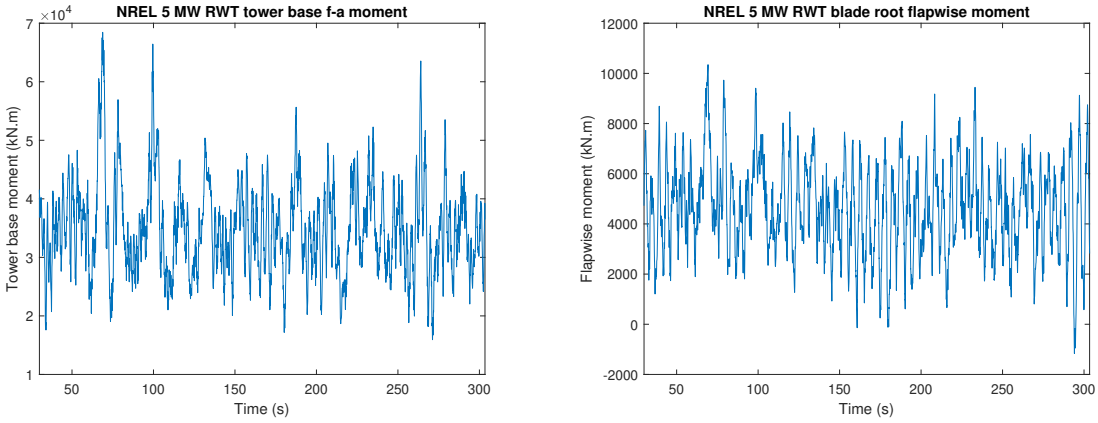

Source: Author (2022)

where, for abuse of notation, the variation of $\Delta\Omega$ with time is only expressed for the integral term. Taking Laplace transform of Eqs. 5.40 and 5.41, and making the appropriate algebraic operations, the final transfer function between rotor speed and wind speed is given by:

$$\frac{\Delta\Omega(s)}{\Delta w(s)} = \frac{B_d s}{(1 - BK_d)s^2 + (-A - BK_p)s + (-BK_i)} \tag{5.42}$$

Analyzing Eq. 5.42, it is possible to identify a second-order system with dynamic response characteristics defined by:

$$\begin{aligned} &s^2 + 2\xi\omega_n + \omega_n^2 = 0 \\ &-A - BK_p = 2\xi\omega_n, -BK_i = \omega_n^2 \end{aligned} \tag{5.43}$$

Thereby, the control gains can be calculated once damping and natural frequency are defined. Following the same method of Baseline DLL Controller, these values are set to $\xi = 1$ and $\omega_n = 0.6$. Nevertheless, a larger damping value compared to the Baseline DLL Controller was defined trying to improve control regulation. The control gains result in:

$$K_p = 0.7830 \tag{5.44}$$

$$K_i = 0.2823 \tag{5.45}$$

$$K_d = 0 \tag{5.46}$$

The same standard values of blade pitch angle saturation and rate limit of the Baseline DLL Controller are considered, i.e., $\theta_{min} = 0°$, $\theta_{max} = 90°$ and $\dot{\theta} = 8°/s$. Regarding generator torque control, the adopted approach from now on is the assumption of constant torque in Region 3. This is different from Baseline DLL Controller which imposes constant generator power in Region 3. The objective is to observe the influence of pitch control on generator torque and dynamic behavior, for future works in generator torque control strategies. Further, the filter in the generator speed signal is removed from now on. Indeed,

Figure 24 – Classical PID Controller - main diagram

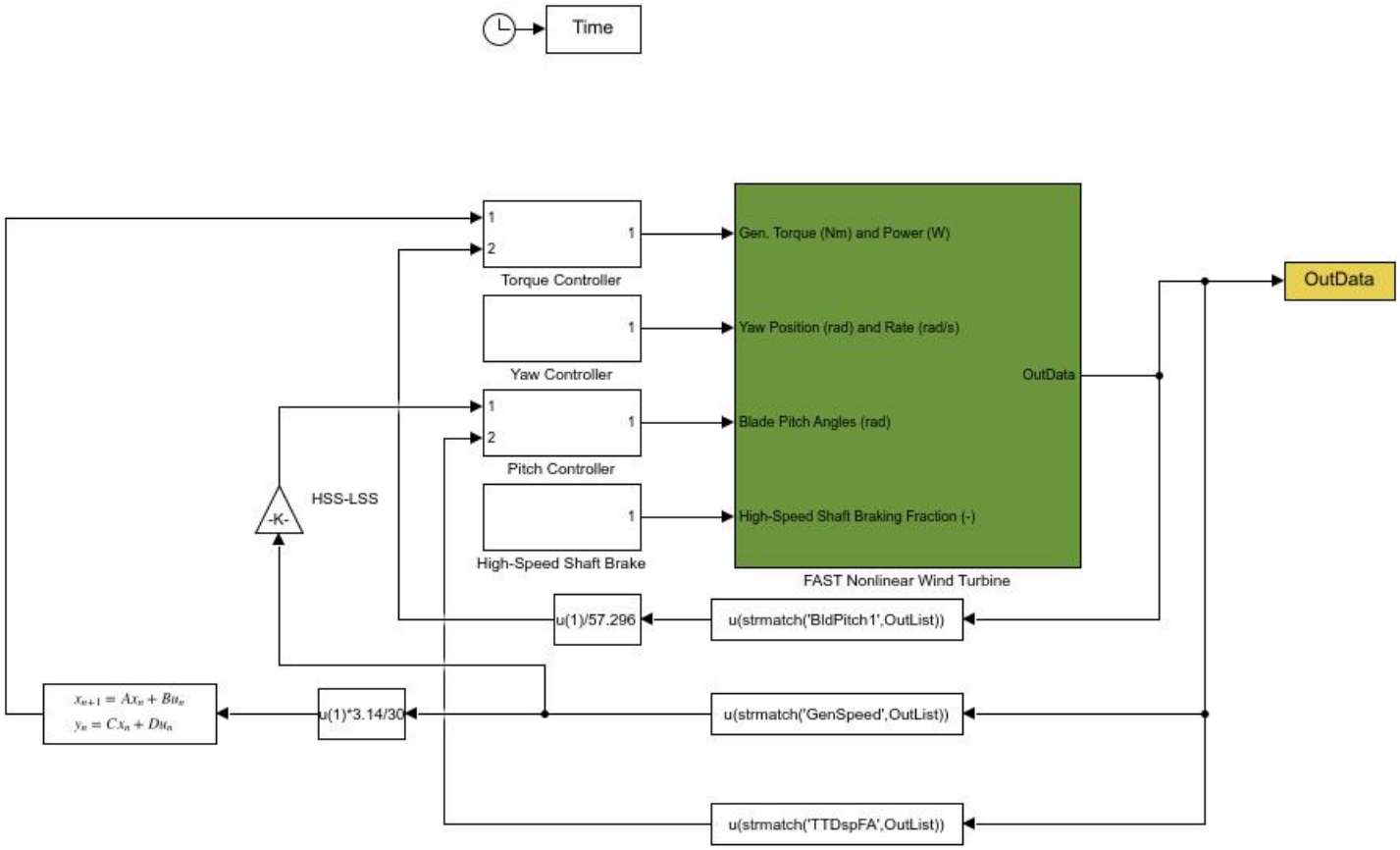

Source: Author (2022)

the inclusion of filter artificially takes out the influence of WT flexible modes that can be excited during operation. It is important to capture all the NREL 5 MW RWT dynamics without filtering.

5.6.1.3.2 Overview of Classical PID Controller based on 1-DOF model

In Fig. 24 we have an overview of the Classical PID Controller. The measured generator speed is directly feed to the pitch controller, without filtering. Only conversion for rotor speed is carried out using the transmission ratio of the WT (corresponding to 1:97). In Fig. 25 the detailing of Pitch Controller block is shown, with the implemented PID controller.

5.6.1.3.3 Results

The set of simulations consider steady wind conditions without wind shear. As it will be clear from the results, Classical PID Controller is insufficient to control the wind turbine when all the WT DOFs are enabled in simulation (this is why turbulent simulations are not presented, since even in steady wind conditions the performance is unsatisfactory).

Figure 25 – Classical PID Controller - Pitch Controller diagram

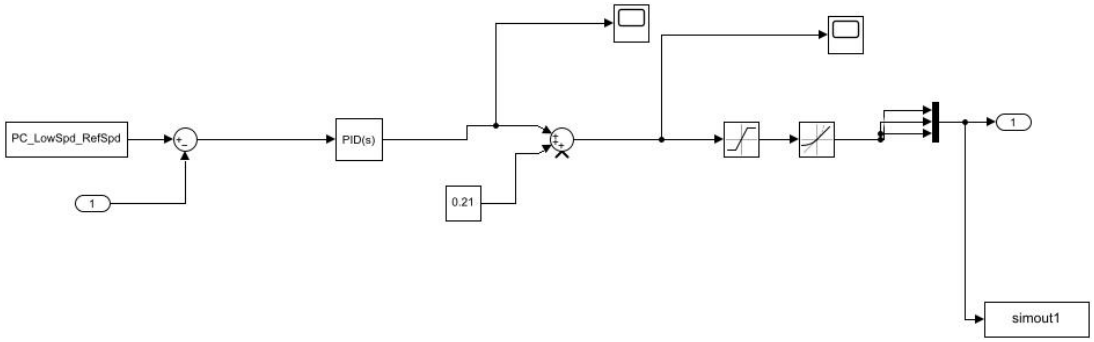

Source: Author (2022)

Indeed, hybrid modal-multibody approach and the employed OpenFAST simulation allow to consider any number of DOFs when simulating. It is possible to consider from one single DOF enabled to all the 22 DOFs enabled to the simulated WT. In this case, since the Classical PID Controller relies on a 1-DOF model, it provides an unstable system behavior when all the DOFs are active in simulation. This happens because the flexible modes associated with WT DOFs and their interaction with rotor speed are not taken into account in control design. The same problem arises in Baseline DLL Controller if the generator speed filter is not included (this result, though, is not included in Sec. 5.6.1.2.4). This will be solved by using state-space control in the next sections.

The WT simulation results with the Classical PID controller are shown in Fig. 26, for a simulation with steady wind of $v = 16m/s$. In the left plot, we have deactivated the blade DOFs of the WT to decrease its flexibility and test the control under these conditions. As one can see in the left plot, the rotor speed is reasonably controlled, however more oscillations are observed. In the right, we have activated the blade DOFs and simulated the WT with all DOFs enabled. The oscillations in rotor speed are completely unacceptable. The same behavior is reflected in the generator power production, shown in detail in the left side of Fig. 27. The variations in produced power range from 4000∼6000 kW and this cannot be tolerated. At last, in the right side of Fig. 27 the simulation is executed with only one DOF enabled (the DOF used in control design, i.e., the rotor azimuth). As can be inferred from the plot, control performance is satisfactory and oscillations are around a very small range.

5.6.1.4 State-space Controller based on 1-DOF model

5.6.1.4.1 Control design

This controller design is based on the full-state feedback method. Thus, it relies on a state-space modeling of the WT. For the baseline case, we are considering a single DOF to build the state-space model. The model for control design is the same from the

Figure 26 – NREL 5 MW RWT rotor speed with blade DOFs inactive (left) and NREL 5 MW RWT rotor speed with all the DOFs active (right) - Classical PID Controller

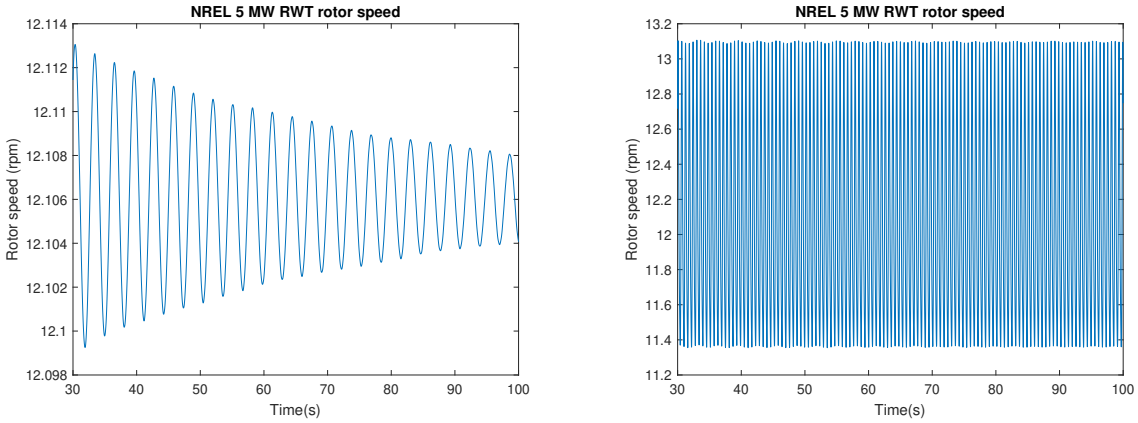

Source: Author (2022)

Figure 27 – NREL 5 MW RWT generator power with all the DOFs active (left) and NREL 5 MW RWT rotor speed with only one DOF (rotor azimuth) active (right) - Classical PID Controller

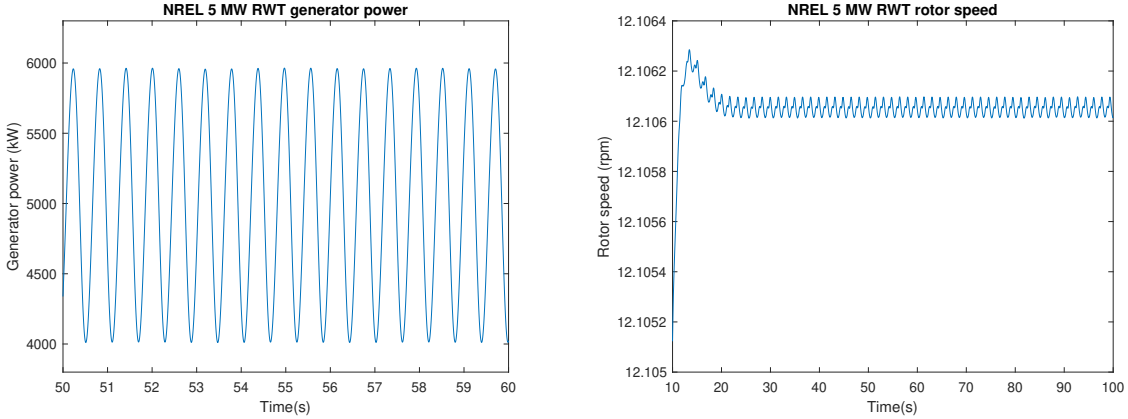

Source: Author (2022)

Classical PID Controller, expressed by

$$\Delta\dot{\Omega} = A\Delta\Omega + B\Delta\theta + B_d\Delta v \tag{5.47}$$

but this time it will not be transformed by Laplace. Instead, we analyze the values of $A = -0.2014$, $B = -1.2754$ and $B_d = 0.029$. A corresponds to the state matrix (in the 1-DOF model, a scalar), B corresponds to the control matrix (in the 1-DOF model, a scalar) and B_d to the disturbance matrix (in the 1-DOF model, a scalar). Following the full-state feedback methodology, the control design is done by placing the poles of the control system in pre-defined positions. In this case, the single pole is coincident to A value. We choose to place this pole at -2 to perform control. Executing the calculations, this demands a control gain $K = -1.41$.

Figure 28 – State-space Controller based on 1-DOF model - Pitch Controller diagram

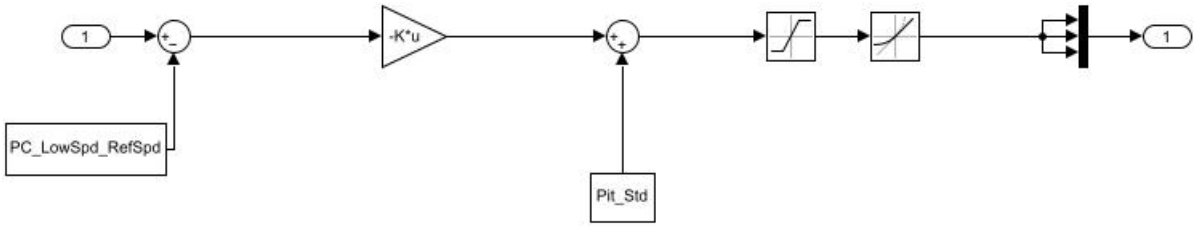

Source: Author (2022)

5.6.1.4.2 Overview of State-space Controller based on 1-DOF model

In Fig. 28 we have an overview of Pitch Controller block of the State-space Controller based on 1-DOF model. The main diagram with the general overview is not shown here because it is equal to the Classical PID Controller (see Fig. 24). The remarkable point here is the absence of PID gains and the presence of a single control gain calculated for full-state feedback. No observer is needed in this 1-DOF model.

5.6.1.4.3 Results

The set of simulations consider steady wind conditions without wind shear at $v = 16m/s$. Likewise the Classical PID Controller, the State-space Controller based on 1-DOF model is insufficient to control the wind turbine when all the WT DOFs are enabled in simulation. The simulation results are presented in Fig. 29, where rotor speed is shown for a simulation with blade DOFs inactive (left) and with all the WT DOFs active (right). The control performance is very similar to Classical PID Controller, however a small difference can be noted in the simulation with all DOFs, where the State-space controller provides a more precise response about 12.1 rpm set-point. Generator power results for the all DOFs enabled is shown in Fig. 30, presenting the same performance of the Classical PID Controller. Also in Fig. 30, result from simulation with steady winds varying from $v = 14m/s$ to $v = 18m/s$ is shown, with only the rotor azimuth DOF enabled. In this case, the great potential of state-space controller is evident, since rotor speed regulation has almost no oscillation.

5.6.2 State-space controllers

5.6.2.1 Developed controllers

The state-space controllers, relying on a multi-input, multi-output (MIMO) approach and on full-state feedback control method, present significant advantages and are a strong alternative to solve the problems of WT control. First of all, being MIMO allows this controller to address multiple control objectives, i.e., there is the possibility of considering simultaneously rotor speed control and load reduction in WT components. Therefore, it

Figure 29 – NREL 5 MW RWT rotor speed with blade DOFs inactive (left) and NREL 5 MW RWT rotor speed with all the DOFs active (right) - State-space Controller based on 1-DOF model

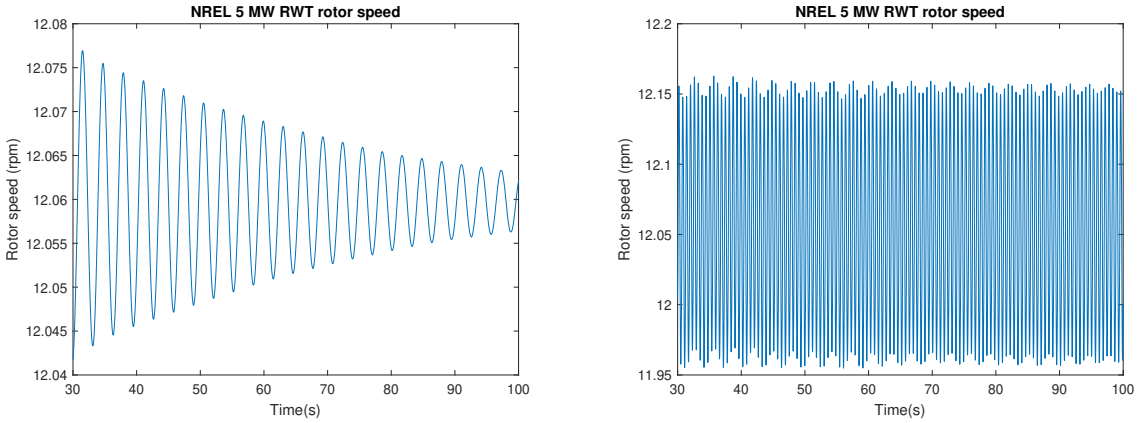

Source: Author (2022)

Figure 30 – NREL 5 MW RWT generator power with all the DOFs active (left) and NREL 5 MW RWT rotor speed with only one DOF (rotor azimuth) active (right) - State-space Controller based on 1-DOF model

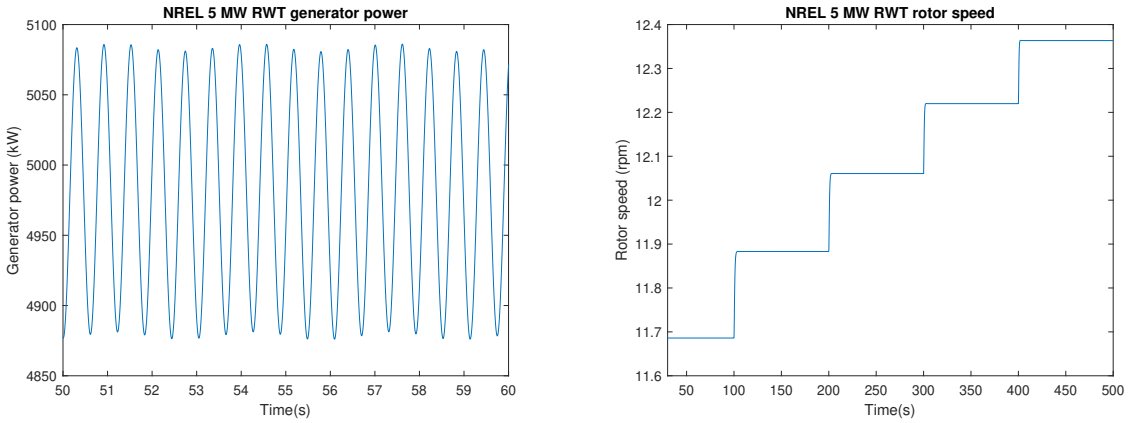

Source: Author (2022)

fits very well to wind turbine structural control. Second, the full-state feedback allows to address several WT flexible modes taken all of them into consideration in the control design, since they are associated with the states of the state-space model. Third, the MIMO control enables the use of more than one control input, and therefore individual pitch control (IPC), where each blade receives a different control signal, is feasible. The state-space controllers developed here are:

- State-space CPC 5-DOF Controller
- State-space IPC 4-DOF Controller

5.6.2.2 State-space CPC 5-DOF Controller

5.6.2.2.1 Control design

The control objectives of this controller are the rotor speed control and the mitigation of tower fore-aft loads. We focus on developing a control that works satisfactorily even with all the WT flexible DOFs considered in simulation. For attaining the proposed objectives, it is necessary to develop a model with 5-DOFs, i.e., rotor azimuth, drive-train torsion, first edgewise blade mode, first flapwise blade mode and first tower fore-aft mode. The term 'mode' is used herein as short for 'flexible mode' (e.g., where there is first flapwise blade mode, it should be understood, first flapwise blade flexible mode). Additionally, the term CPC refers to collective pitch control, since in this controller all the blades will receive the same control command.

The model for control design is established in the state-space form. Each DOF will correspond to 2 states, since both the DOF and its derivative must be included in the model. Thereby, this will result, for this case, in a 10-state model. However, one exception is the rotor azimuth DOF, from which just the derivative needs to be considered (indeed, the rotor azimuth position is of no importance for dynamics). In this way, we obtain a 9-state model in the form,

$$\begin{aligned} \dot{\mathbf{x}} &= \mathbf{A}\mathbf{x} + \mathbf{B}\mathbf{u} + \mathbf{B_d}\mathbf{u_d} \\ \mathbf{y} &= \mathbf{C}\mathbf{x} + \mathbf{D}\mathbf{u} \end{aligned} \tag{5.48}$$

where $\mathbf{A}$ is the 9x9 state matrix, $\mathbf{B}$ is the control matrix, $\mathbf{B_d}$ is the disturbance matrix, $\mathbf{C}$ is the output matrix $\mathbf{D}$ is the direct transmission matrix, and $\mathbf{D_d}$ is the direct transmission disturbance matrix. The state vector is represented by $\mathbf{x}$ and the output vector by $\mathbf{y}$. The values for the state-space matrices are obtained by a linearization around the mid-range Region 3 operating point. For the NREL 5 MW RWT, the 9-state model state and control matrices are written below. These matrices are here to showcase an example. The complete matrices are not shown here for conciseness.

$$A = \begin{bmatrix} 0.000 & 0.000 & 0.000 & 0.000 & 1.000 & 0.000 & 0.000 & 0.000 & 0.000 \\ 0.000 & 0.000 & 0.000 & 0.000 & 0.000 & 0.000 & 1.000 & 0.000 & 0.000 \\ 0.000 & 0.000 & 0.000 & 0.000 & 0.000 & 0.000 & 0.000 & 1.000 & 0.000 \\ 0.000 & 0.000 & 0.000 & 0.000 & 0.000 & 0.000 & 0.000 & 0.000 & 1.000 \\ -4.469 & 22.181 & 0.262 & 0.836 & -0.066 & -0.103 & 0.055 & 0.022 & 0.006 \\ -0.000 & 172.600 & 0.000 & 0.000 & 0.000 & 0.000 & 1.237 & -0.000 & -0.000 \\ 0.047 & -327.075 & 0.377 & -2.993 & -0.056 & -0.126 & -2.471 & 0.012 & -0.004 \\ 8.026 & 6138.907 & -37.024 & 118.705 & -9.425 & -64.900 & -21.225 & -6.831 & -1.808 \\ 7.661 & -12730.370 & 30.709 & -294.299 & -5.037 & -7.790 & -99.154 & 0.602 & -0.522 \end{bmatrix}$$

$$B = \begin{bmatrix} 0.000 \\ 0.000 \\ 0.000 \\ 0.000 \\ -0.812 \\ -0.000 \\ 1.687 \\ -809.046 \\ 106.897 \end{bmatrix} \tag{5.49}$$

5.6.2.2.2 Multiblade Coordinate Transformation (MBC)

At this point, since blade DOFs are included in the WT model, it is necessary to discuss the blades rotation movement and how they are taken into account in the linearization. In fact, the linear models are obtained running a steady wind simulation for a long time, until all the transient behavior disappear, and using a numerical perturbation technique within OpenFAST (RINKER et al., 2020). Since the rotor is in movement (in constant speed, when linearizing), every azimuthal position defines a different operating point, with different dynamic characteristics for the analyzed system, i.e., the WT.

A linearization can be performed in any of these operating points characterized by the infinite azimuthal positions of the blades along the 360° of spinning. The adopted solution is to linearize the WT in several points and take the mean of the obtained linear models. However, since the WT is a periodic system, averaging the linear models would cancel some dynamics due to the existence of the harmonics functions underlying to these models. The solution is to use a Multiblade Coordinate Transformation (MBC), also called the Coleman transform or d-q transform (PETROVIć; JELAVIć; BAOTIć, 2015). It basically consists in a change of reference frame, to express quantities relatives to the blades' coordinate (rotating) systems in a fixed coordinate system. In this way, the effects

of each blade are accounted for as a whole, which is why the new coordinates are also called rotor coordinates (in opposite to individual blades). Following this argument, the MBC transformation is defined as (BIR, 2008):

$$q_0 = \frac{1}{N}\sum_{b=1}^{N} q_b \tag{5.50}$$

$$q_{nc} = \frac{2}{N}\sum_{b=1}^{N} q_b cos(n\psi_b) \tag{5.51}$$

$$q_{ns} = \frac{2}{N}\sum_{b=1}^{N} q_b sin(n\psi_b) \tag{5.52}$$

Where q_b is a generic blade degree-of-freedom. The q_0, q_{nc} and q_{ns} are called the collective, cosine-cyclic and sine-cyclic modes, respectively. Once the MBC transformation is realized, we proceed the averaging process of the linear models without risking of disregard periodic dynamics, and we see the blades individual DOFs as rotor DOFs. Therefore, in the matrices obtained in the previous section, this procedure was employed. The NREL 5 MW RWT was linearized around 36 azimuth positions (each one corresponding to an operating point), the MBC transformation was executed, and the averaging was carried out to get the final matrices (such as the matrix $\mathbf{A}$ shown in this section).

5.6.2.2.3 Pole placement, observers and Disturbance Accommodating Control (DAC)

With the state-space model acquired, one needs to choose the new pole locations to run pole placement. We will execute this task using also an observer and the method of Disturbance Accommodating Control (DAC). Observers are fundamental in state-space control design, because the full-state feedback requires measurements for all the system states, which most often is not possible or feasible. Thus, the observers enable to estimate the states not directly measured from a mathematical model of the system and the values of the states directly measured (GOLNARAGHI; KUO, 2017). For example, in the WTs, variables corresponding to blades, drive-train or nacelle can be unreachable or the cost of installing many sensors can be raised. This situation is common practice in control engineering, and state-space is very frequently accompanied by an observer. The model for a state observer is in Eq. 5.54,

$$\dot{\tilde{\mathbf{x}}} = \mathbf{A}\tilde{\mathbf{x}} + \mathbf{B}\mathbf{u} + \mathbf{K_e}(\mathbf{y} - \tilde{\mathbf{y}}) \tag{5.53}$$

$$\tilde{\mathbf{y}} = \mathbf{C}\tilde{\mathbf{x}} + \mathbf{D}\mathbf{u} \tag{5.54}$$

where $\tilde{x}$ and $\tilde{y}$ are estimates for the states and outputs, $\mathbf{K_e}$ is the observer gain and the other matrices are defined as before. Comparing Eqs.5.67 and 5.54, the error between the state and the estimate is given by

$$\mathbf{e} = \mathbf{x} - \tilde{\mathbf{x}} \tag{5.55}$$

$$\dot{\mathbf{e}} = (\mathbf{A} - \mathbf{K_e}\mathbf{C}\mathbf{e}) \tag{5.56}$$

Thereby, choosing an appropriate observer gain $\mathbf{K_e}$ it is possible to get a decreasing error dynamics. It is noteworthy that not all systems can use observers. In order to adopt this approach, it is required that the system matrices (Eq. 5.67 meets the requirements of observability (NISE, 2015). Also, for pole placement control, the system needs to meet the requirements of controllability (HENRIKSEN; HANSEN; POULSEN, 2012). These will be checked for the present control system. The DAC method is a non-conventional control strategy which uses the presence of an observer to include the estimation of disturbances in the control system (WANG; WRIGHT; BALAS, 2017). By doing that, the effect of such disturbances can be attenuated. For the wind turbines control, this is a very suitable method, since the wind can be seen as a persistent disturbance to the system. DAC relies on an assumed disturbance model:

$$\begin{aligned} \dot{\mathbf{z}}_\mathbf{d} &= \mathbf{F}\mathbf{z}_\mathbf{d} \\ \mathbf{u}_\mathbf{d} &= \mathbf{\Theta}\mathbf{z}_\mathbf{d} \end{aligned} \tag{5.57}$$

where the outputs of this state-space model are the disturbance states $\mathbf{u_d}$. The DAC auxiliary states are $\mathbf{z_d}$ and the state and output matrices are $\mathbf{F}$ and $\mathbf{\Theta}$, respectively. These matrices are chosen according to the kind of disturbance is being modeled. In this State-space CPC 5-DOF Controller, we are interested in uniform wind variations, since the control objectives are rotor speed control and tower loads mitigation. In the next controller, we will be interested in reducing blade asymmetric loads and an asymmetric wind model will be used. Therefore, in State-space CPC 5-DOF Controller we have for the DAC matrices:

$$\begin{aligned} \dot{\mathbf{z}}_\mathbf{d} &= \mathbf{0}\mathbf{z}_\mathbf{d} \\ \mathbf{u}_\mathbf{d} &= \mathbf{z}_\mathbf{d} \end{aligned} \tag{5.58}$$

which reflects a steady wind. Once the disturbances states have been estimated, their effect can be eliminated by considering an additional control gain $\mathbf{K_d}$ as follows,

$$\mathbf{u} = \mathbf{K}_\mathbf{d}\mathbf{z}_\mathbf{d} \tag{5.59}$$

$$||\mathbf{B}\mathbf{K}_\mathbf{d} + \mathbf{B}_\mathbf{d}\mathbf{\Theta}|| = \mathbf{0} \tag{5.60}$$

By comparing Eqs. 5.60 and 5.57 with Eq. 5.67, one can see that using $\mathbf{u}$ (control input) as in Eq. 5.59 will effectively cancel the effect of the disturbance $\mathbf{u_d}$. The condition in Eq. 5.60 is achieved by simply matrix manipulation.

Now, we must determine the pole locations for both the controller and observers, and calculate the disturbance gain. Initially, it is necessary to determine if the system is controllable and observable. The conditions for controllability and observability are well-known (DORF; BISHOP, 2021) The condition for controllability is that the matrix

$$\begin{bmatrix} B & AB & \dots & A^{n-1}B \end{bmatrix} \tag{5.61}$$

has full-rank. The condition for observability is that the matrix,

$$\begin{bmatrix} C \\ CA \\ . \\ . \\ . \\ CA^{n-1} \end{bmatrix} \tag{5.62}$$

has also full-rank. Both conditions are satisfied for the system considered here.

Analyzing the eigenvalues of the state matrix $\mathbf{A}$, we have:

$$\begin{bmatrix} -1.3529 + 22.7188i \\ -1.3529 - 22.7188i \\ -0.2609 + 10.7883i \\ -0.2609 - 10.7883i \\ -3.0844 + 3.4997i \\ -3.0844 - 3.4997i \\ -0.1437 + 2.1035i \\ -0.1437 - 2.1035i \\ -0.2062 + 0.0000i \end{bmatrix} \tag{5.63}$$

Analyzing the corresponding eigenvectors, not written here by conciseness, one can see that the eigenvalue which most contributes to tower fore-aft DOF is located at -0.1437 ± 2.1035 and that the eigenvalue which most contributes to rotor speed is located at -0.2062. In order to obtain a better response, we choose to place these poles at -0.30 ± 2.1035 and -1.5. Additionally, we identify the pole in -0.2609 ± 10.7883 as the least damped pole. In fact, it corresponds to the first edge DOF of the NREL 5 MW RWT, which has already been proven to be causing instability. We choose -0.8 ± 10.8 as its new pole location. With these pole locations, we run pole placement procedure and obtain for the control gain

$$\mathbf{K_{FB}} = [-0.042099 \; -8.1133 \; -0.013691 \; 0.04953 \; -0.03028 \; -0.9409 \; -1.8229 \; -0.0040506 \; 0.024173] \tag{5.64}$$

The disturbance control gain, on the other hand, is calculated as:

$$\mathbf{K_d} = [-0.010305] \tag{5.65}$$

The total control gain is used to form the control input (Eq. 5.10) as

$$\mathbf{u} = -\mathbf{K}\mathbf{x} = -\mathbf{K_{FB}}\mathbf{x} - \mathbf{K_d}\mathbf{u_d} \tag{5.66}$$

where the total control gain $\mathbf{K}$ is composed by the full-state feedback gain $\mathbf{K_{FB}}$ and the control disturbance gain $\mathbf{K_d}$.

Figure 31 – State-space CPC 5-DOF Controller - main diagram

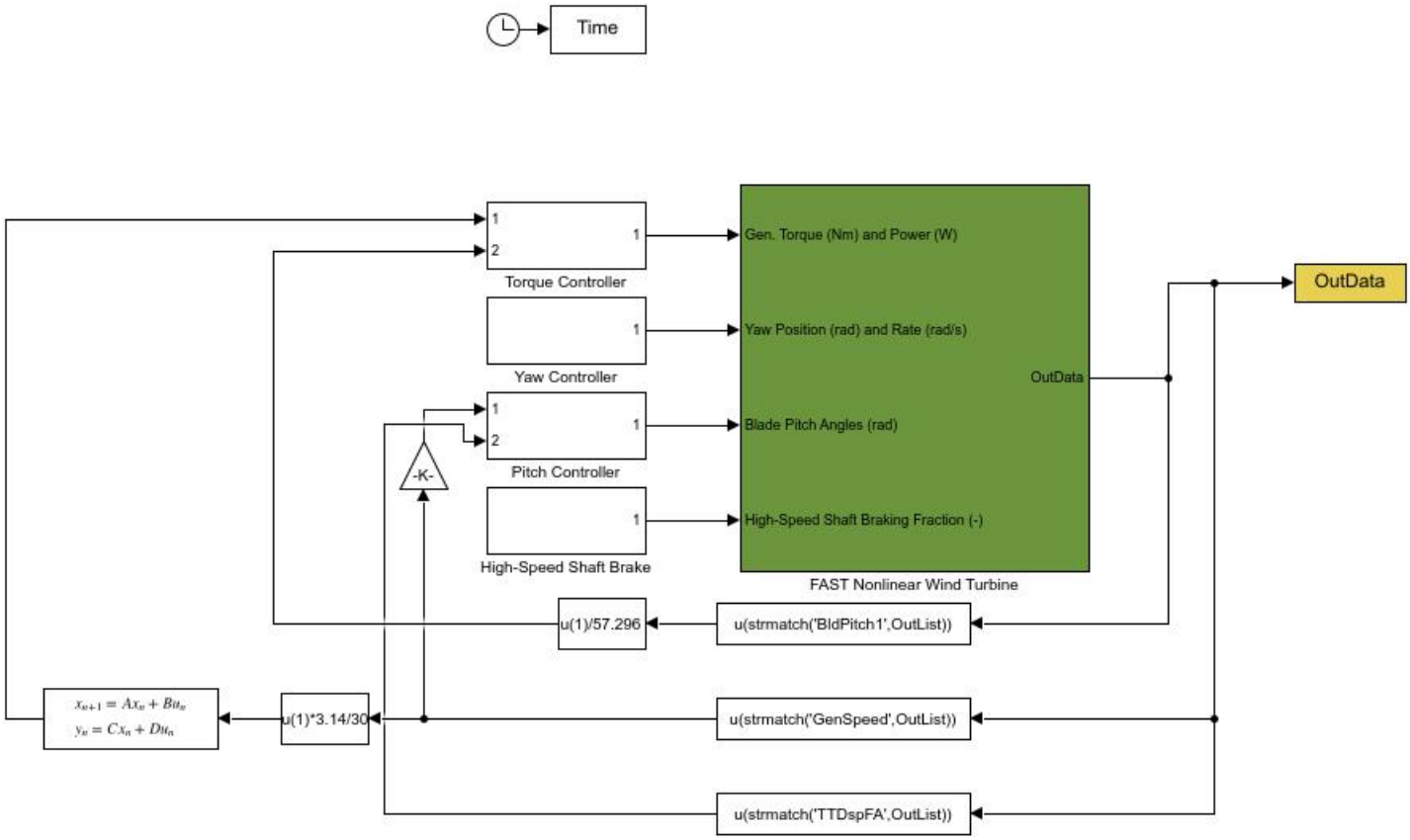

Source: Author (2022)

5.6.2.2.4 Overview of State-space CPC 5-DOF Controller

In Fig. 31 we have an overview of the State-space CPC 5-DOF Controller. The rotor speed and the tower-top displacement fore-aft are used as feedback signals to the pitch controller. This is necessary to ensure observability of the system. In Fig. 32 the detailing of pitch controller is shown. It is possible to see the observer and the collective pitch command for the blades.

5.6.2.2.5 Results

The set of simulations consider steady wind conditions from $v = 14m/s$ to $v = 18m/s$. Afterwards, turbulent wind conditions at $v = 18m/s$ are simulated, with the same turbulence characteristics of Sec. 5.6.1.2.6 (according to IEC 61400-1). The results for steady wind conditions are shown in Fig. 33, along with the blade pitch command signal. As can be seen, the rotor speed is satisfactorily controlled, with little speed overshoot. It is remarkable that this control is being applied without the necessary filter employed in the Baseline DLL Controller. Therefore, even with all the DOFs enabled in simulation and without filtering, the CPC 5-DOF controller performs well. The blade pitch angles are within reasonable limits. The control objective of rotor speed regulation is reached, but we

Figure 32 – State-space CPC 5-DOF Controller - Pitch Controller diagram

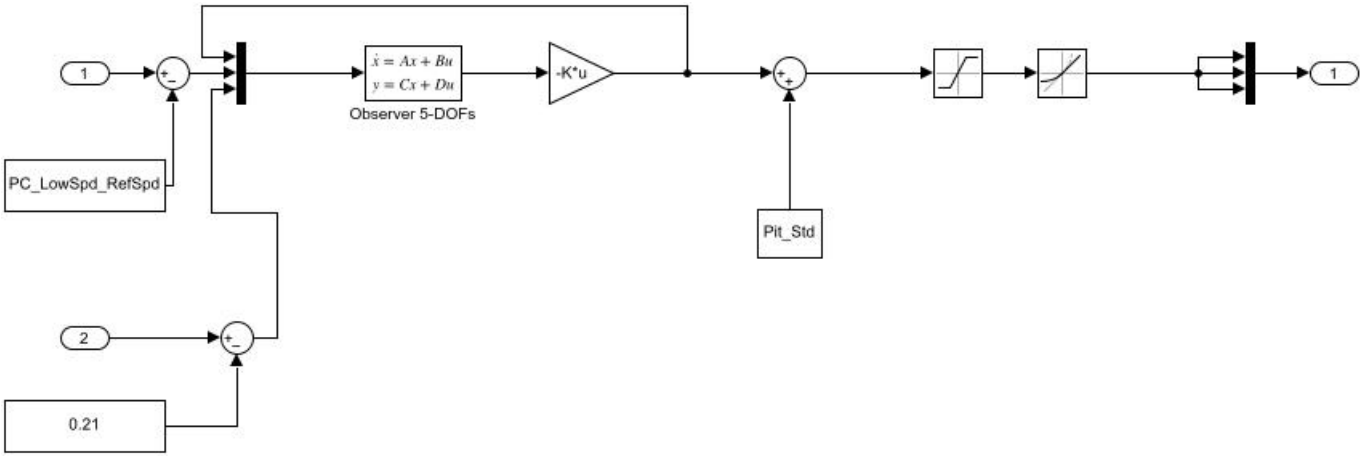

Source: Author (2022)

need to check load mitigation. For this, results are shown in Fig. 34, where a comparison with the Baseline DLL Controller and the Classical PID Controller is done. It is possible to infer from the figure that the State-space CPC 5-DOF Controller indeed reduces the tower oscillations, mainly after a wind change (after each 100s). Performance slightly degrades for high winds. Turbulent simulations are presented in Fig. 35. As expected, the CPC 5-DOF Controller appears to reduce the overall vibration level. This needs to be confirmed using a fatigue analysis method, which will be studied in the next sections of this chapter.

Figure 33 – NREL 5 MW RWT rotor speed (left) and NREL 5 MW RWT commanded pitch angle (right) with all the DOFs active - State-space Controller based on 5-DOF model

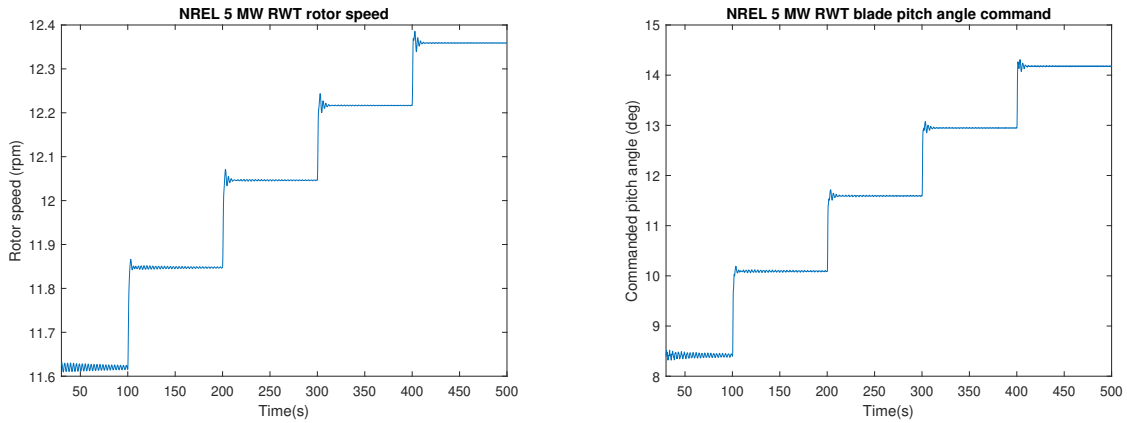

Source: Author (2022)

Figure 34 – NREL 5 MW RWT tower base fore-aft moment with all the DOFs active. Comparisons with Baseline DLL Controller (left) and Classical PID Controller based on 1-DOF model (right) - State-space Controller based on 5-DOF model

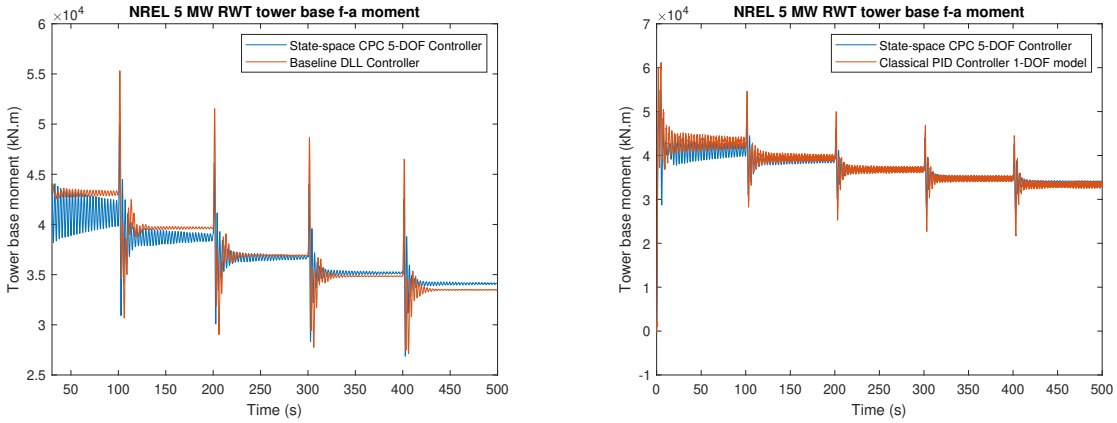

Source: Author (2022)

Figure 35 – NREL 5 MW RWT tower base fore-aft moment with all the DOFs active. Comparisons with Baseline DLL Controller (left) and Classical PID Controller based on 1-DOF model (right), turbulent conditions - State-space Controller based on 5-DOF model

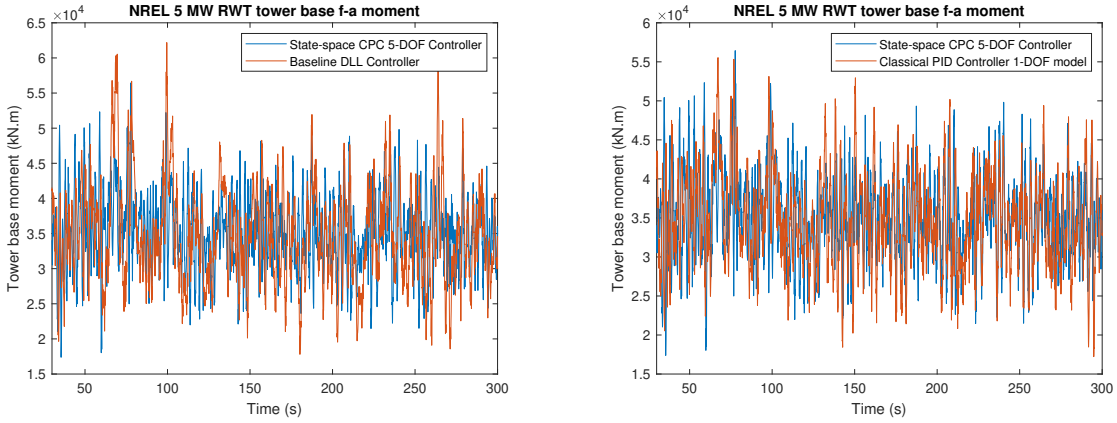

Source: Author (2022)

5.6.2.3 State-space IPC 4-DOF Controller

5.6.2.3.1 Control design

The control objectives of this controller are rotor speed control and the mitigation of blades' loads. Using state-space modeling, it is possible to develop an individual pitch controller (IPC), in which each blade receives different control signals. This is not the standard control used in today's wind turbines, but it is expected to be largely used in the near future. For attaining the proposed objectives, a model with 4-DOF is necessary: rotor azimuth, first collective flapwise blade mode, first cosine flapwise blade mode and first sine flapwise blade mode. Our objective is to mitigate blade flap structural loads.

The model for control design is established in the state-space form. Each DOF will correspond to 2 states, since both the DOF and its derivative must be included in the model. Thereby, this will result, for this case, in a 8-state model. However, with the exception of the rotor azimuth DOF (as in the previous Section of CPC controller), we obtain a 7-state model in the form,

$$\begin{aligned}\dot{\mathbf{x}} &= \mathbf{A}\mathbf{x} + \mathbf{B}\mathbf{u} + \mathbf{B_d}\mathbf{u_d} \\ \mathbf{y} &= \mathbf{C}\mathbf{x} + \mathbf{D}\mathbf{u}\end{aligned} \tag{5.67}$$

where the vectors and matrices are defined as before. The difference here is on the dimensions of the control and disturbance matrices, as well as in control input. Since we are designing an IPC controller, there are 3 control inputs, and the dimension of $\mathbf{u}$ is 3x1. Following this, $\mathbf{B}$ has dimensions 7x3. Regarding the disturbances, $\mathbf{B_d}$ has dimensions 7x2, because in IPC we will consider one disturbance state for uniform wind and another state for wind variations caused by shear. All the matrices are presented in Appendix B. The MBC transformation is applied and the conditions of controllability and observability are checked. Next, analyzing the eigenvalues of state matrix $\mathbf{A}$, one obtains:

$$\begin{bmatrix} -0.20415 + 0i \\ -3.1497 + 4.6739i \\ -3.1497 - 4.6739i \\ -3.1692 + 3.5823i \\ -3.1692 - 3.5823i \\ -3.1521 + 2.1411i \\ -3.1521 - 2.1411i \end{bmatrix} \tag{5.68}$$

Analyzing the corresponding eigenvectors, one can see that the eigenvalue which most contributes to rotor speed is again, as expected, at -0.2014. Besides, the cosine and sine cyclic components of the blade flap movement are strongly influenced by the remaining eigenvectors. We place these poles further to the left in order to increase damping, in $-1, -6.14 + 4.67i, -6.14 - 4.67i, -12.16 + 6.58i, 12.16 - 6.58i, -12.15 + 2.14i$ and $-12.15 - 2.14i$. With these pole locations, we run pole placement procedure and obtain for the control gain

$$\mathbf{K_{FB}} = \begin{bmatrix} -0.12506 & 0.0094572 & -0.085352 & -3.2602 & -0.018406 & 0.0024807 & -0.0052434 \\ 0.024397 & -0.12616 & -0.02935 & 0.55669 & 0.00011573 & -0.019385 & 0.00021675 \\ -0.030771 & 0.077194 & -0.15588 & -0.83368 & -0.002922 & 0.003265 & -0.021382 \end{bmatrix} \tag{5.69}$$

Note that the control gain now has 3 lines, since the control input will be 3-fold in this case. The disturbance gain is calculated as:

$$\mathbf{K_d} = \begin{bmatrix} 0.014754 & 0.014754 \\ -6.9035e-05 & -6.9035e-05 \\ -0.00011301 & -0.00011301 \end{bmatrix} \tag{5.70}$$

Note that the disturbance gain now has 3 lines, corresponding to the 3 control inputs, and 2 columns, because here we are modeling two disturbance types: the uniform wind over the rotor and the variation due to wind shear. In fact, the DAC matrices for this modeling are:

$$\begin{bmatrix} \dot{z}_{d1} \\ \dot{z}_{d2} \\ \dot{z}_{d3} \end{bmatrix} = \begin{bmatrix} 0 & 1 & 0 \\ -\Omega^2 & 0 & 0 \\ 0 & 0 & 0 \end{bmatrix} \begin{bmatrix} z_{d1} \\ z_{d2} \\ z_{d3} \end{bmatrix}$$
$$\begin{bmatrix} u_{d1} \\ u_{d2} \end{bmatrix} = \begin{bmatrix} 1 & 0 & 0 \\ 0 & 0 & 1 \end{bmatrix} \tag{5.71}$$

in which z_{d1}, z_{d2}, z_{d3} are the DAC-states and u_{d1} and u_{d2} are the disturbance states that are estimated by the observer.

5.6.2.3.2 Overview of State-space IPC 4-DOF Controller

In Fig. 36 we have an overview of the State-space IPC 4-DOF Controller. It is possible to see that the inputs to the Pitch Controller include not only rotor speed, but also the flap displacements of the three blades, what is necessary to ensure observability. Additionally, before being input to controller, the flap displacements pass by the MBC-transformation block. This block also receives the rotor azimuth information, to implement Eqs. 5.50-5.52. The Pitch Controller detailing is shown in Fig. 37. Two points deserve emphasis here. The presence of the MBC-inverse transformation is necessary because the calculated control inputs are in the MBC-reference and the blades need the pitch commands in their own reference. The flap references block contain the values of steady blade flaps transformed by MBC, around which the system was linearized. At the output, this block configuration results in three different pitch angles signals for the blades.

5.6.2.3.3 Results

The set of simulations consider steady wind conditions without wind shear, and then with a imposed wind shear of $\alpha = 0.2$. Afterwards, turbulent simulation results are presented. The steady wind conditions without shear are shown in Fig. 38, for a wind varying from $v = 14m/s$ to $v = 18m/s$. It is possible to verify that rotor speed has very little oscillation, despite a small error regarding the desired value of 12.1 rpm. On the other hand, from $v = 17m/s$ and above, high frequency oscillations appear, even though the variation is very reduced in amplitude (in the order of 0.001 rpm). However, for regions around $v = 16m/s$ where the system was linearized, the control performance is completely satisfactory. Results for load reduction are also presented in Fig. 38, comparing to the Baseline DLL Controller. As one can see, the reduction is substantial for wind speeds below and equal to $v = 16m/s$. Performance degrades for superior wind speeds. This

Figure 36 – State-space IPC 4-DOF Controller - main diagram

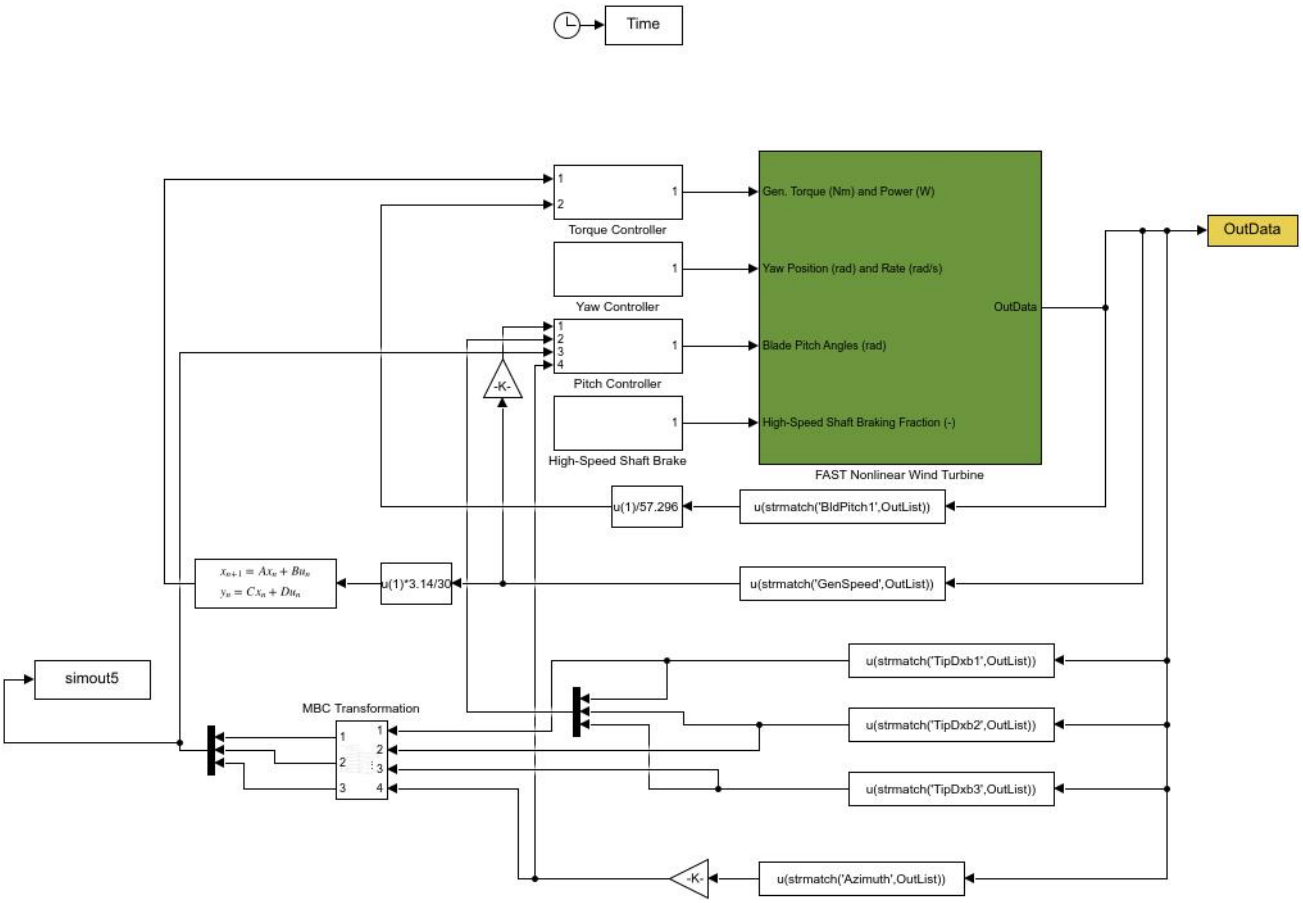

Source: Author (2022)

Figure 37 – State-space IPC 4-DOF Controller - Pitch Controller diagram

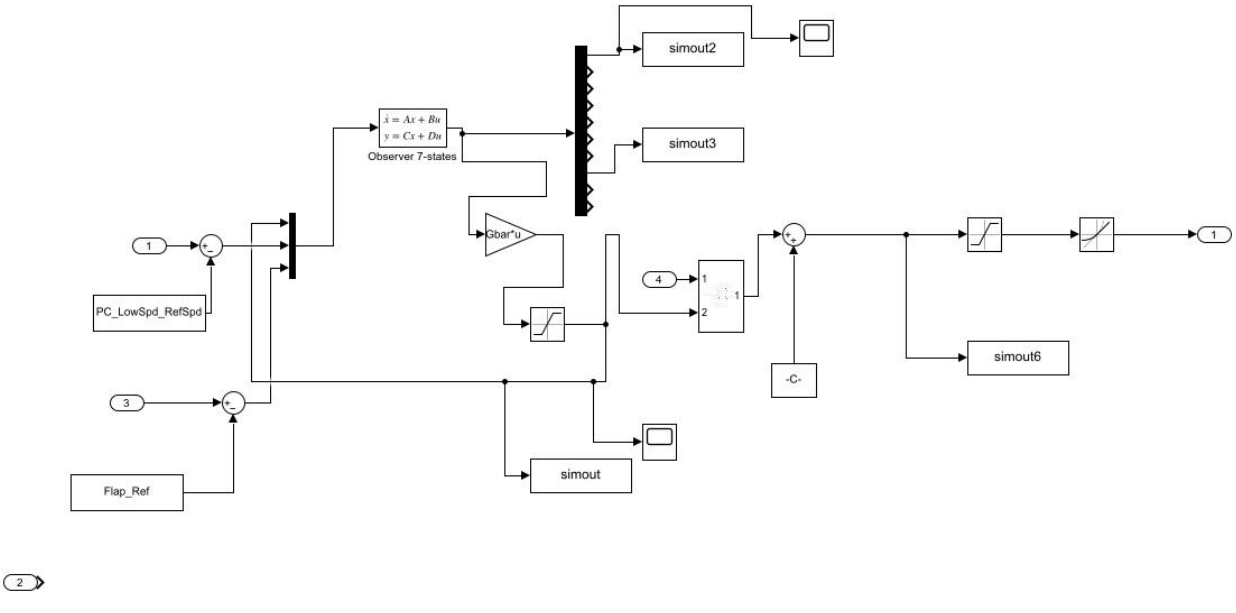

Source: Author (2022)

indicates the need for designing several state-space controllers like the one developed here and applying them as long as the wind changes. It is also noteworthy that the State-space IPC 4-DOF Controller uses no filter, while the Baseline DLL Controller relies on external filtering to work as expected. The results of simulations with wind shear are presented in Fig. 39, for a wind of $v = 16m/s$. The results are outstanding. The State-space IPC 4-DOF controller indeed mitigates the blade root flapwise moments that are increased by wind shear. The blade pitch angles activity is shown in Fig. 40, denoting that the IPC commands are indeed cyclic and different for each blade. At last, turbulent simulation with $v = 16m/s$ and the already discussed turbulent characteristics is presented in Fig. 41. As one can see, the blade root flapwise moment is reduced for the IPC controller.

Figure 38 – NREL 5 MW RWT rotor speed (left) and NREL 5 MW RWT blade root flapwise moment (right) with all the DOFs active - State-space IPC Controller based on 4-DOF model

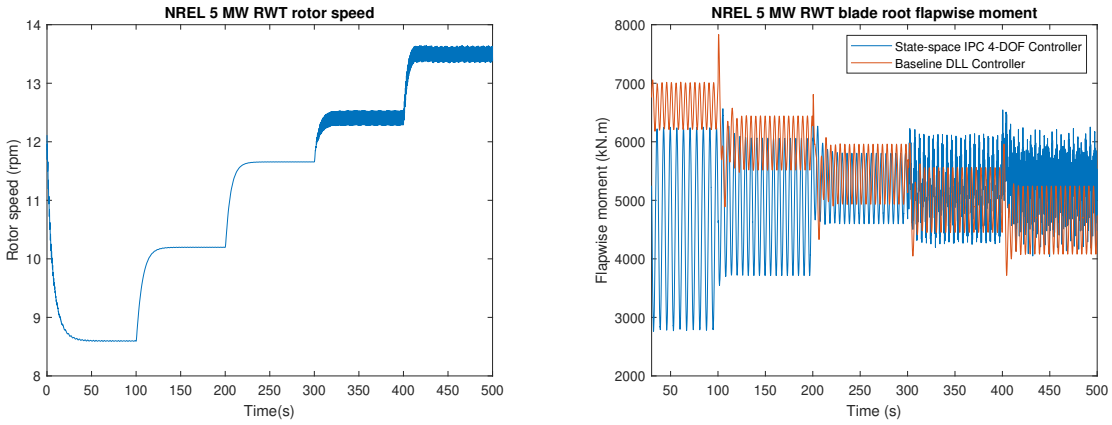

Source: Author (2022)

5.6.3 H_∞ Controller

The work in this section has been submitted for publication in the ***Engineering Structures*** *journal*

5.6.3.1 Control design

H_∞ design allows to obtain the WT controller using an optimization approach. The control objectives of the present H_∞ controller are rotor speed control and tower loads mitigation. Based on that, the number of DOFs in the model should be defined. At this point, given we are interested in the control of tower loads and rotor speed, the model is chosen to have the rotor azimuth, drive-train torsion and tower fore-aft (axial) DOFs. This provides 3x3 mass, damping and stiffness matrices, that for control purposes may be transformed to the state-space representation, resulting in 6x6 state-space matrices. The influence of rotor azimuth is accounted for just for rotor speed and therefore rotor

Figure 39 – NREL 5 MW RWT blade root flapwise moment with all the DOFs active - State-space IPC 4-DOF Controller

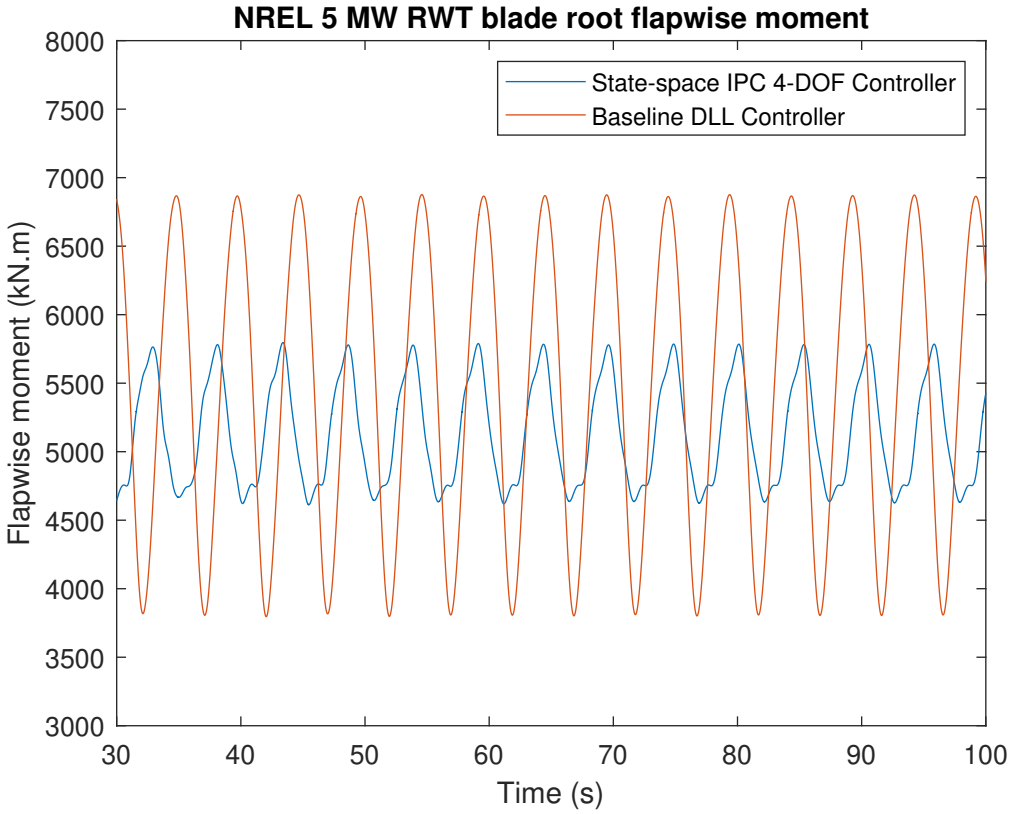

Source: Author (2022)

azimuth position can be discarded. Thus, the state-space model contains 5x5 matrices, written in the usual form presented in the previous sections, and is shown in Eq. 5.72.

$$A = \begin{bmatrix} 0 & 0 & 1 & 0 & 0 \\ 1 & 0 & 0 & 0 & 1 \\ -4.23 & 0.32 & -0.31 & -1.09 & -1.09 \\ 0 & 172.6 & 0 & 0 & 1.24 \\ -9.81e-4 & -194.88 & -0.04 & -0.23 & -1.62 \end{bmatrix} B = \begin{bmatrix} 0 \\ 0 \\ -11.5 \\ 0 \\ -1.44 \end{bmatrix} B_d = \begin{bmatrix} 0 \\ 0 \\ 0.223 \\ -1.48 \cdot 10^{-17} \\ 0.0337 \end{bmatrix}$$

$$C = \begin{bmatrix} 0 & 0 & 0 & 9.55 & 9.55 \\ 1.0 & 0 & 0 & 0 & 0 \end{bmatrix} D = \begin{bmatrix} 0 & 0 \\ 0 & -6.17 \cdot 10^4 \end{bmatrix} \quad (5.72)$$

It is worth noting that the output matrix C has dimension 2x1, with the first line corresponding to the rotor speed and the second one to the tower fore-aft displacement, which are the two relevant system outputs. Also, the system has two inputs, the blade pitch and the wind speed, represented by the matrices B and B_d. In order to apply H_∞ techniques, this state-space model must be converted to transfer function form, originating a transfer function matrix $G(s)$

Figure 40 – NREL 5 MW RWT commanded pitch angles - State-space IPC 4-DOF Controller

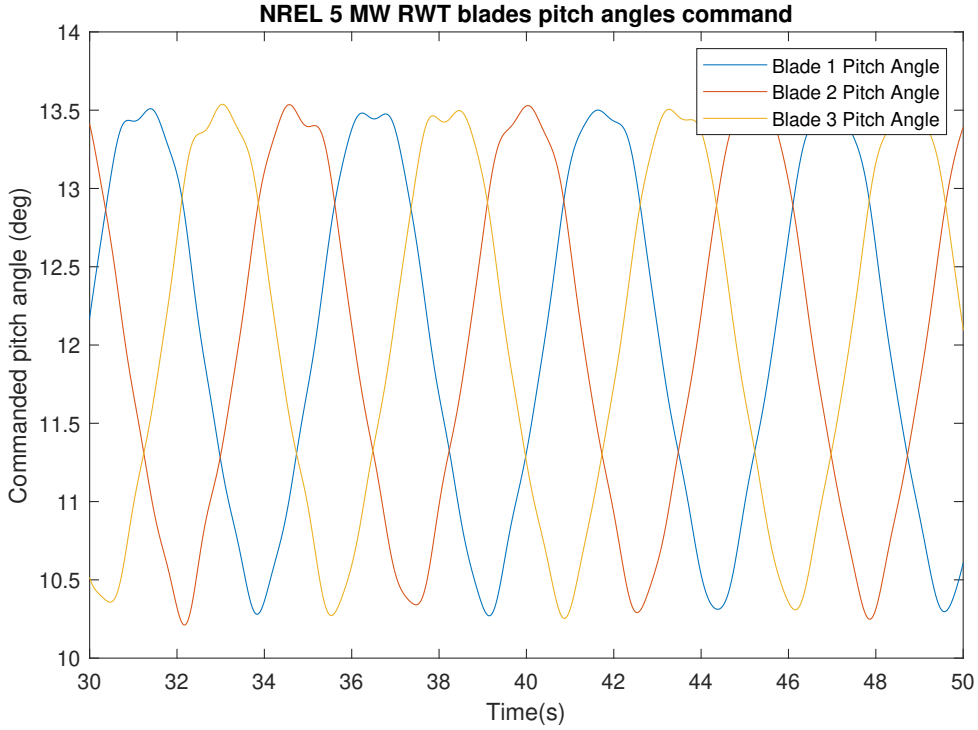

Source: Author (2022)

$$G(s) = \begin{bmatrix} \frac{-13.7s^4-17.3s^3-2432s^2-134s-1000}{s^5+1.9s^4+200s^3+105.7s^2+830.5s+165.7} & \frac{-11.5s^3-17.1s^2-2240s-179}{s^5+1.9s^4+200s^3+105.7s^2+830.5s+165.7} \\ \frac{0.32s^4+0.42s^3+57s^2+5.8+234.7}{s^5+1.9s^4+200s^3+105.7s^2+830.5s+165.7} & \frac{-60000s^5-1.2\cdot10^5s^4-1.2\cdot10^7s^3-6.5\cdot10^6s^2-5.1\cdot10^7s-1\cdot10^7}{s^5+1.9s^4+200s^3+105.7s^2+830.5s+165.7} \end{bmatrix} \tag{5.73}$$

In Eq. 5.73, the first line corresponds to rotor speed and the second line to tower fore-aft displacement; the first column corresponds to the pitch control signal and the second column to the wind speed, which is the disturbance to the control system. This transfer function matrix completely characterizes the system and shall be used for control design purposes.

Given the obtained transfer function matrix $G(s)$, it is possible to design a controller to reduce WT tower structural loads and at the same time maintain the rotor speed under acceptable levels. Since the modeling was done with two outputs, rotor speed and tower displacement, and one control input, the pitch actuator, the plant transfer function is presented in Eq. 5.74, which corresponds to the model developed in the previous section without the wind disturbances, that will be mitigated by the sensitivity function design.

$$G(s) = \begin{bmatrix} \frac{-13.7s^4-17.3s^3-2432s^2-134s-1000}{s^5+1.9s^4+200s^3+105.7s^2+830.5s+165.7} \\ \frac{0.32s^4+0.42s^3+57s^2+5.8+234.7}{s^5+1.9s^4+200s^3+105.7s^2+830.5s+165.7} \end{bmatrix} \tag{5.74}$$

Figure 41 – NREL 5 MW RWT blade root flapwise moment with all the DOFs active, turbulent conditions - State-space IPC 4-DOF Controller

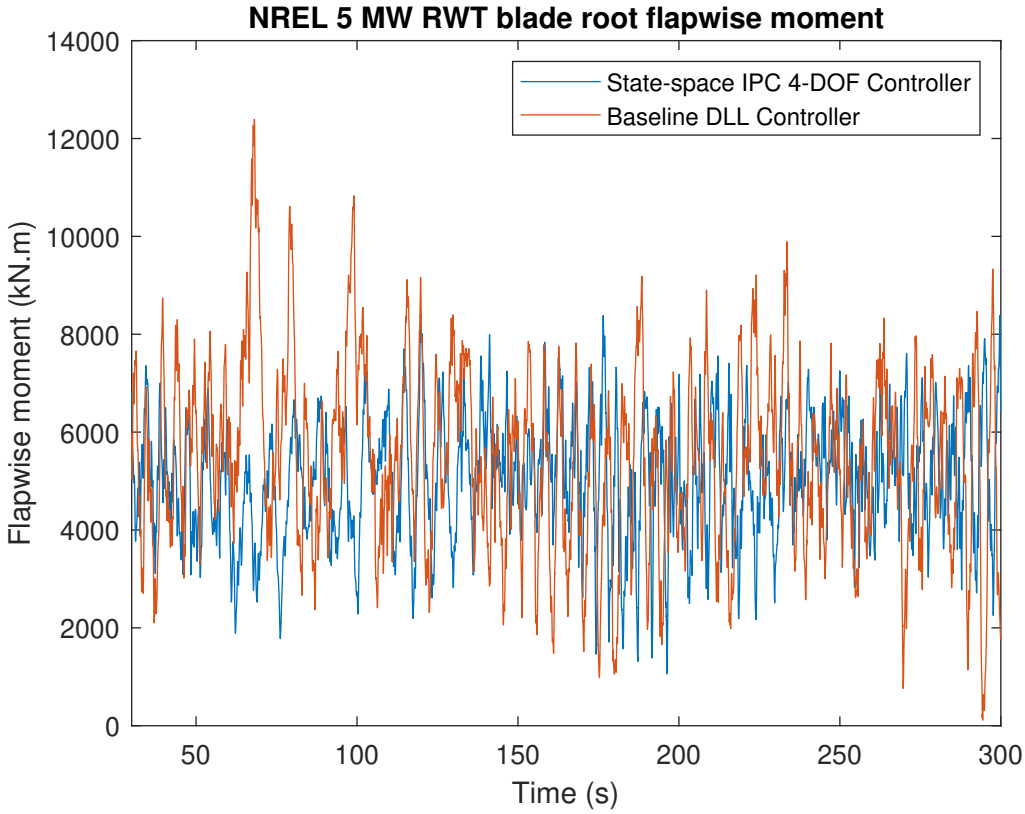

Source: Author (2022)

As previously stated in Sec. 5.4, the sensitivity function S may be obtained as

$$S = (I + GK)^{-1} \tag{5.75}$$

In a multivariable system with two outputs, the S function is actually a 2x2 matrix transfer function. By combining Eqs. 5.74 and 5.75, the sensitivity is given as in Eq. 5.76

$$S(s) = \begin{bmatrix} \frac{s^4+0.37s^3+8.48s^2+0.61s}{s^4+1.87s^3+9.24s^2+8.01s} & \frac{-0.35s^3-0.12s^2-1.49s-0.35}{s^5+8.01s^4+41.24s^3+62.08s^2+130.30s+19.93} \\ \frac{0.02s^3-22.05s^2-6.16s-0.35}{s^5+9.37s^4+48.04s^3+74.38s^2+156.30s+20.77} & \frac{s^5+9.37s^4+48.04s^3+73.97s^2+156.20s+20.76}{s^5+9.37s^4+48.04s^3+74.38s^2+156.30s+20.77} \end{bmatrix} \tag{5.76}$$

The S transfer function matrix was obtained for a unitary controller. To achieve the desired performance, it is necessary to choose the weighting H_∞ functions and minimize the H_∞ norm, based on the desired shape for the sensitivity function. The current frequency response of S is shown through the singular values of S matrix, in Fig. 42. As it can be seen, the frequency response presents several ressonance peaks that must be eliminated. Also, the response magnitude should be maintained small to reduce the effect of wind disturbances in control. Further, it is desirable to keep closeness between the singular values to minimize noisy inputs. Choosing a first-order transfer weighting function given by $W_1 = \frac{s+1}{2s+0.03}$, with high gain in the low frequency range and smooth frequency behavior, these characteristics

of S matrix are ensured when the optimization process is executed. Regarding to W_2, it is sufficient that the H_∞ controller effort does not surpass the maximum value of $W_2 = 1$, so as to the control signal energy does not achieve unfeasible values.

Figure 42 – Sensitivity function frequency-domain response

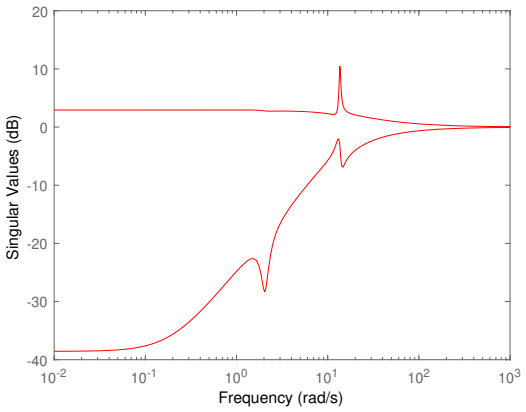

Source: Author (2022)

The frequency response of W_1^{-1} is shown in Fig. 43, along with the resulting new S function after the application of H_∞ optimization procedure. Nevertheless the sensitivity function does not reach perfect following of the target weight, the optimization result provides a much smoother frequency response and with small gain at low frequencies. The resulting optimization procedure considering both W_1 and W_2 provides a final controller given by Eq. 5.77.

$$K = \begin{bmatrix} \frac{-0.49s^6-0.95s^5-97.92s^4-53.25s^3-407.6s^2-87.3s-1.22}{s^7+9.59s^6+213.6s^5+1587s^4+2145s^3+6832s^2+203.5s+1.52} \\ \frac{-0.008s^6-0.017s^5-1.79s^4-0.97s^3-7.47s^2-1.59s}{s^7+9.59s^6+213.6s^5+1587s^4+2145s^3+6832s^2+203.5s+1.52} \end{bmatrix} \tag{5.77}$$

Figure 43 – Sensitivity matrix singular values after H_∞ control

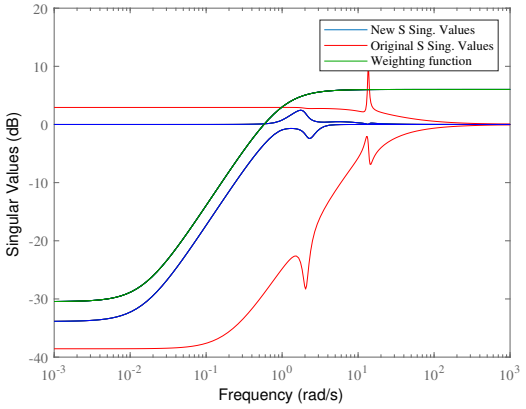

Source: Author (2022)

Figure 44 – H_∞ Controller - Pitch Controller Diagram

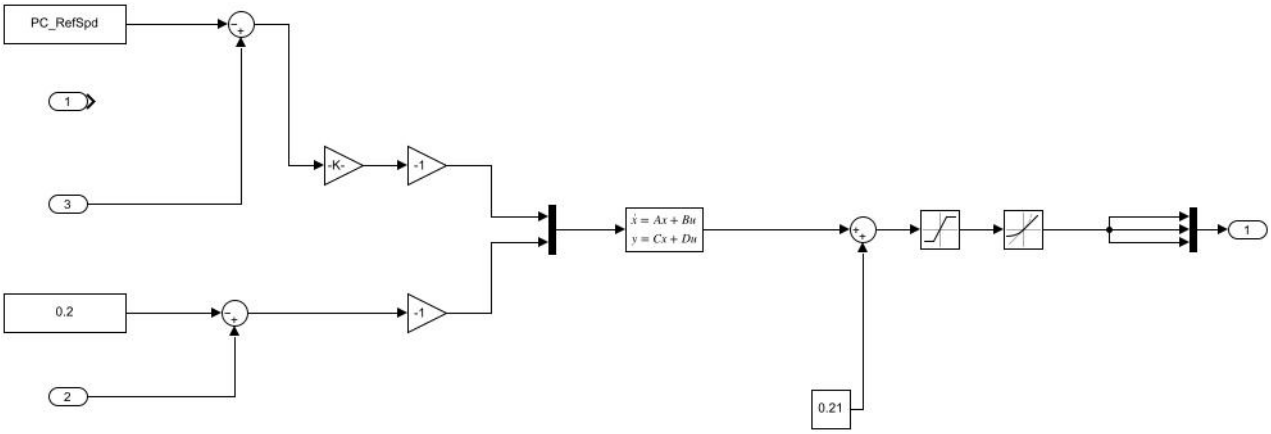

Source: Author (2022)

The designed H_∞ controller will be tested to varied wind conditions and the results will be analyzed from the point of view of tower load reduction and rotor speed control.

5.6.3.2 Overview of the H_∞ Controller

In Fig. 44 we have an overview of the H_∞ Pitch Controller block. The rotor speed and tower displacement are used as the required feedback signals. The H_∞ Controller is implemented in the state-space block, with the calculated transfer functions. The main diagram is not shown because it is identical to previous illustrated diagrams (as the Baseline DLL Controller diagram, Fig. 12).

5.6.3.3 Results

5.6.3.4 Steady wind conditions

The first simulation carried out to test the proposed controller is realized under steady wind conditions. It means that the incident wind in WT rotor is constant and uniform around its diameter, which allows to obtain steady-state controller characteristics. The wind speed (v_w) is chosen in the full-load range of WT, where the pitch control should be active, being $v_w = 18m/s$. Rotor speed control is adjusted with 12.1 rpm set-point, the rated rotor speed. For tower load control, the control reference is set to zero tower displacement. Results of the rotor speed control using the H_∞ controller are shown in Fig. 45. From this result, it is remarkable that the conventional control function of the pitch actuator (rotor speed regulation) is not only maintained, but greatly improved, with much less control overshoot. Reduction of structural loads can be inferred by Fig. 46, where it can be seen that the tower fore-aft base moment is strongly reduced. In this way, the H_∞ controller presents satisfactory results in steady wind condition. On the other hand, the generator power is kept controlled to the rated power of 5MW, as expected and shown in Fig. 47. A simulation result for the whole range of steady wind conditions is shown in Fig.

48, where the robustness of the designed controlled can be confirmed. Tower base moment variations are well controlled, especially in the moments of wind changes (each 100 s of simulation). In addition to the initial validation in steady wind conditions, the designed controller must also be tested in turbulent winds.

Figure 45 – WT rotor speed considering steady wind

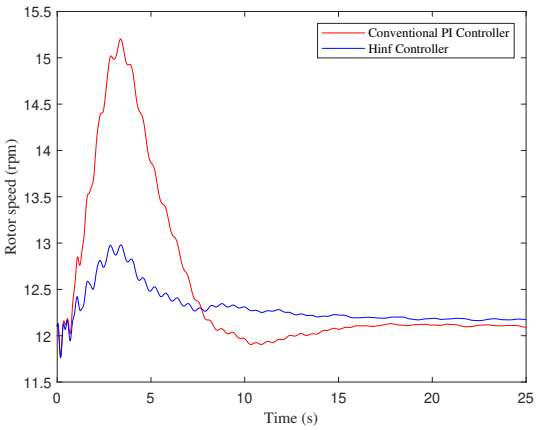

Source: Author (2022)

Figure 46 – Tower fore-aft base moment at steady wind conditions

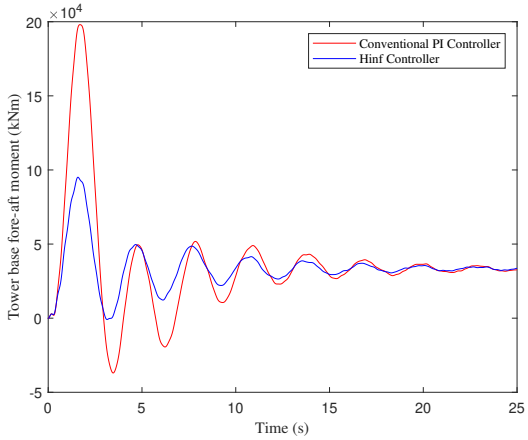

Source: Author (2022)

5.6.3.5 Turbulent wind conditions

The second set of simulations should consider turbulent wind conditions to evaluate the H_∞ controller behavior in more realistic scenarios, as well as its influence in other WT loads beyond the tower base moment for which it was designed. The turbulent wind conditions involve the variation of wind speed in the three spatial directions, and it is generated using the Kaimal spectrum, according to IEC standards (COMMISSION, 2021), following the same characteristics of turbulence employed in the previous Sections of this work. The mean wind speed is set as in the steady wind conditions to $v_w = 18m/s$. Fig. 49

Figure 47 – Generator power production at steady wind conditions

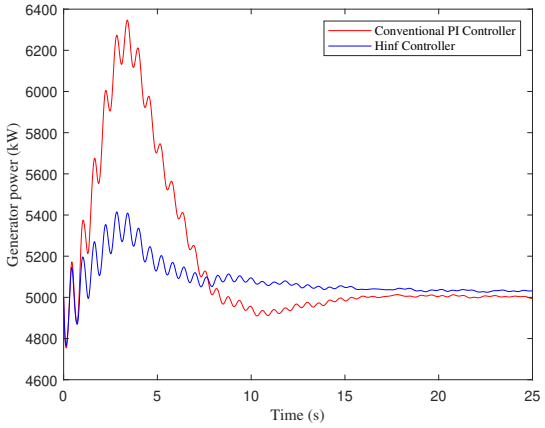

Source: Author (2022)

shows the wind time series for the axial direction, which is the component perpendicular to the rotor plane. The first results of the designed H_∞ controller include the verification of adequate limits of rotor speed and generated power, even in turbulent operation.

Simulations are shown in Figs. 50 and 51, demonstrating the superiority of H_∞ controller regarding maximum overshoot and steady-state response. On the other hand, it is necessary to evaluate controller behavior related to structural load reductions, in the very harsh turbulent conditions.

The major load mitigation should be presented for the tower fore-aft base moment, since this was the design requirement of the H_∞ controller. As pictured in Fig. 52, the tower fore-aft moment is greatly reduced, similar to the steady wind case. However, the reduction of tower base moment is not constrained to the fore-aft direction. Given the coupled wind turbine dynamics, the mitigation of fore-aft loading also provides benefits in the tower side-side (lateral) moment, which undergoes a significant reduction, as shown in Fig. 53. Finally, since the tower fore-aft base moment is directly linked to the blade flap loads, it is possible to verify a similar reduction in the blade flap moment due to the H_∞ controller, especially during the initial transient, as demonstrated in Fig. 54. Results in a larger time window for turbulent simulations are presented in Fig. 55, for rotor speed control and tower fore-aft base moment. Both results show that H_∞ Controller outperforms Baseline DLL Controller.

5.6.3.6 Conclusion

In this paper, the development of a structural control application for WTs was carried out. The objective was to use the traditional WT control systems to increase their functionality through the use of a dynamic modeling that allowed the consideration of structural issues in the control design. The pitch controller, by its ability to influence all

Figure 48 – NREL 5 MW RWT tower base fore-aft moment with all the DOFs active - H_∞ Controller

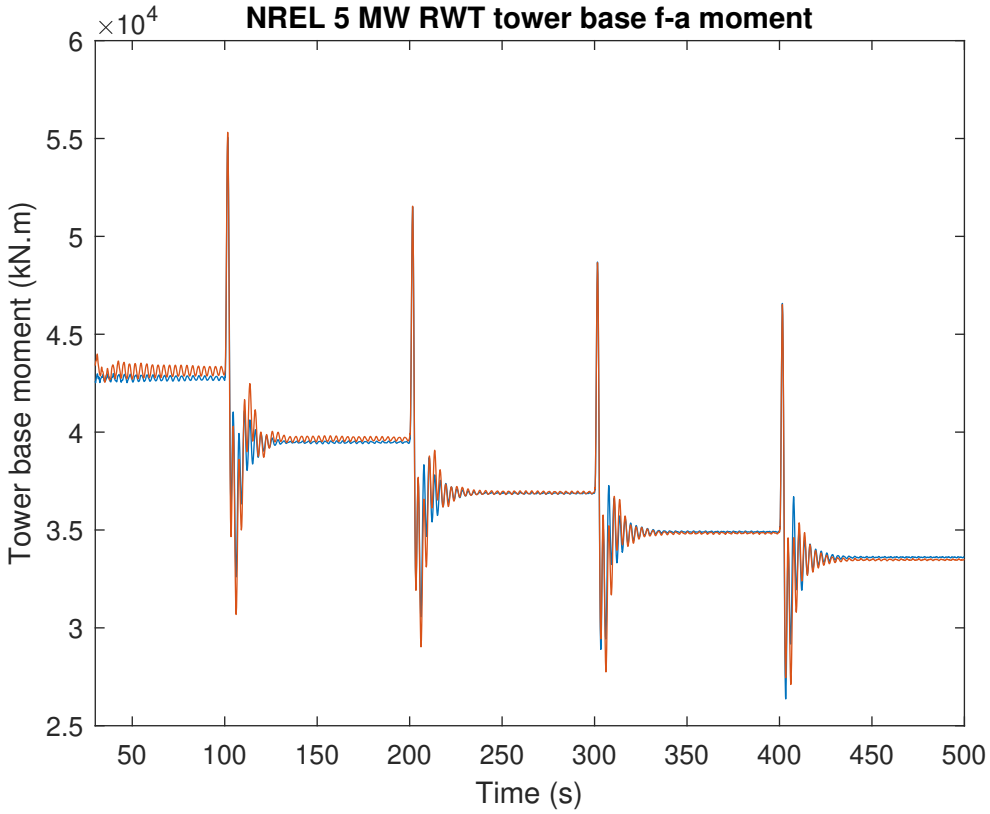

Source: Author (2022)

Figure 49 – Turbulent wind speed used in H_∞ controller simulations

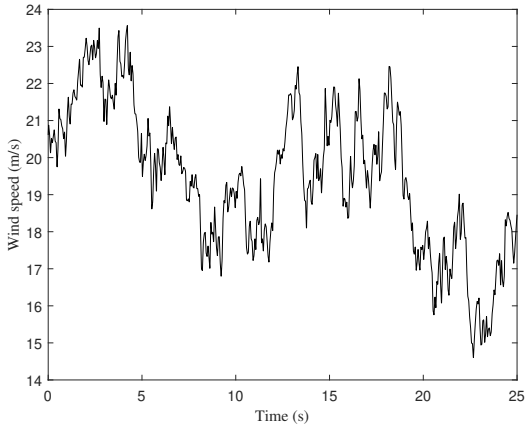

Source: Author (2022)

the WT structural dynamics, was selected to be enhanced. Further, the control design was founded in the H_∞ frequency-domain optimization multivariable methods, allowing to obtain a controller that meets the requirements of rotor speed control and tower load mitigation in an optimal configuration not achieved by traditional PI controllers. Future works include the continuity of turbulent wind simulations to evaluate H_∞ controller

Figure 50 – WT rotor speed in turbulent condition

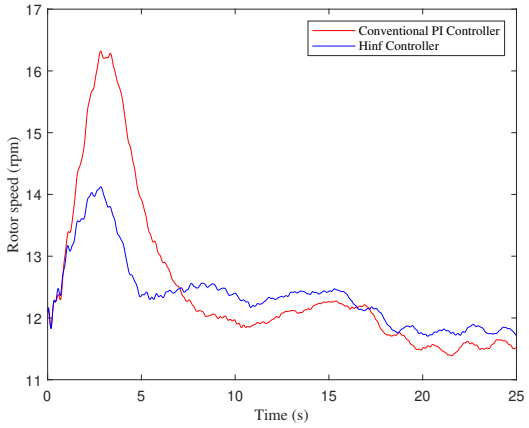

Source: Author (2022)

Figure 51 – Generator power production in turbulent condition

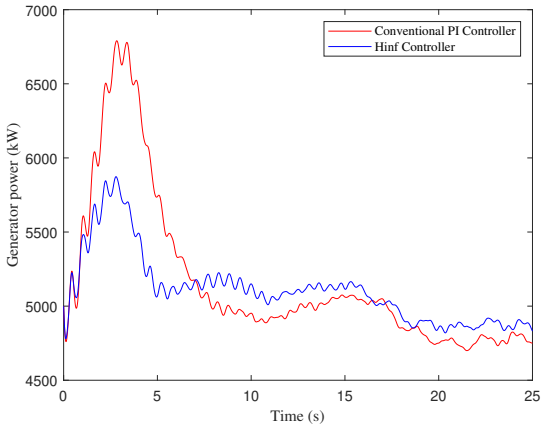

Source: Author (2022)

Figure 52 – Tower base fore-aft moment

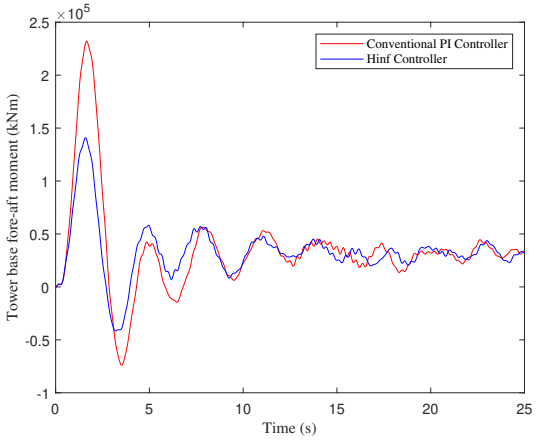

Source: Author (2022)

Figure 53 – Tower base side-side moment

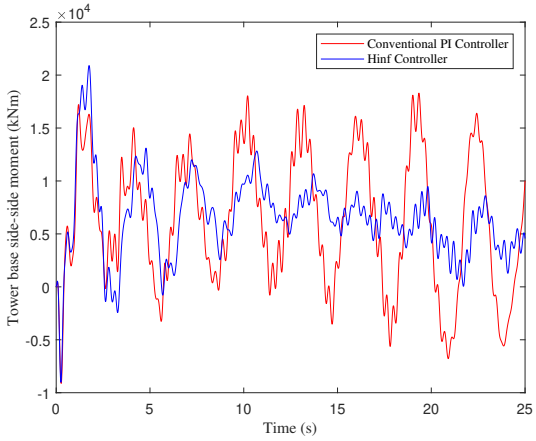

Source: Author (2022)

Figure 54 – Blade flapwise moment, turbulent conditions

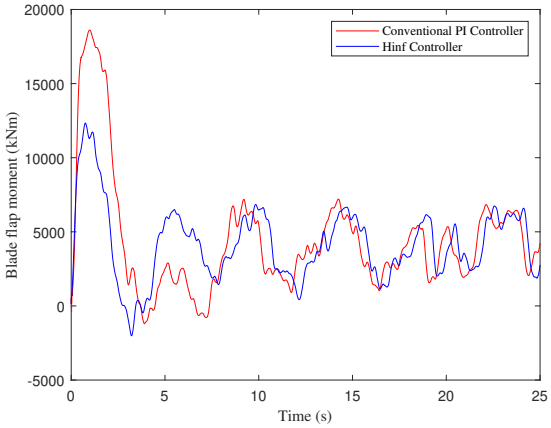

Source: Author (2022)

Figure 55 – NREL 5 MW RWT rotor speed (left) and NREL 5 MW RWT tower base fore-aft moment (right) with all the DOFs active - H_∞ Controller

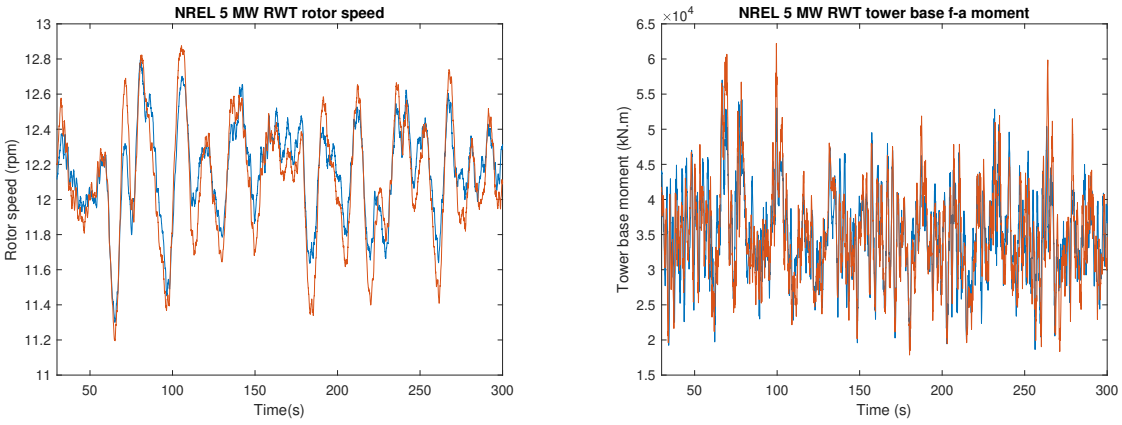

Source: Author (2022)

behavior and the inclusion of other WT loads mitigation as control objectives.

5.6.4 MPC Controller

5.6.4.1 Control design

The Model Predictive Control is a control strategy which uses a mathematical model to predict the future behavior of the system, given the control input in each sample instant. Depending on the type of model being considered, the MPC algorithms receive different names. The most used models are the Dynamic Matrix Control (DMC), based on state-space discrete formulation, and the Generalized Predictive Control (GPC), based on transfer functions in the domain of the z-transformation. Regardless, the first step is the establishment of a system linear model, which in this case will be the same of the H_∞ Controller. The MPC design demands the definition of the relative weight between control effort and reference following, as well as between the references set-points when there are more than one output. In our case, these values were set to 1 for the rotor speed regulation, 0.5 for tower fore-aft displacement and 0.5 for control effort variations. These weights correspond to the ones shown in Eq. 5.18. Since MPC is based on a constraint-handling optimization, it allows the inclusion of constraints directly in the control design. Therefore, we include the values of saturation and rate limit for pitch control used in the simulation of the previous controllers ($0 - 90°$ and $8°/s$). Finally, the control and prediction horizons are set to $N_c = 2$ and $N_p = 10$, respectively.

5.6.4.2 Overview of the MPC Controller

The overview of the MPC Controller is in Fig. 56, for the Pitch Controller block. The main diagram is not shown because it is identical to previous illustrated diagrams (see 12. Similar to the State-space CPC 5-DOF Controller and the H_∞ Controller, the feedback signals are the rotor speed and the tower displacement. On the other hand, the MPC Controller itself is implemented within the block MPC.

Figure 56 – MPC Controller - Pitch Controller diagram

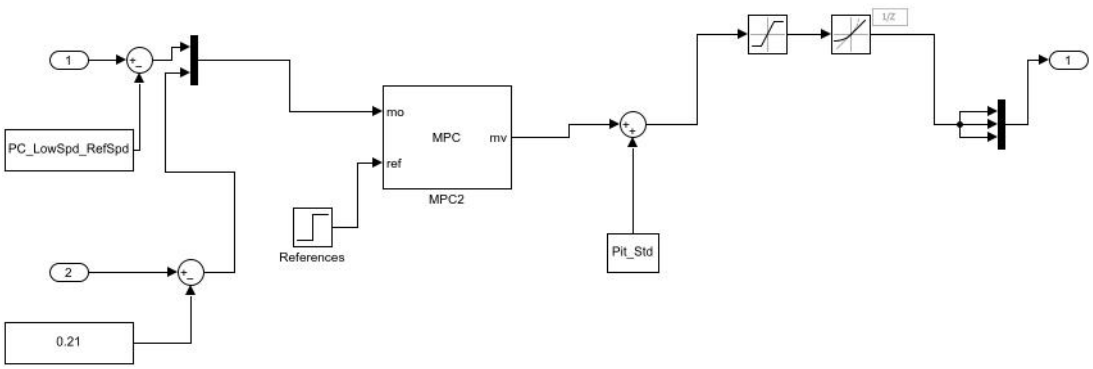

Source: Author (2022)

5.6.4.3 Results

The set of simulations consider steady wind conditions from $v = 14m/s$ to $v = 18m/s$. Afterwards, turbulent wind conditions at $v = 18m/s$ are simulated, with the same turbulence characteristics used in the previous Sections of this work. The results for steady wind conditions are shown in Fig. 57. As it can be seen, rotor speed is satisfactorily controlled. Additionally, tower base fore-aft moment is reduced, mainly in the wind speeds until $v = 16m/s$. Turbulent results are presented in Fig. 58, where it is possible to see that the MPC Controller works as intended, but in rotor speed control it is overcome by the Baseline DLL Controller.

Figure 57 – NREL 5 MW RWT tower base fore-aft moment (left) and NREL 5 MW RWT rotor speed (right) with all the DOFs active - MPC Controller

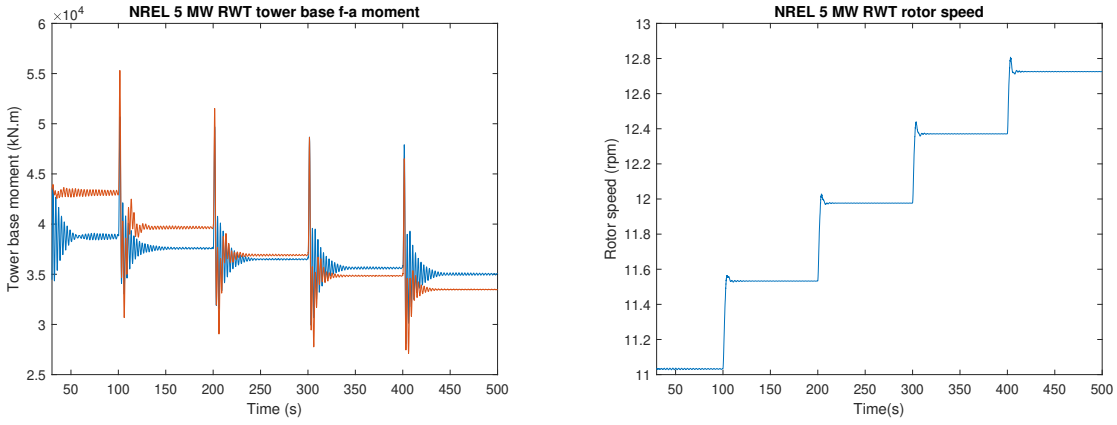

Source: Author (2022)

Figure 58 – NREL 5 MW RWT tower base fore-aft moment (left) and NREL 5 MW RWT rotor speed (right) with all the DOFs active, turbulent conditions - MPC Controller

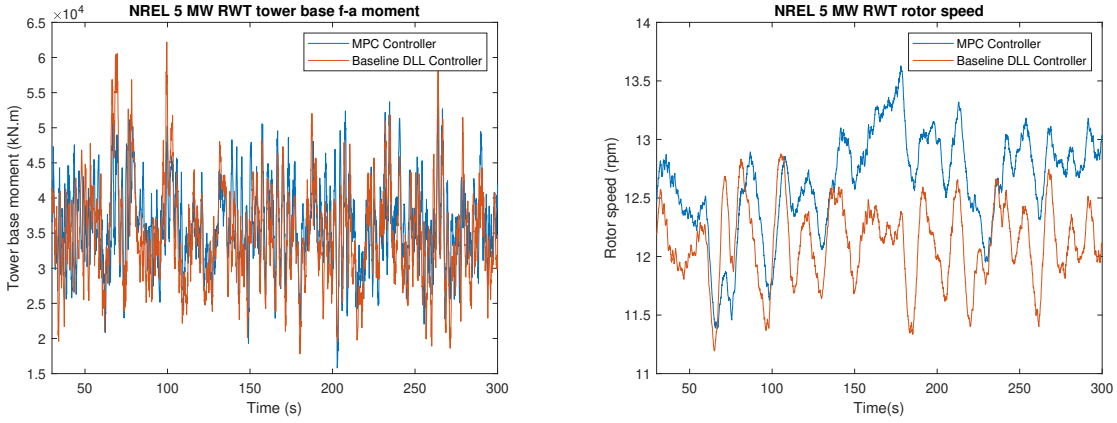

Source: Author (2022)

5.6.5 Comparison of Damage Equivalent Loads (DELs)

In this Section, the objective is to present fatigue behavior differences between the several designed controllers. To do this, it is necessary to have a common basis. Damage Equivalent Load is the value of mechanical loading which, at constant amplitude and frequency, would cause the same fatigue damage to the system. The concept of DELs is largely employed in wind turbine research (MICHALOPOULOS, 2015; SUDHARSAN; XAVIER; RAGHUNATHAN, 2020; NATARAJAN, 2020). It is based on the Miner's rule for damage accumulation,

$$D = \sum_i \frac{n_i}{N_i(S_i)} \tag{5.78}$$

where D is the accumulated damage, n_i is the number of cycles in a time-series under the stress S_i and N_i is the fatigue life in number of cycles at S_i. Assuming an equivalent damage, DEL is calculated as

$$\frac{n_{eq}}{N_{eq}} \sum_i \frac{n_i}{N_i(S_i)} \tag{5.79}$$

$$n_{eq} = f_{eq} T \tag{5.80}$$

where n_{eq} is the equivalent number of cycles, which is dependent on the considered DEL frequency f_{eq} and the time-series total time T. N_{eq} is the number of cycles to failure calculated from the material fatigue curve m. In this work, we will be assuming as typical values $m = 4$ for the steel WT tower and $m = 10$ for the composite WT blades. The equivalent frequency f_{eq} is taken to be $f_{eq} = 1$ Hz. We use the program MLife (HAYMAN, 2012) to run the fatigue calculations. MLife uses Rainflow counting method to estimate number of cycles and load amplitudes from a given time series. Results are given in the following Tables 5, 6, 7, 8, 9, and 10, for turbulent winds. The controllers are evaluated in terms of the target reducing load for which they were designed. In this way, tower base fore-aft moments and blade root flapwise moments have their statistics calculated. As can be inferred from the results presented in the Tables, the H_∞ controller appears to be the most promising load reducing controller. It reduces the tower fore-aft DEL even for conditions where controller performance degrades from the nominal design point. Indeed, the H_∞ Controller was designed around $v = 16m/s$ and steady simulations show that around $18m/s$ it does not perform as designed. Nevertheless, H_∞ presents a similar DEL reduction to better load reducing controller in this wind speed (the CPC 5-DOF Controller, see Table 10. Another remarkable point is the performance of the IPC 4-DOF Controller. As expected, it has reduced blade root flapwise moments. This reduction is even bigger if wind shear loads are considered in conditions without turbulence. As a side effect, it is expected that this reduction in flapwise loads reduce several structural loads in the WT, given the coupled dynamics. Since rotor speed control is the primary function of pitch control system, the reduction of loads cannot interfere with the rotor speed regulation. As previously discussed, rotor speed control ensures power control in

Table 5 – Comparison between CPC 5-DOF Controller and Baseline DLL Controller, turbulent wind (v=18m/s)

Tower base fore-aft moment	CPC 5-DOF Controller	Baseline DLL Controller
Mean (kNm)	3.51E4	3.48E4
Std Dev (kNm)	5.47E3	6.93E3
DEL (kNm)	1.55E4	1.67E4

Source: Author (2022)

Table 6 – Comparison between IPC 4-DOF Controller and Baseline DLL Controller, turbulent wind ($v = 16m/s$)

Blade root flapwise moment	IPC 4-DOF Controller	Baseline DLL Controller
Mean (kNm)	5.03E3	5.46E3
Std Dev (kNm)	1.23E3	1.84E3
DEL (kNm)	6.16E4	9.27E5

Source: Author (2022)

Table 7 – Comparison between H_∞ Controller and Baseline DLL Controller, turbulent wind ($v = 18m/s$)

Tower base fore-aft moment	H_∞ Controller	Baseline DLL Controller
Mean (kNm)	3.48E4	3.48E4
Std Dev (kNm)	6.62E3	6.93E3
DEL (kNm)	1.59E4	1.67E4

Source: Author (2022)

WT Region 3, and therefore is fundamental for a good WT operation. In this context, the rotor speed statistics are presented for all controllers in Table 11. The table shows that the controllers have preserved a properly operation of rotor speed control, even though they have added the objective of structural loads mitigation.

Table 8 – Comparison between MPC Controller and Baseline DLL Controller, turbulent wind (v=18m/s)

Tower base fore-aft moment	MPC Controller	Baseline DLL Controller
Mean (kNm)	3.47E4	3.48E4
Std Dev (kNm)	6.44E3	6.93E3
DEL (kNm)	1.63E4	1.67E4

Source: Author (2022)

Table 9 – Comparison between MPC Controller and H_∞ Controller, turbulent wind (v=18m/s)

Tower base fore-aft moment	MPC Controller	H_∞ Controller
Mean (kNm)	3.47E4	3.48E4
Std Dev (kNm)	6.44E3	6.62E3
DEL (kNm)	1.63E4	1.59E4

Source: Author (2022)

Table 10 – Comparison between CPC 5-DOF Controller and Baseline DLL Controller, turbulent wind (v=18m/s)

Tower base fore-aft moment	CPC 5-DOF Controller	H_∞ Controller
Mean (kNm)	3.51E4	3.48E4
Std Dev (kNm)	5.47E3	6.62E3
DEL (kNm)	1.55E4	1.59E4

Source: Author (2022)

Table 11 – Comparison between the different NREL 5 MW RWT Controllers regarding rotor speed, turbulent wind (v=18m/s)

Rotor speed	Baseline DLL Controller	CPC 5-DOF Controller	IPC 4-DOF Controller	H_∞ Controller	MPC Controller
Min (rpm)	11.2	11.7	10.5	11.2	10.9
Max (rpm)	12.9	12.6	16	12.9	12.9
Mean (rpm)	12.1	12.3	13.3	12.2	12.2
Std Dev (rpm)	0.332	0.169	1.16	0.293	0.361

Source: Author (2022)

6 CONCLUSIONS

The current wind turbines are very different from the initial wind energy first impulse in the 1970s. The WTs were machines which hardly reached 1 MW of power capacity and 50 m of tower height. Nowadays, the environmental and energetic crises have been taking wind turbines to another level of rated capacity, dimensions and performance. Today, the WTs can reach several MWs of power and have tower in the range of 90-120 m and blades of 70-m span. This WT configuration raises many structural issues, which are key for attaining WT lifetime increase, cost reduction and, consequently, wind energy competitiveness.

On the other hand, control systems design is a field of engineering with many applications and that has been developing very fast in the recent decades. Part of that is due to the advancement in simulation and design computational power with the evolution of digital computers. Control theory has been used for digital communication, robotics, chemical processing industry, automotive and aeronautics industry, O&G industry and, more recently, for artificial intelligence and machine learning. Its benefits are recognized all over these fields. In wind energy, control was initially used for simple generator torque and pitch commands. More recently, the growth in the size of WTs has created the need for structural controllers, capable of reducing WT loads. Indeed, structural control aggregates the structural dynamics analysis with control theory to make possible the design of load-mitigating controllers, without degradation of the primary functions, such as rotor speed control.

Recognizing the need for such structural controllers and structural analysis, this thesis has focused on both, to obtain the maximum efficiency in the controllers design. First of all, a review of the wind turbine control systems was executed, in order to identify the main control functions, methods and tools used in the literature. After that, a research on WT structural analysis was carried out, in order to provide the structural models used for control design. The next thesis step was the development of a proprietary structural dynamics software, to identify the flexible modes of WTs. Afterwards, control systems were designed and tested using different control methods. Results are shown for the main WT parameters, such as rotor speed, power and blade pitch angles, as well as in terms of damage equivalent loads (DELs).

For the WT structural analysis, it was demonstrated that the most suitable modeling for control is based on the hybrid modal-multibody approach. Control design model has to be complex enough to capture the main dynamics, but simple enough to enable proper manipulation. In this sense, purely finite-element approaches are not indicated for control

purposes. Hybrid modal-multibody allows the inclusion of finite-element in the calculation of the flexible modes, and the treatment of the WT dynamics in terms of various DOFs. Besides, being a multibody method, it takes into account the constraints and relative movements between the WT components, considering, e.g., the movement of the rotor relative to the blades or the yaw rotation of the nacelle relative to the tower top.

The finite-element software developed allows the user to enter with geometric and structural characteristics and get axial and bending modes, based on Bernoulli beam elements. The stiffness, damping and mass matrices are mounted and the obtaining of natural frequencies and mode shapes is carried out through the calculation of eigenvectors and eigenvalues of a defined level of discretization. Additionally to that, the program also admits the calculation of dynamic responses using Newmark method for the temporal solution. The user is also allowed to define simple geometric characteristics that are used internally by the program to calculate aggregated parameters, such as inertia moment from the tower thickness and diameter variations, and the generalized stiffness from the elasticity modulus, density, inertia moment and area. This is a difference from the NREL program 'Modes', which has the same objective of the herein developed tool, but demand these properties already calculated as inputs.

The wind turbine controllers were developed according to the WT dynamics models derived from the discussed modeling. The controllers included baseline designs, based on PID control algorithms, and non-conventional control methods. The baseline designs are example of the current utilised WT pitch control systems and perform well for rotor speed control. However, their design does not consider structural load reduction. The structural control of the WT was then proposed, using state-space controllers, H_∞ controllers, and MPC controllers. In all of them, structural load reduction was explicitly included as a control objective. The control was designed for a reference large-size wind turbine, the NREL 5 MW RWT, which is a model used as benchmark in the large majority of wind turbine research. All the controllers were tested in steady and turbulent conditions, presenting good results. At last, comparison metrics between the different control systems were established. Overall, as discussed in Chapter 5, the H_∞ controller has presented itself as the better control method. However, it is worth noting that this is just an initial validation. A large number of simulations are still needed to evaluate the controllers performance in several wind conditions. Nonetheless, the good behavior in a harsh turbulent environment, as was demonstrated here, is an excellent evidence of satisfactory performance.

Finally, the work developed here should be extended and continuously improved. Future works include the further development of the structural dynamics software, to encompass all the hybrid modal-multibody approach. Also, the consideration of blades rotation speed in the calculation of flexible modes is envisaged. For the control systems, we plan to advance in the H_∞ control to mitigate another dynamic loads, including especially

the design of an IPC controller. Additionally, we expect to develop hybrid controllers, considering combined control methods responsible for different control objectives. The use of H_∞ to mitigate tower loads and state-space for the blades is seen as the first step in this strategy. Turbulent simulations encompassing all the range of WT operating speeds are also a next step, along with the use of fatigue analysis and statistical tools to evaluate the results. Finally, we plan to move forward with the control design, including offshore wind turbines and even larger WTs than the NREL 5 MW RWT (such as the IEA 15 MW currently being developed).

Bibliography

ABBAS, N. J.; WRIGHT, A.; PAO, L. An update to the national renewable energy laboratory baseline wind turbine controller. In: . [S.l.]: Institute of Physics Publishing, 2020. v. 1452. ISSN 17426596. Citado na página 26.

ABBAS, N. J. et al. A reference open-source controller for fixed and floating offshore wind turbines. *Wind Energy Science*, Copernicus GmbH, v. 7, p. 53–73, 1 2022. ISSN 23667451. Citado na página 43.

AHO, J.; PAO, L.; HAUSER, J. Optimal trajectory tracking control for wind turbines during operating region transitions. p. 1426–1431, 2013. Citado na página 30.

ATA, R. Artificial neural networks applications in wind energy systems: a review. *Renewable and Sustainable Energy Reviews*, v. 49, p. 534–562, 9 2015. ISSN 1364-0321. Disponível em: <http://www.sciencedirect.com/science/article/pii/S1364032115004360>. Citado na página 26.

BADIHI, H.; ZHANG, Y. Fault-tolerant individual pitch control of a wind turbine with actuator faults. In: . [S.l.]: Elsevier B.V., 2018. v. 51, p. 1133–1140. ISSN 24058963. Citado na página 26.

BAK, C. . et al. *The DTU 10-MW Reference Wind Turbine). The DTU 10-MW Reference Wind Turbine.* 2013. Citado na página 43.

BATHE, K. J. *Finite Element Procedures*. Prentice Hall, 2006. ISBN 9780979004902. Disponível em: <https://books.google.com.br/books?id=rWvefGICfO8C>. Citado na página 38.

BEAZLEY, D.; JONES, B. K. *Python Cookbook: Recipes for Mastering Python 3*. [S.l.: s.n.], 2018. Citado na página 60.

BI K.; HAO, H. Z. H. Using multiple tuned mass dampers to control offshore wind turbine vibrations under multiple hazards. *Engineering Structures*, 2017. Citado na página 24.

BINSBERGEN, D. W. van; WANG, S.; NEJAD, A. R. Effects of induction and wake steering control on power and drivetrain responses for 10 mw floating wind turbines in a wind farm. *Journal of Physics: Conference Series*, IOP Publishing, v. 1618, p. 022044, 2020. ISSN 1742-6588. Disponível em: <http://dx.doi.org/10.1088/1742-6596/1618/2/022044>. Citado na página 64.

BIR, G. S. User ' s guide to mbc3 (multi-blade coordinate transformation utility for 3-bladed wind turbines). *NREL*, v. 3, 2008. Citado na página 81.

BOSSANYI, E. The design of closed loop controllers for wind turbines. *Wind Energy*, v. 3, p. 149–163, 2000. Citado na página 24.

BOSSANYI, E. Gh bladed. 2003. Citado na página 34.

BOSSANYI, E. A. Further load reductions with individual pitch control. *Wind Energy*, John Wiley Sons, Ltd., v. 8, p. 481–485, 10 2005. ISSN 1099-1824. Disponível em: <http://dx.doi.org/10.1002/we.166>. Citado na página 34.

BOSSANYI, E. a; FLEMING, P. a; WRIGHT, A. D. Validation of individual pitch control by field tests on two-and three-bladed wind turbines. *IEEE Transactions on Control Systems Technology*, v. 21, p. 1067–1078, 2013. Disponível em: <http://ieeexplore.ieee.org/xpls/abs_all.jsp?arnumber=6515638>. Citado na página 35.

BOTTASSO, C. et al. Lidar-enabled model predictive control of wind turbines with real-time capabilities. *Renewable Energy*, Elsevier Ltd, v. 71, p. 442–452, 2014. ISSN 09601481. Disponível em: <http://linkinghub.elsevier.com/retrieve/pii/S0960148114003024>. Citado na página 35.

BOUOUDEN, S. et al. Fuzzy model based multivariable predictive control of a variable speed wind turbine: Lmi approach. *Renewable Energy*, Elsevier Ltd, v. 37, p. 434–439, 2012. ISSN 09601481. Disponível em: <http://dx.doi.org/10.1016/j.renene.2011.06.025>. Citado na página 33.

BOYCE, W. E.; DIPRIMA, R. C. *Elementary Differential Equations and Boundary Value Problems, 10th Edition*. Wiley, 2012. ISBN 9780470458310. Disponível em: <https://books.google.com.br/books?id=PYhxhRfleJUC>. Citado na página 37.

BRIGGS, H. *Why is the Paris climate agreement important for COP26?* 2021. Disponível em: <https://www.bbc.com/news/science-environment-35073297>. Citado na página 22.

BUHL, M. L.; MANJOCK, A. A comparison of wind turbine aeroelastic codes used for certification. *Renewable Energy*, p. 1–14, 2006. Disponível em: <http://www.nrel.gov/docs/fy06osti/39113.pdf>. Citado na página 70.

BURTON, T. et al. *Wind Energy Handbook*. Wiley, 2011. ISBN 9781119993926. Disponível em: <https://books.google.com.br/books?id=dip2LwCRCscC>. Citado na página 29.

CHAABAN, R.; FRITZEN, C. peter. Reducing blade fatigue and damping platform motions of floating wind turbines using model predictive control. In: . [S.l.: s.n.], 2014. p. 3581–3588. ISBN 9789727521654. Citado na página 35.

CHAPRA, S.; CANALE, R. *Numerical Methods for Engineers*. [S.l.]: McGraw Hill, 2021. Citado na página 61.

CHEN, C. et al. Stall-induced vibrations analysis and mitigation of a wind turbine rotor at idling state: Theory and experiment. *Renewable Energy*, Elsevier Ltd, v. 187, p. 710–727, 3 2022. ISSN 18790682. Citado na página 24.

CHEN, Z. J.; STOL, K. a. An assessment of the effectiveness of individual pitch control on upscaled wind turbines. *Journal of Physics: Conference Series*, v. 524, p. 012045, 2014. ISSN 1742-6596. Disponível em: <http://stacks.iop.org/1742-6596/524/i=1/a=012045?key=crossref.e4963ef2106644677e2f60beaede9e98>. Citado na página 26.

CHEN, Z. J.; STOL, K. a. An assessment of the effectiveness of individual pitch control on upscaled wind turbines. *Journal of Physics: Conference Series*, v. 524, p. 012045, 2014. ISSN 1742-6596. Disponível em: <http://stacks.iop.org/1742-6596/524/i=1/a=012045?key=crossref.e4963ef2106644677e2f60beaede9e98>. Citado na página 35.

COMMISSION, I. E. *IEC 61400-1:2019*. 2021. Disponível em: <www.cleanpower.org>. Citado na página 96.

DNV. *Guidelines for Design of Wind Turbines*. [S.l.: s.n.], 2002. 294 p. ISBN 87-550-2870-5. Citado na página 26.

DNV. *Wind turbine design software - Bladed*. 2022. Citado na página 24.

DORF, R. C.; BISHOP, R. H. *Modern Control Systems (thirteenth Edition)*. Dian zi gong ye chu ban she, 2021. ISBN 9787121343940. Disponível em: <https://books.google.com.br/books?id=x4TyvgEACAAJ>. Citado na página 82.

DTU. *HAWC2*. 2022. Citado na página 24.

DUNNE, F. Comparison of two independent lidar-based pitch control designs comparison of two independent lidar-based pitch control designs. 2012. Citado na página 34.

DUNNE, F. et al. Mechatronics adding feedforward blade pitch control to standard feedback controllers for load mitigation in wind turbines q. *Mechatronics*, Elsevier Ltd, v. 21, p. 682–690, 2011. ISSN 0957-4158. Disponível em: <http://dx.doi.org/10.1016/j.mechatronics.2011.02.011>. Citado na página 33.

DUONG, M. Q. et al. Pitch angle control using hybrid controller for all operating regions of scig wind turbine system. *Renewable Energy*, Elsevier Ltd, v. 70, p. 197–203, 2014. ISSN 09601481. Disponível em: <http://dx.doi.org/10.1016/j.renene.2014.03.072>. Citado na página 33.

EHLERS, J.; DIOP, A.; BINDNER, H. *Sensor Selection and State Estimation for Wind Turbine Controls*. American Institute of Aeronautics and Astronautics, 2007. Doi:10.2514/6.2007-1019. Disponível em: <http://dx.doi.org/10.2514/6.2007-1019>. Citado na página 34.

ENERGY, D. O. of E. E. . R. *Wind Turbines: the Bigger, the Better*. 2021. Disponível em: <https://www.energy.gov/eere/articles/wind-turbines-bigger-better>. Citado na página 23.

EPBR. *Eólica chega a 21 GW de capacidade instalada no Brasil*. 2022. Disponível em: <https://epbr.com.br/eolica-chega-a-21-gw-de-capacidade-instalada-no-brasil/>. Citado na página 23.

EUROPE, W. *History of Europe's wind industry*. 2022. Disponível em: <https://windeurope.org/about-wind/history/>. Citado na página 22.

FENG, J.; SHENG, W. Z. Operating wind turbines in strong wind conditions by using feedforward-feedback control. *Journal of Physics: Conference Series*, v. 555, p. 012035, 2014. ISSN 1742-6588. Disponível em: <http://stacks.iop.org/1742-6596/555/i=1/a=012035?key=crossref.d539d3f2aef05ead994fe0b41d5bcc75>. Citado na página 26.

FLEMING, P. et al. Field test of wake steering at an offshore wind farm. *Wind Energy Science Discussions*, p. 1–17, 2017. ISSN 2366-7621. Disponível em: <http://www.wind-energ-sci-discuss.net/wes-2017-4/>. Citado na página 65.

FROST, S. A.; BALAS, M. J.; WRIGHT, A. D. Direct adaptive control of a utility-scale wind turbine for speed regulation. *International Journal of Robust and Nonlinear Control*, v. 19, p. 59–71, 2009. Citado na página 33.

GAERTNER, E. et al. *Definition of the IEA Wind 15-Megawatt Offshore Reference Wind Turbine Technical Report*. 2020. Disponível em: <www.nrel.gov/publications.> Citado na página 22.

GEYLER, M.; CASELITZ, P. Individual blade pitch control design for load reduction on large wind turbines. *European Wind Energy Conference (EWEC 2007)*, 2007. Disponível em: <http://proceedings.ewea.org/ewec2007/allfiles2/178_Ewec2007fullpaper.pdf>. Citado na página 34.

GOLNARAGHI, F.; KUO, B. C. *Automatic Control Systems, Tenth Edition*. McGraw-Hill Education, 2017. ISBN 9781259643835. Disponível em: <https://books.google.com.br/books?id=TMHRjwEACAAJ>. Citado 2 vezes nas páginas 57 and 81.

GU, D. W.; PETKOV, P. H.; KONSTANTINOV, M. M. *Advanced Textbooks in Control and Signal Processing with Matlab*. [S.l.: s.n.], 2005. 392 p. ISBN 9781852339838. Citado na página 59.

GWEC, G. W. E. C. *GWEC GLOBAL WIND REPORT 2022*. 2022. Citado na página 23.

HALVO, E. *CFD Analysis of Topographically Induced Turbulence and its Effect on a Fatigue Life Analysis of a Wind Turbine Yaw Gear*. 2019. Citado na página 24.

HAN, Y.; LEITHEAD, W. E. Combined wind turbine fatigue and ultimate load reduction by individual blade control. *Journal of Physics: Conference Series*, v. 524, p. 012062, 2014. ISSN 1742-6596. Disponível em: <http://stacks.iop.org/1742-6596/524/i=1/a=012062?key=crossref.5dd81b8b40151443b3f42661c17fb102>. Citado na página 24.

HAND, M. M.; BALAS, M. J. Systematic controller design methodology for variable-speed wind turbines systematic controller design methodology for variable-speed wind turbines. 2002. Citado na página 33.

HANSEN, M.; HANSEN, A.; LARSEN, T. *Control design for a pitch-regulated, variable speed wind turbine*. [S.l.: s.n.], 2005. v. 1500. 84 p. ISSN 15231739. ISBN 8755034098. Citado na página 63.

HARRIS, M. et al. Lidar for turbine control lidar for turbine control. 2006. Citado na página 33.

HAYMAN, G. J. *MLife Theory Manual for Version 1.00 NREL IS A NATIONAL LABORATORY OF THE U.S. DEPARTMENT OF ENERGY, OFFICE OF ENERGY EFFICIENCY RENEWABLE ENERGY, OPERATED BY THE ALLIANCE FOR SUSTAINABLE ENERGY, LLC*. 2012. Disponível em: <http://www.osti.gov/bridge>. Citado na página 103.

HENRIKSEN, L.; HANSEN, M.; POULSEN, N. Wind turbine control with constraint handling: a model predictive control approach. *IET Control Theory Applications*, v. 6, p. 1722, 2012. ISSN 17518644. Citado na página 82.

HENRIKSEN, L. C. Model predictive control of a wind turbine. *Mathematical Modelling*, p. 1–7, 2007. Disponível em: <http://www2.imm.dtu.dk/pubdb/views/edoc_download.php/5256/pdf/imm5256.pdf>. Citado na página 35.

HOU, W. et al. Estimation and control of wind turbine tower vibrations based on individual blade-pitch strategies. 2019. Citado na página 26.

IEA. *Russia's war on Ukraine*. 2022. Disponível em: <https://www.iea.org/topics/russia-s-war-on-ukraine>. Citado na página 23.

IPCC. *Global Warming of 1.5°C. An IPCC Special Report on the impacts of global warming of 1.5°C above pre-industrial levels and related global greenhouse gas emission pathways, in the context of strengthening the global response to the threat of climate change, sustainable development, and efforts to eradicate poverty*. 2018. Citado na página 22.

JAIN, A. et al. On the design and tuning of linear model predictive control for wind turbines. *Renewable Energy*, Elsevier Ltd, v. 80, p. 664–673, 2015. ISSN 18790682. Disponível em: <http://dx.doi.org/10.1016/j.renene.2015.02.057>. Citado na página 26.

JELAVIć, M.; PETROVIć, V.; PERIć, N. Estimation based individual pitch control of wind turbine. *Automatika*, v. 51, p. 181–192, 2010. ISSN 00051144. Citado na página 34.

JOHNSON, K. et al. Special issue on "past, present and future modeling and control of wind turbines". *Mechatronics*, v. 21, p. 633, 2011. ISSN 09574158. Citado na página 32.

JOHNSON, K. E. et al. Control of variable-speed wind turbines: Standard and adaptive techniques for maximizing energy capture. *IEEE Control Systems Magazine*, v. 26, p. 70–81, 2006. ISSN 02721708. Citado na página 29.

JONKMAN, J. *Definition of the Floating System for Phase IV of OC3*. 2010. Disponível em: <http://www.osti.gov/bridge>. Citado na página 24.

JONKMAN, J. et al. Definition of a 5-mw reference wind turbine for offshore system development. *Contract*, p. 1–75, 2009. Disponível em: <http://tethys-development.pnnl.gov/sites/default/files/publications/Jonkman_et_al_2009.pdf>. Citado na página 61.

JONKMAN, J.; JR., M. B. Fast user's guide. *Technical Report NREL/EL-500-38230, National Renewable Energy Laboratory (NREL)*, 2005. Citado 2 vezes nas páginas 39 and 40.

JONKMAN, J. M. Dynamics modeling and loads analysis of an offshore floating wind turbine. *National Renewable Energy Laboratory (NREL)*, v. 68, p. 233, 2007. Disponível em: <http://www.nrel.gov/docs/fy08osti/41958.pdf>. Citado 2 vezes nas páginas 43 and 63.

JONKMAN, J. M.; JR, M. L. B. Fast user ' s guide. 2005. Citado na página 41.

KANE, T. R.; LEVINSON, D. A. *Dynamics: Theory and Applications*. [S.l.]: McGraw-Hill, 1985. Citado na página 42.

KOERBER a; KING, R. Combined feedback and feedforward control of wind turbines using state-constrained model predictive control. *Control Systems Technology, IEEE Transactions on*, v. 21, p. 1117–1128, 2013. Disponível em: <http://ieeexplore.ieee.org/ielx7/87/6532340/06522174.pdf?tp=&arnumber=6522174&isnumber=6532340>. Citado 2 vezes nas páginas 26 and 33.

KOUTROMANOS, I. *Fundamentals of Finite Element Analysis: Linear Finite Element Analysis*. Wiley, 2018. ISBN 9781119260080. Disponível em: <https://books.google.com.br/books?id=0FU8DwAAQBAJ>. Citado na página 45.

KRAGH, K.; HANSEN, M. Model predictive individual pitch control based on local inflow measurements. *7th PhD Seminar on Wind Energy in Europe*, p. 3–6, 2010. Disponível em: <http://proceedings.ewea.org/ewec2010/allfiles2/108_EWEC2010presentation.pdf%5Cnhttp://scholar.google.com/scholar?hl=en&btnG=Search&q=intitle:Model+Predictive+Individual+Pitch+Control+Based+on+Local+Inflow+Measurements#0>. Citado na página 35.

KUMAR, A.; STOL, K. *Scheduled Model Predictive Control of a wind Turbine*. American Institute of Aeronautics and Astronautics, 2009. Doi:10.2514/6.2009-481. Disponível em: <http://dx.doi.org/10.2514/6.2009-481>. Citado na página 35.

LAKS, J. et al. Mechatronics the use of preview wind measurements for blade pitch control. *Mechatronics*, Elsevier Ltd, v. 21, p. 668–681, 2011. ISSN 0957-4158. Disponível em: <http://dx.doi.org/10.1016/j.mechatronics.2011.02.003>. Citado na página 34.

LARSEN, J.; NIELSEN, S. Non-linear dynamics of wind turbine wings. *International Journal of Non-Linear Mechanics*, v. 41, p. 629–643, 2006. ISSN 00207462. Citado na página 29.

LI, P. et al. Control and monitoring for grid-friendly wind turbines : Research overview and suggested approach. v. 30, p. 1979–1986, 2015. Citado na página 33.

LIO, W. H. et al. A review on applications of model predictive control to wind turbines. p. 673–678, 2014. Citado na página 60.

LIU, X.; WU, Q.; KONG, X. Economic model predictive control for wind turbine. In: . [S.l.: s.n.], 2019. p. 2919–2923. ISSN 1934-1768. Citado na página 26.

LUBOSNY, Z. et al. Supervisory control of a wind farm. *IEEE Transactions on Power Systems*, v. 22, p. 985–994, 2007. Bom! Frequency control. Citado na página 29.

LUZAR, M.; WITCZAK, M. Robust mpc for a non-linear system – a neural network approach. *Journal of Physics: Conference Series*, v. 570, p. 032002, 2014. ISSN 1742-6588. Disponível em: <http://stacks.iop.org/1742-6596/570/i=3/a=032002?key=crossref.e3d97acee69f364de30d82620c609df7>. Citado na página 33.

MANWELL, J. F.; MCGOWAN, J. G.; ROGERS, A. L. *Wind Energy Explained: Theory, Design and Application*. Wiley, 2010. ISBN 9780470686287. Disponível em: <https://books.google.com.br/books?id=roaTx_Of0vAC>. Citado 2 vezes nas páginas 21 and 37.

MATHWORKS, C. User ' s guide r 2017 a. 2017. Citado na página 60.

MAZARE, M.; TAGHIZADEH, M.; GHAF-GHANBARI, P. Fault tolerant control of wind turbines with simultaneous actuator and sensor faults using adaptive time delay control. *Renewable Energy*, v. 174, p. 86–101, 2021. ISSN 0960-1481. Disponível em: <https://www.sciencedirect.com/science/article/pii/S0960148121005978>. Citado na página 33.

MENEZES, E. J. N. et al. Active load control of large wind turbines using state-space methods and disturbance accommodating control. *Energy*, v. 150, p. 310–319, 2018. ISSN 03605442. Citado 2 vezes nas páginas 26 and 57.

MENEZES, E. J. N.; ARAúJO, A. M.; SILVA, N. S. B. da. A review on wind turbine control and its associated methods. *Journal of Cleaner Production*, v. 174, p. 945–953, 2018. ISSN 09596526. Citado 2 vezes nas páginas 32 and 65.

MENG, H. et al. Study on fatigue life of bend-twist coupling wind turbine blade based on anisotropic beam model and stress-based fatigue analysis method. *Composite Structures*, Elsevier, v. 208, p. 678–701, 1 2019. ISSN 0263-8223. Citado na página 24.

MICHALOPOULOS, V. *Simplified fatigue assessment of offshore wind support structures accounting for variations in a farm*. 2015. Citado na página 103.

MULJADI, E.; PIERCE, K.; MIGLIORE, P. *Control Strategy for Variable-Speed, Stall-Regulated Wind Turbines Work performed under task number WE803020 Control Strategy for Variable-Speed, Stall-Regulated Wind Turbines*. 1998. Citado na página 29.

MUYAN, C.; COKER, D. Finite element simulations for investigating the strength characteristics of a 5m composite wind turbine blade. *Wind Energy Science*, Copernicus GmbH, v. 5, p. 1339–1358, 10 2020. ISSN 23667451. Citado na página 24.

NAJD, A.; GOREL, G.; HAMMOOD, H. Pitch angle control using neural network in wind turbines. *IOP Conference Series: Materials Science and Engineering*, v. 928, p. 22118, 8 2020. Citado na página 33.

NAMIK, H.; STOL, K. Performance analysis of individual blade pitch control of offshore wind turbines on two floating platforms. *Mechatronics*, Elsevier Ltd, v. 21, p. 691–703, 2011. ISSN 09574158. Disponível em: <http://dx.doi.org/10.1016/j.mechatronics.2010.12.003>. Citado na página 35.

NASA. Scientific and technical aerospace report. 1977. Disponível em: <https://play.google.com/store/books/details?id=Jrf-C3XAfgsC&rdid=book-Jrf-C3XAfgsC&rdot=1>. Citado na página 24.

NATARAJAN, A. Damage equivalent load synthesis and stochastic extrapolation for fatigue life validation. *Wind Energy Science Discussions*, 2020. Disponível em: <https://doi.org/10.5194/wes-2021-125>. Citado na página 103.

NAVALKAR, S. T. et al. Subspace predictive repetitive control to mitigate periodic loads on large scale wind turbines. *Mechatronics*, Elsevier Ltd, v. 24, p. 916–925, 2014. ISSN 09574158. Disponível em: <http://dx.doi.org/10.1016/j.mechatronics.2014.01.005>. Citado 2 vezes nas páginas 26 and 35.

NEJAD, A. R. et al. Drivetrain load effects in a 5-mw bottom-fixed wind turbine under blade-pitch fault condition and emergency shutdown. *Journal of Physics: Conference Series*, IOP Publishing, v. 753, p. 112011, 2016. ISSN 1742-6588. Disponível em: <http://dx.doi.org/10.1088/1742-6596/753/11/112011>. Citado na página 64.

NING, S. A. et al. *Development and Validation of a New Blade Element Momentum Skewed-Wake Model within AeroDyn: Preprint*. 2015. Disponível em: <www.nrel.gov/publications.> Citado 2 vezes nas páginas 43 and 65.

NISE, N. S. *Control Systems Engineering, 7th Edition*. Wiley, 2015. ISBN 9781118800829. Disponível em: <https://books.google.com.br/books?id=BwTYBgAAQBAJ>. Citado na página 82.

NISE, N. S. *Control Systems Engineering*. [S.l.: s.n.], 2019. Citado na página 60.

NJIRI, J. G.; SöFFKER, D. State-of-the-art in wind turbine control: Trends and challenges. *Renewable and Sustainable Energy Reviews*, Elsevier, v. 60, p. 377–393, 2016. ISSN 18790690. Disponível em: <http://dx.doi.org/10.1016/j.rser.2016.01.110>. Citado 2 vezes nas páginas 30 and 32.

NOEVER-CASTELOS, P.; MELCHER, D.; BALZANI, C. Model updating of a wind turbine blade finite element timoshenko beam model with invertible neural networks. *Wind Energy Science*, Copernicus GmbH, v. 7, p. 623–645, 3 2022. ISSN 23667451. Citado na página 38.

NREL. *OpenFAST Documentation*. 2022. Disponível em: <https://openfast.readthedocs.io/en/main/>. Citado na página 24.

OGATA, K. *Modern Control Engineering*. Prentice Hall, 2010. ISBN 9780136156734. Disponível em: <https://books.google.com.br/books?id=Wu5GpNAelzkC>. Citado na página 59.

OSSMANN, D. et al. Field testing of multi-variable individual pitch control on a utility-scale wind turbine. *Renewable Energy*, v. 170, p. 1245–1256, 2021. ISSN 0960-1481. Disponível em: <https://www.sciencedirect.com/science/article/pii/S096014812100207X>. Citado na página 35.

PEREIRA, A. de L. *Análise aeroelástica de turbinas eólicas de eixo horizontal*. 1993. Citado na página 24.

PETROVIć, V.; JELAVIć, M.; BAOTIć, M. Advanced control algorithms for reduction of wind turbine structural loads. *Renewable Energy*, v. 76, p. 418–431, 2015. ISSN 09601481. Citado 2 vezes nas páginas 34 and 80.

POULTANGARI, I.; SHAHNAZI, R.; SHEIKHAN, M. Rbf neural network based pi pitch controller for a class of 5-mw wind turbines using particle swarm optimization algorithm. *ISA Transactions*, Elsevier, v. 51, p. 641–648, 2012. ISSN 00190578. Disponível em: <http://dx.doi.org/10.1016/j.isatra.2012.06.001>. Citado na página 26.

PRODAN, I.; ZIO, E. A model predictive control framework for reliable microgrid energy management. *International Journal of Electrical Power Energy Systems*, Elsevier Ltd, v. 61, p. 399–409, 2014. ISSN 01420615. Trata de quot;enegy managementquot; em microgrids.
É tipo analisar quando carregar a bateria, quando usar a

fonte eólica ou quando usar a solar, etc. num sistema integrado. Disponível em: <http://www.sciencedirect.com/science/article/pii/S0142061514001197>. Citado na página 60.

RINKER, J.; DYKES, K. *WindPACT Reference Wind Turbines*. 2018. Disponível em: <https://www.nrel.gov/docs/fy18osti/67667.pdf.> Citado na página 43.

RINKER, J. et al. Comparison of loads from hawc2 and openfast for the iea wind 15 mw reference wind turbine. In: . [S.l.]: IOP Publishing Ltd, 2020. v. 1618. ISSN 17426596. Citado 2 vezes nas páginas 24 and 80.

RITTEL, F. M. *Load Reduction of a Multi-Rotor Wind Turbine using a Gain-Scheduled LQR Controller*. 2021. Citado na página 26.

ROHATGI, J.; VAUGHN, N. *Wind Characteristics: an analysis for the generation of wind power*. [S.l.]: Alternative Energy Institute, 1994. Citado na página 31.

SCHLIPF, D. et al. Field testing of feedforward collective pitch control on the cart2 using a nacelle-based lidar scanner. *Journal of Physics: Conference Series*, v. 555, p. 012090, 2014. ISSN 1742-6588. Disponível em: <http://stacks.iop.org/1742-6596/555/i=1/a=012090?key=crossref.31b710eca91078489eeada3b048cb2bb>. Citado 2 vezes nas páginas 34 and 72.

SOLINGEN, E. van et al. Field testing of linear individual pitch control on the two-bladed controls advanced research turbine. *Wind Energy*, p. n/a–n/a, 4 2015. ISSN 10954244. Disponível em: <http://doi.wiley.com/10.1002/we.1841>. Citado 2 vezes nas páginas 26 and 34.

SPENCER, M. D. et al. Model predictive control of a wind turbine using short-term wind field predictions. *Wind Energy*, v. 16, p. 417–434, 4 2013. ISSN 1099-1824. Disponível em: <http://dx.doi.org/10.1002/we.1501>. Citado na página 35.

STRESSER, J. F. *ESTUDO DO CONTROLE DE VIBRAÇÃO DE UMA VIGA ENGASTADA POR MEIO DE ABSORVEDORES DINÂMICOS DE VIBRAÇÃO*. 2021. Citado na página 54.

SUDHARSAN, G. S.; XAVIER, S. A. E.; RAGHUNATHAN, V. R. Fatigue load mitigation in wind turbine using a novel anticipatory predictive control strategy. *Proceedings of the Institution of Mechanical Engineers. Part I: Journal of Systems and Control Engineering*, SAGE Publications Ltd, v. 234, p. 60–80, 1 2020. ISSN 20413041. Citado na página 103.

SULLIVAN, T. A review of resonance in large horizontal-axis wind turbines. *Solar Energy*, 1982. Citado na página 24.

SYSTEMS, R. *Repower 5MW*. 2005. Citado na página 65.

T. LINDENBURG, C. W. D. H. J.; HOOFT, E. L. K. van der. *DOWEC 6 MW Pre-Design: Aero-elastic modeling of the DOWEC 6 MW pre-design in PHATAS*. 2003. Citado na página 65.

TAKAHASHI, K. et al. Output control of three-axis pmsg wind turbine considering torsional vibration using h infinity control. *Energies*, MDPI AG, v. 13, 7 2020. ISSN 19961073. Citado na página 26.

TANG, S. et al. Individual pitch controller characteristics analysis and optimization under aerodynamic imbalanced loads of wind turbines. *Energy Reports*, Elsevier Ltd, v. 7, p. 6489–6500, 11 2021. ISSN 23524847. Citado 2 vezes nas páginas 34 and 58.

TAVARES, R. P.; BOUWMAN, V.; PAEPEGEM, W. V. Finite element analysis of wind turbine blades subjected to torsional loads: Shell vs solid elements. *Composite Structures*, Elsevier, v. 280, p. 114905, 1 2022. ISSN 0263-8223. Citado na página 24.

TOMCZAK, J. S. *Finite-element analysis of post-tensioned concrete wind turbine towers*. 2021. Citado na página 38.

VAN, T. L. et al. Advanced pitch angle control based on fuzzy logic for variable-speed wind turbine systems. v. 30, p. 578–587, 2015. Citado na página 26.

WANG, H. et al. Finite element analysis of smart wind turbine blades sandwiched with magnetorheological fluid. *Journal of Vibroengineering*, JVE International, v. 18, p. 3858–3868, 9 2016. ISSN 13928716. Citado na página 38.

WANG, N. et al. Lidar-assisted preview controllers design for a mw-scale commercial wind turbine model. *Proceedings of the IEEE Conference on Decision and Control*, p. 1678–1683, 2013. ISSN 01912216. Citado na página 29.

WANG, N.; WRIGHT, A. D.; BALAS, M. J. Disturbance accommodating control design for wind turbines using solvability conditions. *Journal of Dynamic Systems, Measurement, and Control*, v. 139, 2 2017. ISSN 0022-0434. Disponível em: <https://doi.org/10.1115/1.4035097>. Citado na página 82.

YANG, W.; TIAN, S. W. Research on a power quality monitoring technique for individual wind turbines. *Renewable Energy*, Elsevier Ltd, v. 75, p. 187–198, 2015. ISSN 09601481. Disponível em: <http://linkinghub.elsevier.com/retrieve/pii/S0960148114006028>. Citado na página 29.

Appendix

APPENDIX A – Main finite-element program

The following code is the main part of the developed finite-element program to model flexible beams. Besides the main, the program contains submodules to input turbine properties and to generate the finite-element mesh. Both of them can be reached under a direct request to the author.

```
%% Program v.1.0.0
parametros
malha2;
%parametros_torre_NREL5MW;
%malha;
%dados;
%matrizes e vetores
sza=nnos; szf=2*nnos;
Ma=zeros(nnos,nnos);
Ca=zeros(nnos,nnos);
Ka=zeros(nnos,nnos);
Fa=zeros(nnos,1);
nCD=size(CD,1);
nCDa=0;
for i=1:nCD
    dir=CD(i,2);
    if dir==1
        nCDa=nCDa+1;
    end
end
nCDf=nCD-nCDa;
HDa=zeros(nnos,nCDa);
Mf=zeros(2*nnos,2*nnos);
Cf=zeros(2*nnos,2*nnos);
Kf=zeros(2*nnos,2*nnos);
Ff=zeros(2*nnos,1);
Hf=zeros(2*nnos,2*nnos);
HDf=zeros(2*nnos,nCDf);
for i=1:nel
```

```
    nos=AresVert(i,:);
    x1=X(nos(1));
    x2=X(nos(2));
    he=norm(x2-x1);
    A=(area(x1)+area(x2))/2;
    C=(amortx(x1)+amortx(x2))/2;
    ro=(rho(x1)+rho(x2))/2;
    E=(Elast(x1)+Elast(x2))/2;
% axial - início
Mae=ro*A*he*[2 1; 1 2]/6;
Kae=E*A*[1 -1; -1 1]/he;
Kx=(rigKx(x1)+rigKx(x2))/2;
Kae=Kae+[2 1; 1 2]*Kx*he/6;
Cae=C*A*[1 -1; -1 1]/he;
fa=[Fx0; Fx0]/6;
fae=he*[2 1; 1 2]*fa;

for r=1:2
    Fa(nos(r))=Fa(nos(r))+fae(r);
    for s=1:2
        Ka(nos(r),nos(s))=Ka(nos(r),nos(s))+Kae(r,s);
        Ca(nos(r),nos(s))=Ca(nos(r),nos(s))+Cae(r,s);
        Ma(nos(r),nos(s))=Ma(nos(r),nos(s))+Mae(r,s);
    end
end
end
for i=1:nnos
    azi(i)=area(X(i));
    dli(i)=azi(i)*8500;
    momi(i)=momI(X(i))*Elast(X(i));
end
%flexão-início
for i=1:nel
    nos=AresVert(i,:);
    x1=X(nos(1));
    x2=X(nos(2));
    he=norm(x2-x1);
    A=(area(x1)+area(x2))/2;
    E=(Elast(x1)+Elast(x2))/2;
```

```
I=(momI(x1)+momI(x2))/2;
C=(amorty(x1)+amorty(x2))/2;
Ky=(rigKy(x1)+rigKy(x2))/2;
ro=(rho(x1)+rho(x2))/2;
Mfe=(ro*A*he/420)*[156 22*he 54 -13*he;
                  22*he 4*he*he 13*he -3*he*he;
                   54 13*he 156 -22*he;
                   -13*he -3*he*he -22*he 4*he*he];
Cfe=(C*I/(he*he*he))*[12 6*he -12 6*he;
                      6*he 4*he*he -6*he 2*he*he;
                      -12 -6*he 12 -6*he;
                     6*he 2*he*he -6*he 4*he*he];
Kfe=(E*I/(he*he*he))*[12 6*he -12 6*he;
                      6*he 4*he*he -6*he 2*he*he;
                      -12 -6*he 12 -6*he;
                     6*he 2*he*he -6*he 4*he*he];
Kfe=Kfe+(Ky*he/420)*[156 22*he 54 -13*he;
                     22*he 4*he*he 13*he -3*he*he;
                     54 13*he 156 -22*he;
                     -13*he -3*he*he -22*he 4*he*he];
fy=(Fy0+Fy0)/2;
ffe=(fy*he/12)*[6;
                he;
                6;
                -he];
for r=1:2
    lai=2*(r-1)+1; %posição p/ elemento
    glai=2*(nos(r)-1)+1; %posição global
    laf=lai+1;
    glaf=glai+1;
    Ff(glai:glaf)=Ff(glai:glaf)+ffe(lai:laf);
for s=1:2
    lbi=2*(s-1)+1;
    glbi=2*(nos(s)-1)+1;
    lbf=lbi+1;
    glbf=glbi+1;
    Mf(glai:glaf,glbi:glbf)=Mf(glai:glaf,glbi:glbf)+Mfe(lai:laf,lbi:lbf);
    Cf(glai:glaf,glbi:glbf)=Cf(glai:glaf,glbi:glbf)+Cfe(lai:laf,lbi:lbf);
    Kf(glai:glaf,glbi:glbf)=Kf(glai:glaf,glbi:glbf)+Kfe(lai:laf,lbi:lbf);
```

```
    end
    end
end
% Cargas concentradas
nCN=size(CN,1);
for i=1:nCN
    no=CN(i,1);
    dir=CN(i,2);
    fc=cargN(no,dir);
    if dir==1
        pa=no;
        Fa(pa)=Fa(pa)+fc;
    else
        pa=2*(no-1)+dir-1;
        Ff(pa)=Ff(pa)+fc;
    end
end
% Massa concentrada
nMC=size(MC,1);
for i=1:nMC
    no=MC(i,1);
    Mci=MC(i,2);
    Jci=MC(i,3);
    pa=no;
    pf=2*(no-1)+1;
    Ma(pa,pa)=Ma(pa,pa)+Mci;
    Mf(pf,pf)=Mf(pf,pf)+Mci;
    pf=pf+1;
    Mf(pf,pf)=Mf(pf,pf)+Jci;
end
% Molas
nRC=size(RC,1);
for i=1:nRC
    no=RC(i,1);
    dir=RC(i,2);
    Kc=RC(i,3);
    um=rigC(no,dir,t);
    if dir==1
        pa=no;
```

```
        Ka(pa,pa)=Ka(pa,pa)+Kc;
        Fa(pa,pa)=Fa(pa)+Kc*um;
    else
        pa=2*(no-1)+dir-1;
        Kf(pa,pa)=Kf(pa,pa)+Kc;
        Ff(pa)=Ff(pa)+Kc*um;
    end
end
% Amortecimento concentrado
nAC=size(AC,1);
for i=1:nAC
    no=AC(i,1);
    dir=AC(i,2);
    Cc=AC(i,3);
    vc=amC(no,dir,t);
    if dir==1
        pa=no;
        Ca(pa,pa)=Ca(pa,pa)+Cc;
        Fa(pa)=Fa(pa)+Cc*vc;
    else
        pa=2*(no-1)+dir-1;
        Cf(pa,pa)=Cf(pa,pa)+Cc;
        Ff(pa)=Ff(pa)+Cc*vc;
    end
end
% Condições iniciais
Un=zeros(sza,1);
Upn=Un;
Uppn=Un;
Un1=Un;
Upn1=Un;
Uppn1=Un;
Vn=zeros(szf,1);
Vpn=Vn;
Vppn=Vn;
Vn1=Vn;
Vpn1=Vn;
Vppn1=Vn;
for i=1:nnos
```

```
    pa=i;
    pf=2*(i-1)+1;
    x=X(i);
%     Un(pa)=CondIniX(x,0); Upn(pa)=CondIniX(x,1);
%     [Vn(pf) Vn(pf+1)]=CondIniY(x,0); [Vpn(pf) Vpn(pf+1)]=CondIniY(x,1);
    Un(pa)=0; Upn(pa)=0;
    Vn(pf)=0; Vn(pf+1)=0; Vpn(pf)=0; Vpn(pf+1)=0;
end
Fa=Fa-Ka*Un-Ca*Upn;
Ff=Ff-Kf*Vn-Cf*Vpn;
nCD=size(CD,1); Mfeig=Mf(3:42,3:42); Kfeig=Kf(3:42,3:42);
for i=1:nCD
    no=CD(i,1);
    dir=CD(i,2);
    ac=condD(no,dir);
    if dir==1
        pa=no;
        g=Ma(:,pa);
        Ma(:,pa)=0;
        Ma(pa,:)=0;
        Ma(pa,pa)=1;
        Fa=Fa-ac*g;
        Fa(pa)=ac;
    else
        pa=2*(no-1)+dir-1;
        g=Mf(:,pa);
        Mf(:,pa)=0;
        Mf(pa,:)=0;
        Mf(pa,pa)=1;
        Ff=Ff-ac*g;
        Ff(pa)=ac;
    end
end
[v1,d1]=eig(Ka,Ma);
[v2,d2]=eig(Kfeig,Mfeig); amr=2*0.01*sqrt(diag(d2));
amr_aux=eye(40,40);
for i=1:40
    amr_aux(i,i)=amr(i);
end
```

```
%Meig=v1'*Ma*v1; Keig=v1'*Ka*v1; Feig=v1'*Fa; Ceig=v1'*Ca*v1;
Uppn=Ma\Fa; %Uppneig=Meig\Feig; t1=Uppn;t2=Uppneig; Uppp=Uppn;
Vppn=Mf\Ff;
gCt=0;
 nCol=(npt/npg)+1;
    gU=zeros(sza,nCol); gUeig=zeros(sza,nCol); gUeigt=zeros(sza,nCol);
    gV=zeros(szf,nCol);
    % Reações
    gCD=zeros(3*nCD,nCol);
    gU(:,1)=Un; %gUeig(:,1)=Uneig; % gUeigt(:,1)=v*Uneig;
    gV(:,1)=Vn;
    tempo=zeros(nCol,1);
    tempo(1)=0;
    gCD(:,1)=0;
    t=dt;
    ngr=2;
    % Matrizes permanentes
    a1=(1+2/dt); a2=a1*a1;
    Ha=a2*Ma+a1*Ca+Ka; %Haeig=a2*Meig+a1*Ceig+Keig; a11=2/dt;a22=a11*a11;
    Hf=a2*Mf+a1*Cf+Kf;
    sa=1;
    sf=1;
    for i=1:nCD
        no=CD(i,1);
        dir=CD(i,2);
        if dir==1
            pa=no;
            HDa(:,sa)=Ha(:,pa); %HDaeig(:,sa)=Haeig(:,pa);
            Ha(:,pa)=0; % Haeig(:,pa)=0;
            Ha(pa,:)=0; %Haeig(pa,:)=0;
            Ha(pa,pa)=1; %Haeig(pa,pa)=1;
            sa=sa+1;
        else
            pa=2*(no-1)+dir-1;
             HDf(:,sf)=Hf(:,pa);
            Hf(:,pa)=0;
            Hf(pa,:)=0;
            Hf(pa,pa)=1;
            sf=sf+1;
```

```
        end
    end
    while (t<= Int)
        Fa(:)=0; Feig(:)=0;
        Ff(:)=0;
%         for i=1:nel
          nCN=size(CN,1);
          for i=1:nCN
          no=CN(i,1);
          dir=CN(i,2);
          fc=cargN(no,dir);
          if dir==1
                      pa=no;
        Fa(pa)=Fa(pa)+fc; %fceigmat=zeros(9,1); fceigmat(pa)=fc; fceig=v'*fceigmat;
%         Feig(pa)=Feig(pa)+fceig(pa);

          else
          pa=2*(no-1)+dir-1;
          Ff(pa)=Ff(pa)+fc;
          end
          end
%           Feig=v'*Fa;
        Fa=Fa+Ma*(a2*Un+2*a1*Upn+Uppn)+Ca*(a1*Un+Upn);
%         Feig=Feig+Meig*(a2*Uneig+2*a1*Upneig+Uppneig)+Ceig*(a1*Uneig+Upneig);
        Ff=Ff+Mf*(a2*Vn+2*a1*Vpn+Vppn)+Cf*(a1*Vn+Vpn);
        sa=1;
        sf=1;
        for i=1:nCD
            no=CD(i,1);
            dir=CD(i,2); %auxi=zeros(9,1);
            ud=condD(no,dir); %auxi(no)=ud; ad=v'*Ma*auxi; udeig=ad(no);
            if dir==1
                g=HDa(:,sa);% geig=HDaeig(:,sa);
                Fa=Fa-ud*g; %Feig=Feig-udeig*geig;
                pa=no;
                Fa(pa)=ud; %Feig(pa)=udeig;
                sa=sa+1;
            else
                g=HDf(:,sf);
```

```
                Ff=Ff-ud*g;
                pa=2*(no-1)+dir-1;
                Ff(pa)=ud;
                sf=sf+1;
            end
        end
%        Feig=v'*Fa; Haeig=v'*Ha*v;
        Un1=Ha\Fa; % Un1eig=Haeig\Feig;
        Vn1=Hf\Ff;
        Upn1=a1*(Un1-Un)-Upn;   %Upn1eig=a1*(Un1eig-Uneig)-Upneig;
        Uppn1=a1*(Upn1-Upn)-Uppn;% Uppn1eig=a1*(Upn1eig-Upneig)-Uppneig;
        Vpn1=a1*(Vn1-Vn)-Vpn;
        Vppn1=a1*(Vpn1-Vpn)-Vppn;
        % trocar estados
        Un=Un1; Vn=Vn1; % Uneig=Un1eig;
        Upn=Upn1; Vpn=Vpn1; %Upneig=Upn1eig;
        Uppn=Uppn1; Vppn=Vppn1; %Uppneig=Uppn1eig;
        gCt=gCt+1;
        if gCt>=npg
            gU(:,ngr)=Un; %gUeig(:,ngr)=Uneig; gUeigt(:,ngr)=v*Uneig;
            gV(:,ngr)=Vn;
            tempo(ngr)=t;
            gCt=0;

    %Cálculo reações
    for i=1:nCD
        no=CD(i,1);
        dir=CD(i,2);
        pos=3*(i-1);
        ares=VertAres(no,:);
        if dir==1
            Re=zeros(2,1);
            for s=1:2
                if ares(s)>0
                    i=ares(s);
                    nos=AresVert(i,:);
                    x1=X(nos(1));
                    x2=X(nos(2));
                    he=norm(x2-x1);
```

```
                A=(area(x1)+area(x2))/2;
                C=(amortx(x1)+amortx(x2))/2;
                ro=(rho(x1)+rho(x2))/2;
                E=(Elast(x1)+Elast(x2))/2;
                % axial - início
                Mae=ro*A*he*[2 1; 1 2]/6;
                Kae=E*A*[1 -1; -1 1]/he;
                Kx=(rigKx(x1)+rigKx(x2))/2;
                Kae=Kae+[2 1; 1 2]*Kx*he/6;
                Cae=C*A*[1 -1; -1 1]/he;
                fa=[Fx0; Fx0]/6;
                fae=he*[2 1; 1 2]*fa;
                Ue=[Un1(nos(1)); Un1(nos(2))];
                Upe=[Upn1(nos(1));Un1(nos(2))];
                Uppe=[Uppn1(nos(1)); Uppn1(nos(2))];
                    Re=Re+Mae*Uppe+Cae*Upe+Kae*Ue-fae;
            end
        pos=pos+1;
        if no==nos(1)
        gCD(pos,ngr)=Re(1);
        else
            gCD(pos,ngr)=Re(2);
        end
        end
    else
        Re=zeros(4,1);
        for s=1:2
            if ares(s)>0
                i=ares(s);
                nos=AresVert(i,:);
x1=X(nos(1));
x2=X(nos(2));
he=norm(x2-x1);
A=(area(x1)+area(x2))/2;
E=(Elast(x1)+Elast(x2))/2;
I=(momI(x1)+momI(x2))/2;
C=(amorty(x1)+amorty(x2))/2;
Ky=(rigKy(x1)+rigKy(x2))/2;
ro=(rho(x1)+rho(x2))/2;
```

```
Mfe=(ro*A*he/420)*[156 22*he 54 -13*he;
                  22*he 4*he*he 13*he -3*he*he;
                   54 13*he 156 -22*he;
                   -13*he -3*he*he -22*he 4*he*he];
Cfe=(C*I/(he*he*he))*[12 6*he -12 6*he;
                      6*he 4*he*he -6*he 2*he*he;
                      -12 -6*he 12 -6*he;
                     6*he 2*he*he -6*he 4*he*he];
Kfe=(E*I/(he*he*he))*[12 6*he -12 6*he;
                      6*he 4*he*he -6*he 2*he*he;
                      -12 -6*he 12 -6*he;
                     6*he 2*he*he -6*he 4*he*he];
Kfe=Kfe+(Ky*he/420)*[136 22*he 54 -13*he;
                     22*he 4*he*he 13*he -3*he*he;
                     54 13*he 156 -22*he;
                     -13*he -3*he*he -22*he 4*he*he];
fy=(Fy0+Fy0)/2;
ffe=(fy*he/12)*[6;
                he;
                6;
                -he];
            pa1=2*(nos(1)-1)+1;
            pa2=pa1+1;
            pb1=2*(nos(2)-1)+1;
            pb2=pb1+1;
            Ve=[Vn1(pa1:pa2);Vn1(pb1:pb2)];
            Vpe=[Vpn1(pa1:pa2);Vpn1(pb1:pb2)];
            Vppe=[Vppn1(pa1:pa2);Vppn1(pb1:pb2)];
            Re=Re+Mfe*Vppe+Cfe*Vpe+Kfe*Ve-ffe;
            end
        pa=pos+2; pb=pa+1;
        if no==nos(1)
            gCD(pa:pb,ngr)=Re(1:2);
        else
            gCD(pa:pb,ngr)=Re(3:4);
        end
        end
    end
end
```

```
  ngr=ngr+1;
end
      t=t+dt;
end
```